Analog-to-Digital Conversion Schemes in Beyond-Fifth and Sixth Generation Wireless Communication Systems

July 2022

GAO, Peng

A Thesis for the Degree of Ph.D. in Engineering

Analog-to-Digital Conversion Schemes in Beyond-Fifth and Sixth Generation Wireless Communication Systems

July 2022

Graduate School of Science and Technology
Keio University

GAO, Peng

ACKNOWLEDGEMENTS

I would like to thank my esteemed supervisor – Prof. Yukitoshi Sanada, for his invaluable supervision, support, and teaching during my Ph.D. degree. My gratitude extends to the Graduate School of Science and Technology for the funding opportunity to undertake my studies at Keio University. Additionally, I would like to express gratitude to Prof. Sasase, Prof. Ohtsuki, and Prof. Ikehara for their treasured advice and support, which was influential in improving my dissertation and critiquing my results. My appreciation also goes out to my family and friends for their encouragement and support throughout my studies.

TABLE OF CONTENTS

LIST OF TABLES

LIST OF FIGURES

ACRONYMS

1G first-generation

2D two dimensional

2G second-generation

3D three dimensional

3D-InteCom Three-dimensional integrated communications

3G third-generation

4G fourth-generation

4K 4000 pixels

5G fifth-generation

6G sixth generation

ADC analog-to-digital converter

AGC automatic gain control

AMPS advanced mobile phone system

APs access points

AQNM additive quantization noise model

AR adaptive-resolution/augmented reality

BER bit error rate

BigCom Big communications

BS base station

CDMA code-division multiple access

CPU central processing unit

CSI channel state information

D2D device-to-device

DAS distributed antenna system

DFT discrete Fourier transform

EE energy efficiency

EHF extremely high-frequency bands

eMBB Enhance mobile broadband

FDMA frequency-division multiple access

FOM figure-of-merit

GPRS general packet radio service

GSM global system for mobile

HSPA high-speed packet access

IAD inter-antenna distance

ICN information centric networking

IDFT inverse discrete Fourier transform

i.i.d. independent and identically distributed

IMT International Mobile Telecommunications

inf-ADC infinite-resolution ADC

IoT Internet of things

IPL-Rayleigh ideal pathloss model with Rayleigh

ITU-R International Telecommunication Union Radiocommunication Sector

IUI inter-user interference

LOS line-of-sight

LS Least-square

LTE long-term evolution

MAP maximum a posteriori

MIMO multiple-input and multiple-output

ML maximum likelihood

MMSE minimum mean square error

mMTC massive machine type communications

MRC maximum ratio combining

MSDE mean square distortion error

MSE mean square error

MSQE mean square quantization error

MU multi-user

MUI multi-user interference

NFV network functions virtualization

NLOS non-line-of-sight

NTT Nippon Telegraph and Telephone

OFDM orthogonal frequency-division multiplexing

OFDMA orthogonal frequency-division multiple access

PDFs probability density functions

QoS quality of service

RAT radio access technology

RF radio frequency

RFFE radio frequency front-end

SAR successive approximation register

SDMA space-division multiple access

SDQNR signal-to-distortion-quantization noise ratio

SDR software defined radio

SE spectral efficiency

SHF super-high frequency

SINR signal-to-interference-plus-noise ratio

SIQNRs signal-to-interference-plus-quantization-and-noise ratios

SISO single-input and single-output

SNDR Signal-to-noise-and-distortion ratio

SNR signal-to-noise ratio

SR serving range

SURLLC Secure ultra-reliable low-latency communications

TDD time division duplexing

TDMA time-division multiple access

THF tremendously high frequency

UCDC Unconventional data communications

UE user equipment

URLLC ultra-reliable low-latency communications

UVA unmanned aerial vehicles

VR virtual reality

ZF zero-forcing

NOTATIONS

A	the quantatization range
B	number of blocks
$\mathcal{B}$	the resolution set of ADCs
b	the block
C	the clipping factor
C_{op}	the set of different clipping coefficients C corresponding to $\mathcal{B}$
d_{LOS}	the distance between the AP and the user under the LOS condition
d_{mk}	the distance between the kth UE and the mth AP
$\mathbf{E}[v]$	the quantization noise vector
$E_m[v]$	the quantization noise on vth subcarrier
$e_m[u]$	the quantization noise at time u
$\mathrm{erfc}(\cdot)$	the complementary error function
f_c	the carrier frequency
$G_{mk}[v]$	the channel response including pathloss between the kth user and mth antenna of the AP in frequency domain
g_{mk}	the channel gain between AP m and UE k
H_{mkn}	the channel response between the nth antenna of the kth user and the mth antenna of the BS in frequency domain
$\mathbf{H}_{ij}[v]$	the channel responses between the jth antenna of the ith user and the base station antennas in the vector form
$\hat{\mathbf{H}}_{kn}^{b}$	the estimated channel vector in the bth block for the nth antenna of user k
$\hat{\mathbf{H}}_{m}^{b}$	the estimated channel vector in the bth block for the mth antenna of the BS

h_{mkn}	the channel response between the nth antenna of the kth user and the mth antenna of the BS in time domain
$\Im(\cdot)$	the imaginary part for quantization
K	number of users/UEs
$\mathcal{K}$	Rician factor
L	number of streams
L_{ap}	number of APs
L_q	the quantization level
M	number of receive antennas/serving APs
N_{cp}	the length of a cyclic prefix
N_{dft}	the size of an inverse discrete fourier transform
N_{sc}	number of subcarriers
N_{sym}	number of OFDM symbols
N_u	number of antennas for kth user in massive MIMO
P_k	the transmit power of the kth user
PC_k	the power consumption of the ADC
$PL[\text{dB}]$	the pathloss in dB
$P_{\text{LOS}}(d_{mk})$	the LOS probability
$P_{q_m}(C)$	the power of the undistorted signal component
p^{ul}	the transmit power for each UE
$Q(\cdot)$	quantization operation
$q_m[u]$	the quantization signal at the time u
R	the resolution bits of an ADC
$\Re(\cdot)$	the real part for quantization
r_m	the input signal of the kth UE at the m AP
$\mathcal{R}_k$	an ergodic rate per arbitrary user k
$S_{kn}[v]$	the transmit signal from the nth antenna of user k on vth subcarrier

$s_{kn}[u]$	the transmit signal from the nth antenna of user k at time u
$\hat{S}_k[v]$	the estimate of $S_k[v]$ at AP m, ($N_u = 1$ case)
SE	an achievable uplink SE
V	number of subcarriers in one block
W_{mk}	the MRC coefficient
$\mathbf{W}_{kn}^b$	the MRC coefficient of the b th block in the vector form
$\mathcal{W}_{kn}^b$	the MMSE coefficient of the b th block in the vector form
$Y_m[v]$	the received signal of the mth antenna of the BS on vth subcarrier
$y_m[u]$	the received signal of the mth antenna of the BS at time u
$Y_{q_m}[v]$	the ADC output of the mth AP on vth subcarrier
$\hat{y}_{mi}$	the ith original quantization threshold value and q_i is the amplitude of the ith original quantization interval
$Z_m[v]$	the thermal noise on vth subcarrier
$z_m[u]$	the thermal noise at time u
Δ	allowable distortion parameter through quantization
δ	the quantization step-size
η_{EE}	uplink EE
$\theta_m[u]$	the filtered distortion noise at time u
λ	the subcarrier
λ_w	the wavelength
μ	the coefficient of the Bussgang decomposition
σ'	the sum of the variance of the thermal noise and the quantization noise
σ_n^2	the variance of the thermal noise
$\sigma_{q_m}^2$	the total power of the output of the quantizer at the mth AP
$\sigma_{y_{mk}}^2$	the ADC input power of the kth UE at the mth AP
Ω_k	the instantaneous SIQNR of the MRC output of the kth UE

SUMMARY

With a marked rise in a plethora of wireless devices and emerging use cases in the future, larger data traffic needs to be supported. The development of the existing fifth-generation (5G) network is designed to satisfy these demands. Furthermore, increasing factory automation and the transition from Industry 4.0 to the upcoming Industry X.0 paradigm will accelerate the demands of wider coverage and higher connection density in 5G designs. One of the main keys to improve the spectrum efficiency is massive multiple-input and multiple-output (MIMO) technology. In recent years, massive MIMO has been implemented in two ways, namely centralized and distributed antenna deployment. Centralized massive MIMO deploys a large number of antennas at the base station (BS); distributed massive MIMO is that the BS antennas are geographically distributed over the cell. For reducing cost and power consumption, massive MIMO communications adopt hybrid transceivers, which combine analog phase shifters and power amplifiers with digital signal processing units. However, hybrid-mode implementations are confronted with inter-user interference (IUI) due to a larger beamwidth. On the other hand, using a low-resolution analog-to-digital converter (ADC) in the BS can also achieve better energy efficiency (EE), but it will cause severe quantization distortion in a received signal. With the trends of ADCs, current research indicates that low-resolution ADCs are very promising for massive MIMO and cell-free networks. Therefore, the focus of this thesis tends to address the above challenges to improve the spectral efficiency (SE) and the EE of the system, and we assert that the ongoing research on massive MIMO and cell-free distributed antennas are the key to future wireless communications. To this end, a low-complexity and low-power full-digital receiver with a practical quantized signal detection scheme is designed. Further, an adaptive-resolution (AR) ADC scheme is proposed to the cell-free distributed antenna system to mitigate the serious quantization distortion.

Chapter one is the introduction. It mainly describes the evolution of wireless commu-

nication systems, the major demands of beyond-5G and the sixth generation (6G), the key issues of current 5G networks, and related research motivations. The first section introduces the evolution of wireless communications; the second section introduces beyond-5G and 6G; The third section is the trends of ADCs. The fourth section is the research motivations based on the above-related issues.

Chapter two is the design of a low-power and low-cost massive MIMO system. Since low-resolution ADCs can bring low power consumption, they have been equipped to massive MIMO systems. However, low-resolution ADCs can also bring severe quantization distortions that degrade the performance of the system. The first section addresses the conventional schemes that have been studied on reducing the impacts of the quantization distortion, including power allocation schemes, signal detection schemes, channel estimation schemes, coding schemes, and the conventional ADC design. The main concern is to reduce a quantization noise generated by the ADC through the design of the quantization process. The second section is a quantization range control scheme in a massive MIMO system with low-resolution ADCs. Therein, the quantization process in the ADC is introduced. By analyzing an additive quantization noise model (AQNM), the quantization range limit coefficient of the ADC is derived. When a thermal noise in a received signal dominates, the noise at the receiver can be clipped by adjusting the quantization range limit coefficient. Further, this section represents related numerical results based on quantization range control, including mean square distortion error (MSDE) performance, mean square error (MSE) performance, and the SE performance. The third section presents the selection of interference reduction schemes. Based on the quantization range control scheme, the coarse quantization noise introduced by the low-resolution ADC can be effectively suppressed. Furthermore, since the quantization distortion effect is weakened, it also has an impact on the effects of interference suppression schemes. By comparing and analyzing minimum mean square error (MMSE), we propose to adopt maximum ratio combining (MRC) for quantized signals to reduce the computational complexity of the very large-scale antenna systems. Moreover, the related numerical results based on the MRC detection scheme and their related conclusions are represented.

Chapter three is the design of ADCs in the access points (APs) of a cell-free distributed antenna system (DAS). Different from conventional cellular communications, the cell-free DAS architecture removes boundary between cells and deploys APs over an area and all APs communicate with a central processing unit (CPU). When users request services, all APs distributed in the service area provide services for them. This kind of an AP ubiquitous service mode can provide extremely large channel gain and coverage. However, the system still faces larger energy consumption caused by infinite-resolution ADC (inf-ADC) components or a lower system throughput that is caused by low-resolution ADC components. The first section presents the conventional schemes for a tradeoff between SE and EE, i.e., a maximum-minimum fairness power optimization scheme, and a hybrid-ADC scheme and a bit allocation scheme. Under the premise of ensuring power consumption, the throughput of the system can be improved through those schemes. The second section is the proposed cell-free DAS with AR-ADCs. Although the existing hybrid ADC scheme can improve a SE, studies have shown that the energy consumption of ADCs will still be dominated by inf-ADCs. The proposed AR-ADC scheme for each AP can refer to factors such as propagation loss, quantization distortion, and IUI, and then reasonably switch a flexible low-resolution ADC component to improve system throughput and reduce energy consumption. We conduct simulation for verification of this scheme in different scenarios. Compared with the conventional hybrid ADC scheme with inf-ADCs, it can guarantee the EE while greatly increase the SE to realize a higher throughput for beyond-5G and 6G networks. The third section analyzes the relevant numerical results and draws conclusions.

CHAPTER 1
INTRODUCTION

1.1 Evolution of Wireless Communications

The first-generation (1G) system appeared around 1980. It adopted frequency-division multiple access (FDMA), which divides system bandwidth into many sub-bandwidths and then allocates the different sub-frequency bands to the different users. A bandpass filter is utilized to further reduce the interference among users. However, low spectral efficiency, complex equipment, and limited capacity became the problems in the 1G.

The second-generation (2G) system appeared around 1990. The difference from the 1G is that it made voice digitized and adopted digital multiple access technologies, FDMA and time-division multiple access (TDMA). Therein, the digital modulation can make the characteristics of the transmission signal match with the characteristics of the channel. In TDMA, one carrier frequency is shared by several users. Different users are distinguished by non-overlapping time slots so that a signal is transmitted discontinuously. Since multiple users share one frequency in TDMA, additional frequency generators are not needed, and the cost of shared equipment is reduced. Compared with 1G, the advantages of 2G are high SE, large system capacity, strong abilities on anti-interference, and anti-multipath fading.

The third-generation (3G) system was launched in early 2000. It mainly adopted code-division multiple access (CDMA), in which multiple users use the same frequency resource and time resource and orthogonal codes as the sets of sequences are allocated to users. Different users are distinguished by different codes. Co-channel interference can be reduced by the dispreading process of spread-spectrum technique, 3G system owns strong abilities on anti-interference and anti-multipath fading. Based on CDMA, the 3G system can increase the number of users through introducing less noise. The capacity of CDMA obviously increases tenfold more than that of FDMA. However, since the assigned codes are not orthogonal completely, multiple access interference during the dispreading process limits the capacity of the system.

The fourth-generation (4G) system mainly adopted orthogonal frequency-division multiple access (OFDMA), which modulates the serial data onto the parallel multiple orthogonal subcarriers to reduce the symbol rate of each subcarrier and to increase the symbol period. Since this, the abilities of anti-interference and anti-multipath fading are improved. Furthermore, due to the orthogonality of the subcarriers, spectral efficiency is greatly improved. A MIMO technology was also adopted, which utilizes the independence of spatial channels between antennas to distinguish and provide services for users. In the MIMO system, the diversity technique uses two or more antennas to transmit the same signals for reliability; spatial multiplexing sends data to user equipment (UE)s that have more than one received antenna. MIMO can use independent spatial resources to improve capacity.

The 5G system extends the MIMO technology and scales up it as a massive MIMO technology which uses tens of antennas to increase the capacity of the system by using space as three dimensions; beamforming is used for directive signal transmission or reception to improve a signal-to-noise ratio (SNR). The number of antennas is generally no more than 16 in the conventional, while the number of antennas in a massive MIMO scenario can reach tens to hundreds. The following sections will describe the impacts of massive MIMO on system capacity and spectral efficiency [1–4].

Throughout the development of wireless communications, the improvement in performance is a leap every ten years as Fig. 1.1 shows. From 1G to 3G, they have their own representative technologies, respectively. However, radio access technology (RAT) is expanded to a variety of new orthogonal frequency-division multiplexing (OFDM)-based composite technologies from 4G. Since OFDM-based technology has already achieved communication quality close to Shannon limit in 5G, technological fields of 6G will become more abundant.

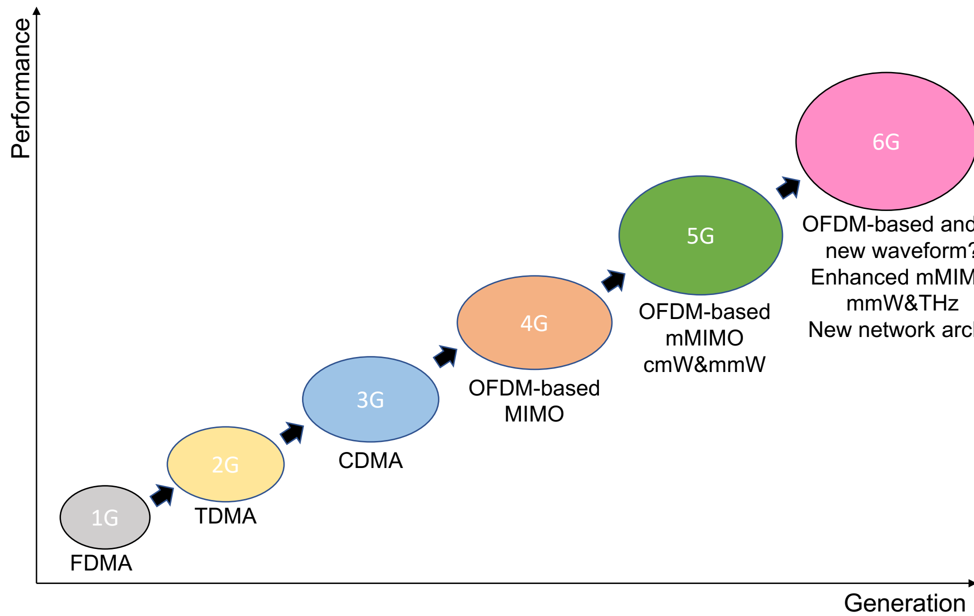

Figure 1.1: Evolution of wireless technologies 1G to 6G in mobile communication.

1.2 Next Generation-6G

As a new generation mobile communication technology, 6G needs to significantly improve the transmission capacity and the quality of service (QoS) as compared with 5G. From the perspective of research, the transformative technologies are mainly dedicated to increasing the system capacity and the data rates supporting a surge of device connections, and saving energy and cost. In theory, a 6G network will deliver a peak date rate of 1000 Gbps that is a hundred times faster than that of the current 5G network with enhanced reliability and wider network coverage.

In 6G, there are two key technologies to fulfil the demands for the rapid development of the mobile internet and to drive full reality of Internet of things (IoT) [5]. They are the use of a tremendously high frequency (THF) band and the implementation of a distributed network architecture.

i. Terahertz wave

Nowadays, most mobile communication networks operate in low-frequency bands. The advantage of low-frequency bands is better propagation performance. The disadvantage of it is that continuous frequency resources are limited, which means less bandwidth is available for each user, and this limitation causes slower network services and more connection interruptions. The highest carrier frequency of the 4G long-term evolution (LTE) band is around 2GHz, and its available spectrum bandwidth is the only 100MHz. Comparing 5G and 6G, 5G is the first-generation communication system to use a high frequency band, which is allocated for low band (sub-6 GHz) and high band (above 24.25 GHz as millimeter wave), respectively. Such as the 28 GHz band, it can provide the available spectrum bandwidth of up to 1 GHz. 6G will be in the domains of terahertz band communications, the wider spectrum bandwidth and the faster transmission rate can be obtained. However, larger propagation loss becomes its disadvantages.

ii. Cell-free network architecture

Use cases of future wireless communications significantly increase and they demands wireless communications to improve the capacity. As we all know, the antenna diversity scheme has developed from "single-input and single-output (SISO)" to "MIMO", then to "massive MIMO", and even larger MIMO has more capacity and ability to improve communication quality. However, the classic cell-based or centralized antenna architecture of wireless networks cannot be expanded to meet the aera traffic capacity and the device connection density requirements of 6G. Cell-free network architecture can reduce path loss and shadowing effects by closer distances between APs and users. The reliability of links is improved as each user is served by many APs and there is less probability of blockage.

1.2.1 Use Cases in 6G

Based on the above-mentioned new technologies, 6G will provide faster transmission speeds, stronger outdoor and indoor coverage capabilities, more extensive connection capability, and lower latency user experience. The following introduces 5G use cases based on International Mobile Telecommunications (IMT)-2020 radio interface standardization trends in International Telecommunication Union Radiocommunication Sector (ITU-R) and 6G use cases based on the outlook for the next decade [6, 7]. These are shown in Fig. 1.2.

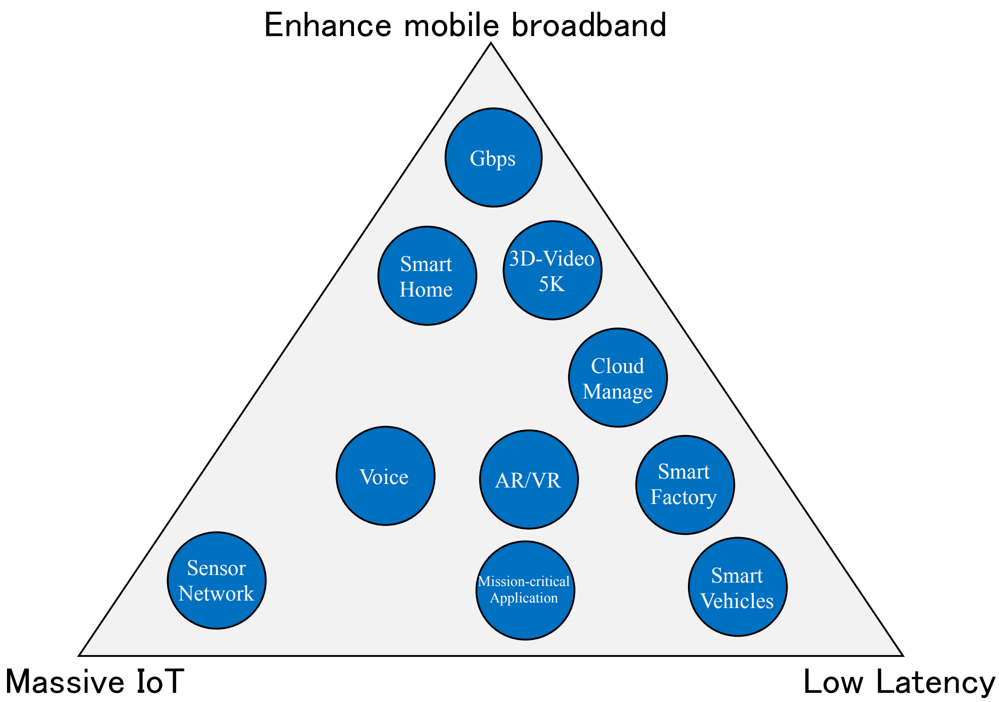

(a) IMT-2020 (5G) typical usage scenarios.

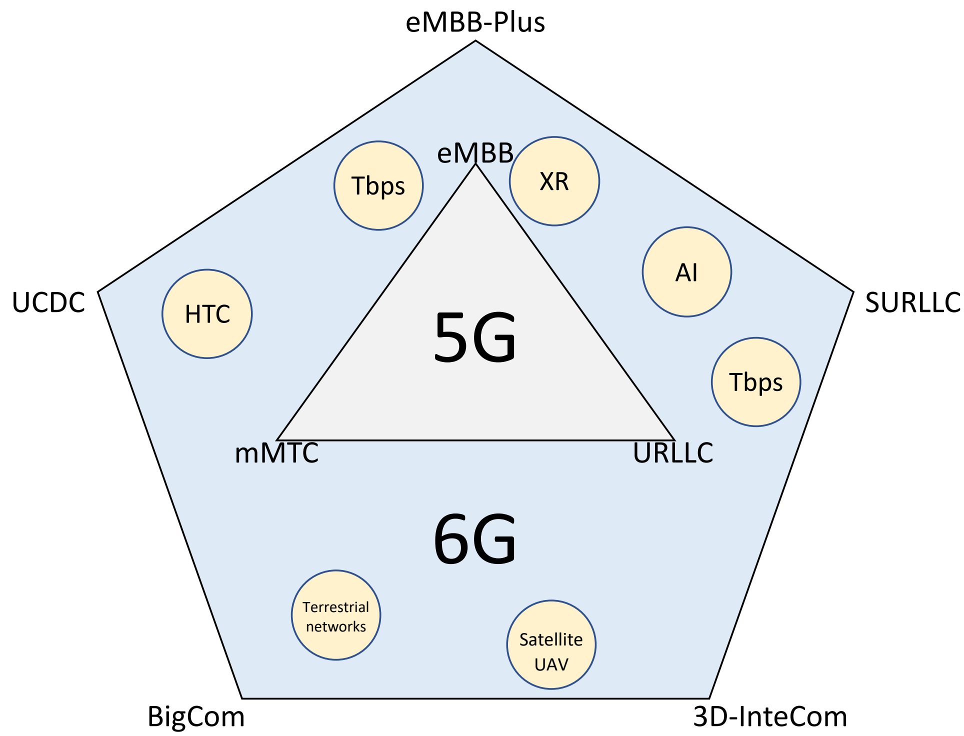

(b) 6G typical usage scenarios.

Figure 1.2: Requirements for 5G&6G wireless technology.

5G Typical Usage Scenarios

Enhance mobile broadband (eMBB): high-speed data transmission can support real-time broadcast at 4000 pixels (4K) and above. Massive data processing can be carried out on cloud platforms.

Massive IoT: stronger signal coverage and improved terminal access capacity make it easier to connect people to things and things to things. Therefore, 5G becomes more widespread in the application of the IoT.

Low latency: because of very low latency and extremely high reliability of 5G, the user experience of augmented reality (AR) and virtual reality (VR) can be greatly improved, which promotes the implementation of applications such as telemedicine surgery, autonomous driving, and remote control.

6G Typical Usage Scenarios

The next generation network supports not only features of the current 5G but also enhanced features to extend new fields, such as faster data rate, lower latency, wider coverage, higher reliability, among others [8].

The eMBB-Plus: much higher requirements and standards will serve the conventional mobile communications and optimize cellular networks in terms of interference, handover, and big data stream.

Secure ultra-reliable low-latency communications (SURLLC): a joint upgrade of ultra-reliable low-latency communications (URLLC) and massive machine type communications (mMTC) has higher reliability and lower latency. It mainly provides the technological support to smart industry and military communications.

Big communications (BigCom): For dense areas, the extremely good data service can be guaranteed like 5G. Although, the same service quality cannot be guaranteed for remote areas, it will realize the wider coverage range of networks to cover and provide acceptable data service.

Three-dimensional integrated communications (3D-InteCom): This feature focuses on network analysis, planning, and optimization from two dimensional (2D) to three dimensional (3D), where the heights of communication nodes need to be considered. For example, satellite unmanned aerial vehicles (UVA) and underwater communications will benefit from this feature of 6G. Therefore, the original two-dimensional wireless communication analysis framework based on random geometry and graph theory needs to be upgraded to a 3D perspective [9]. Considering the height of the node, this can also realize the elevation beamforming of the full-dimensional MIMO architecture, which provides another direction for network optimization [10].

Unconventional data communications (UCDC): According to the expansion of 6G technical advantages, the development of IoT will be more comprehensive. Interdisciplinary applications are being explored, including medicine, sociology, biology, and so on. Novel application scenarios include holographic, tactile, and human bond communication.

These benefits of 5G&6G can be realized through technical processing. Among them, its large capacity/high speed, and wide coverage can be resolved using massive MIMO technology, high frequency band and cell-free with distribution antenna architecture, as shown in Fig. 1.3.

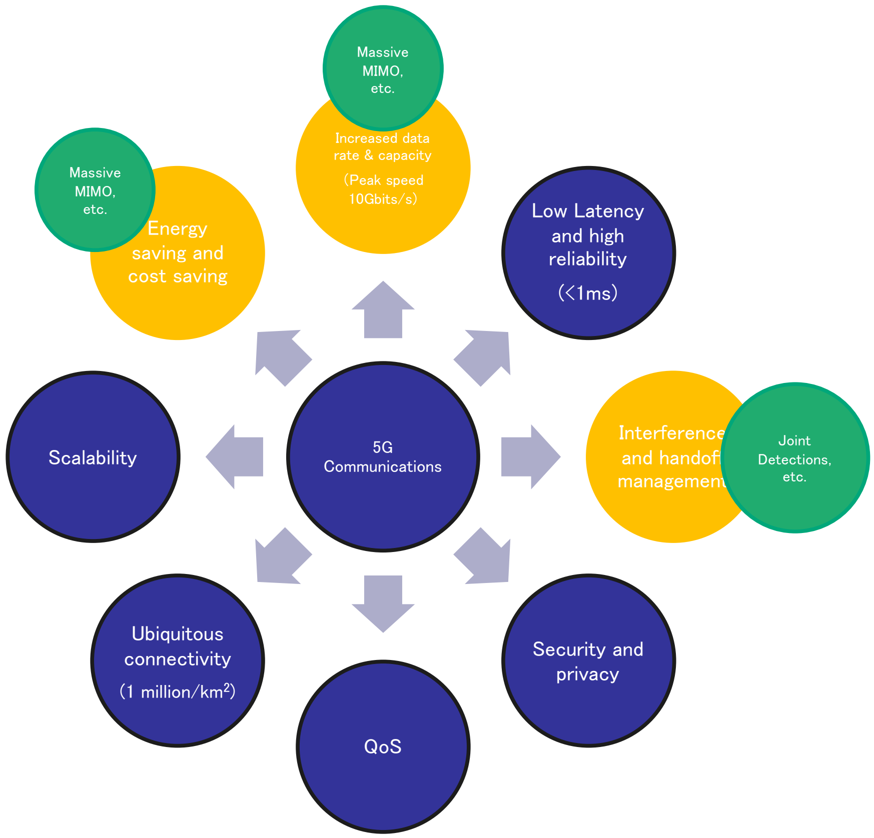

(a) 5G technological pros.

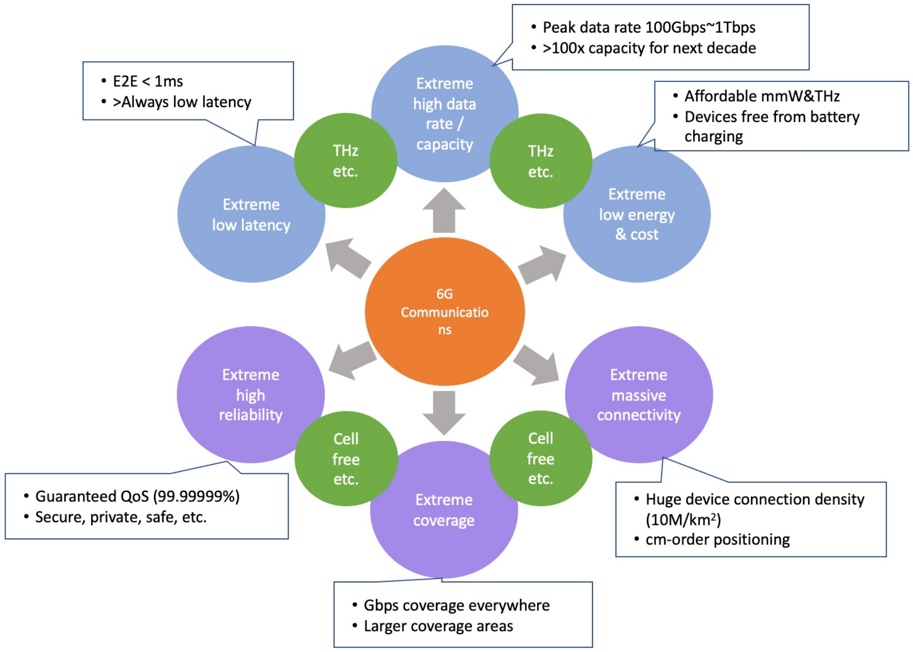

(b) 6G technological pros.

Figure 1.3: Benefits of 5G&6G.

The advanced requirements described in 6G will be met by a combination of technologies.

1.2.2 Spectrum for 5G&6G

The spectrum of 5G is based on the ITU-R spectrum allotment plans, which is made to manage the international radio-frequency spectrum and to develop standards for radiocommunication systems with the objective of ensuring the effective use of the spectrum [11]. ITU-R identifies frequency bands for mobile services, especially IMT. Global spectrum assignment for different services and applications are done within the ITU-R and have been documented in the ITU Radio Regulations. ITU-R describes the use of IMT bands worldwide and the frequency bands that 6G will plan to use in the future in Table 1.

Table 1.1: International review of 5G&6G frequency

<table>
<tr><th>Country</th><th colspan="5">5G frequency bands</th><th>6G</th></tr>
<tr><th></th><th>Sub-6GHz</th><th>28GHz</th><th>30GHz</th><th>40GHz</th><th>60-70GHz</th><th>THz</th></tr>
<tr><td>Japan</td><td>3.48-3.6GHz: Assigned
3.6-4.2GHz: Consideration
4.4-4.5GHz: Consideration</td><td>27.5-29.5GHz:
Consideration</td><td colspan="3"></td><td rowspan="5">0.1-10THz:
Undivided
0.15-0.3THz
(Beyond 5G)</td></tr>
<tr><td>USA</td><td>600MHz: Incentive auction
3.55-3.7GHz: Consideration</td><td>27.5-28.35GHz:
Promulgation</td><td>37-38.6GHz:
Promulgation</td><td>38.6-40GHz:
Promulgation</td><td>64-71GHz:
Promulgation</td></tr>
<tr><td>Korea</td><td>3.4-3.7GHz: Promulgation</td><td>27.5-29.5GHz:
Promulgation
24.75-27.5GHz:
Consideration</td><td>31.8-33.4GHz:
Consideration</td><td>37-40.5GHz:
Consideration</td><td></td></tr>
<tr><td>China</td><td>3.3-3.6GHz: Promulgation
4.4-4.5GHz: Consideration</td><td>24.75-27.5GHz:
Promotion</td><td colspan="3">37.5-42.5GHz: Promotion</td></tr>
<tr><td>Europe</td><td>700MHz: Coverage&indoor use
3.4-3.8GHz: Consideration</td><td>24.75-27.5GHz:
Pioneer band</td><td></td><td>40.5-43.5GHz:
Promotion</td><td>66-71GHz:
Promotion</td></tr>
</table>

From Table 1, all frequency bands in 5G & 6G belong to super-high frequency (SHF), extremely high-frequency bands (EHF) and THF. In these frequency bands, massive MIMO and enhanced massive MIMO features wideband signals and a larger number of antennas in the same space.

1.2.3 Trends of Analog-to-Digital Converters

For 5G and 6G, wider transmission bandwidth and more advanced multi-antenna technologies are required. hundredfold increment on bandwidth will be available. As a result, higher-speed ADC components are required to meet radio frequency (RF) sampling. Furthermore, the trade-off between SE and EE will be considered a more worthy issue. Since the smaller value of figure-of-merit (FOM) means a better quality of ADCs, low-resolution ADCs will be appropriately applied to reduce the power consumption in full-digital communication systems.

The ADC is a vital module of a coherent transceiver chip solution and is widely used in digital communication systems. Due to the continued growth of a wireless network and communications market, mobile data traffic (mainly generated by smartphones) is expected to grow tenfold in the next five years. As a result, expectations for ADCs continue to increase. The performance of the ADC will determine the ultimate performance of the digital system.

In 5G, the greater bandwidth available will challenge data conversion interfaces between analog and digital domains in receivers and transmitters. Signal-to-noise-and-distortion ratio (SNDR)-based FOM is a widely accepted metric for ADCs as defined in [12].

Generally, for lower resolution ADCs, the energy efficiency can be doubled in every 1 to 6 years, but it is difficult for high-resolution ADCs to achieve this energy efficiency improvement due to thermal noise limitations. Therefore, in order to analyze the FOM trend, we will learn about the most commonly used FOM:

$$FOM = \frac{Power}{2BW \times 2^{ENOB}}, \tag{1.1}$$

where BW is the bandwidth, ENOB is the effective number of bits defined by the SNDR.

$$ENOB = \frac{SNDR - 1.76}{6.02}. \tag{1.2}$$

FOM is sometimes referred to as the Walden and relates the ADC power dissipation to its performance, represented by the bandwidth and the conversion error amplitude. The best reported FOM value each year has been plotted in Fig. 1.4 [13]. Trajectories for state-of-the-art have been indicated and trends have been fitted to these state-of-the-art data points [14].

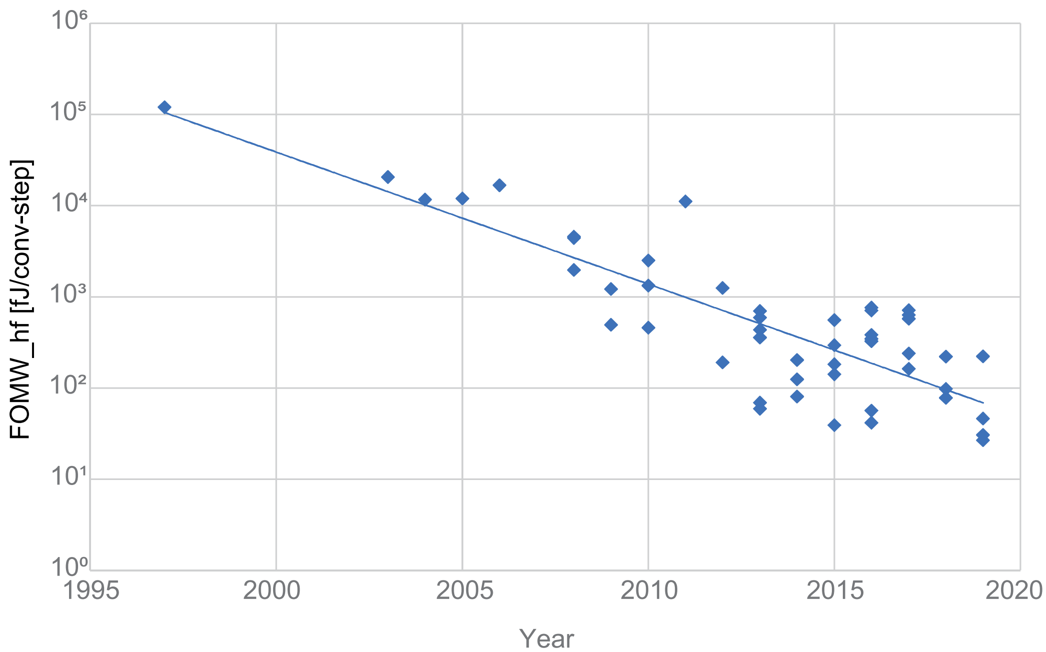

Figure 1.4: FOMW of ADCs.

Based on the FOM index, the performance ADC elements will be improved in future, which means less power-loss and error from the ADC itself, even low-resolution ADCs.

1.2.4 Network Architectures in 5G&6G

The cellular technology was developed by Bell Laboratories in 1947 [15]. A cellular network is a radio network distributed over land through cells, where each cell includes a fixed location transceiver known as the BS. These cells together provide radio coverage over larger geographical areas, and hexagonal cells are conventional. The architecture of the hexagonal cell consists of a central cell surrounded by other cells as Fig. 1.5 [16].

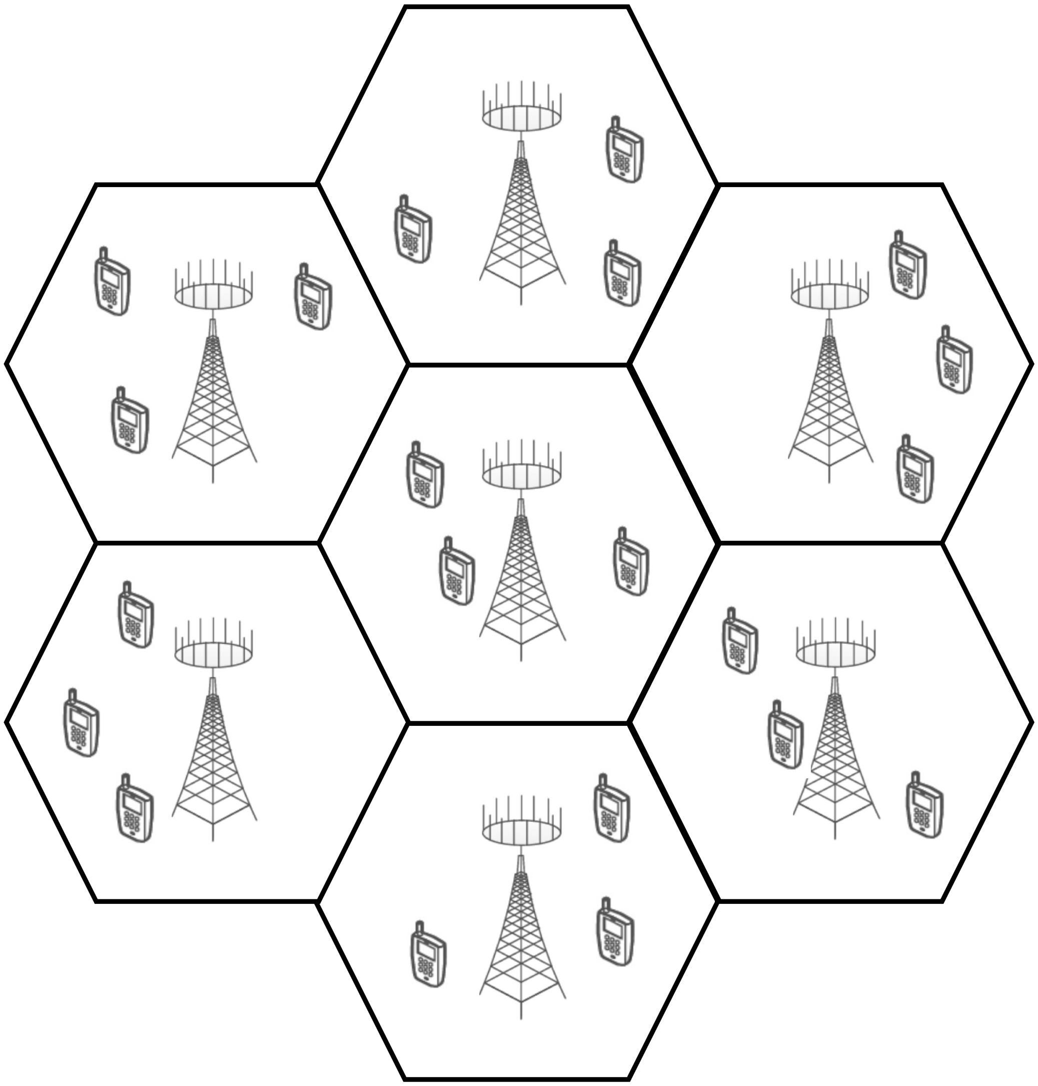

Figure 1.5: Conventional cellular network architecture.

The first commercial cellular network for 1G in Japan was launched by Nippon Telegraph and Telephone (NTT) in 1979 [17]. In 1G cellular network, an advanced mobile phone system (AMPS) provided basic voice services based on an analog transmission technology. In 2G cellular network, mobile data services were provided by general packet radio service (GPRS) in addition to basic voice services. In 1999, 3G retains the basic architecture of global system for mobile (GSM)/GPRS networks, with wideband CDMA for enhanced capabilities. In CDMA, all the cells share the same frequency band. Starting from 2002, high-speed packet access (HSPA) was introduced to achieve higher-speed downlink and uplink packet access by using new techniques such as multicode transmission, short transmission time interval, adaptive modulation and coding, fast dynamic scheduling and hybrid automatic repeat request [18]. From 2009, a 4G cellular network capable of transmitting high-quality video images and high-quality images has been developed. Meanwhile, a heterogeneous network was employed in 4G. To avoid network congestion, add multiple 4G small BSs supplying customers with service jointly in the area already having been covered with 4G signal, especially for the crowded places or the place that demands better signal [19]. From beyond-4G to the current 5G cellular networks, the data rate, capacity, service range and stability requirements are getting higher and higher. Current cell network architectures can achieve high data rates in the cell centers based on massive MIMO [20–23]. Since there are still essential rate variations to UE in each cell, the large variations within each cell lead to the unreliable QoS. This is not sufficient for the future ubiquitous wireless communications to provide the uniform QoS. The cellular-free network architecture is considered not only to increase the data rate, but more importantly to ensure the QoS for users in almost all locations within the geographic coverage area [24].

Next, the basic architecture of a cell-free network is introduced in detail. It consists of L geographically distributed access points (APs) that are jointly serving the UEs that reside in the area. Each AP is connected via a fronthaul to a central processing unit (CPU), which is responsible for the AP cooperation. In a very large areas, multiple CPUs can be used all connected via fronthaul links [25–27]. Through the fronthaul links, sharing physical-layer signals that will be transmitted in the downlink, forwarding received uplink data signals that are yet to be decoded, and sharing channel state information (CSI) related to the physical channels can be processed. A cell-free network with single-antenna APs is shown in Fig. 1.6.

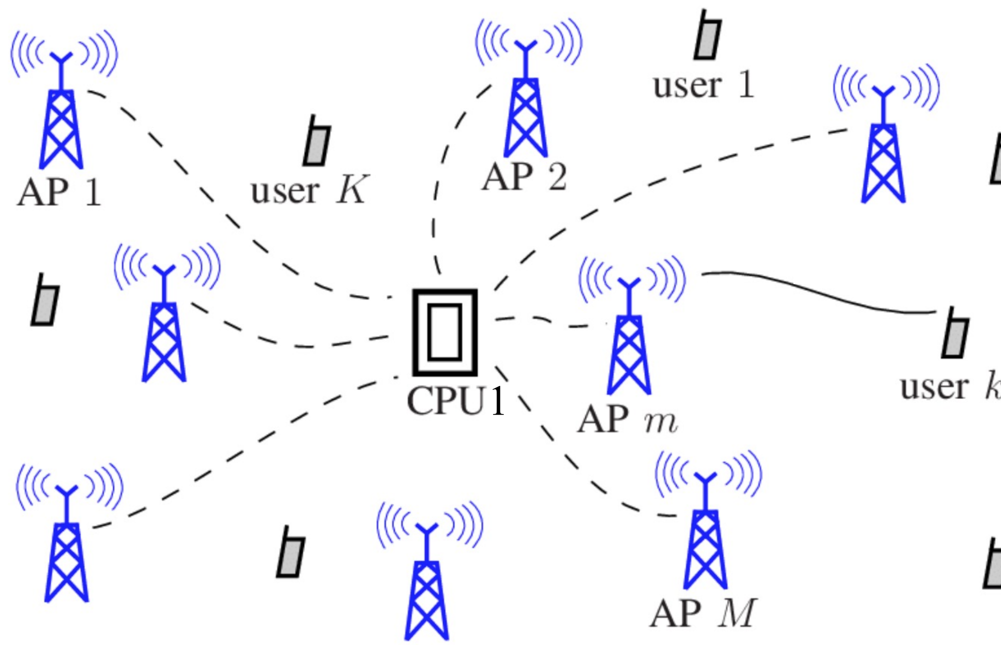

Figure 1.6: Cell-free network architecture.

Due to high-density deployment in cell-free networks, the average propagation distance between a UE and the closest AP is significantly reduced. Furthermore, the main reason is that data is jointly transmitted to the UE by all the surrounding APs, thereby alleviating the inter-cell interference issue that is one of the main causes of the large rate variations in cellular networks.

Last, the antennas setups are different in the above-mentioned network architectures to bring their own benefits. Therein, the benefits of cell-free networks are a better ability to manage interference and a higher uniform SNR in the coverage area.

1.2.5 Massive-Antenna Transmission

In the previous generation of mobile communication systems, both BSs and UEs had been designed to use multiple antennas for radio transmission and reception [28,29]. Three main multi-antenna technologies have different goals and are achieved in different ways. The first one is diversity processing, which increases the power of the received signal and reduces the amount of fading by using multiple antennas on the transmitter, the receiver, or both.

Diversity processing has been used since the early days of mobile communications. In spatial multiplexing, both the transmitter and the receiver use multiple antennas to increase the data rate. Finally, beamforming uses multiple antennas at the BS to increase cell coverage. Spatial multiplexing is often described as using MIMO antennas. This name derives from the inputs and outputs of the air interface, so "multiple inputs" refers to the transmitter and "multiple outputs" refers to the receiver. MIMO technology is applied to a multi-antenna transmission system. Based on the spectrum of 5G in the previous section, the high frequency bands will be adopted. Since the high frequency band can reduce the size of antenna elements, the 5G communication system allows to setup more antennas in the same space, which forms a step into massive MIMO with a very large number of steerable antenna elements [30, 31].

Digital Massive MIMO

The massive MIMO concept was proposed in the paper [32] and described in the patent [31]. The massive MIMO is defined as a special multi-user MIMO system with M antennas and K single-antenna users per BS. The system is characterized by $M \gg K$ and operates in time division duplexing (TDD) mode using linear uplink and downlink processing as Fig. 1.7.

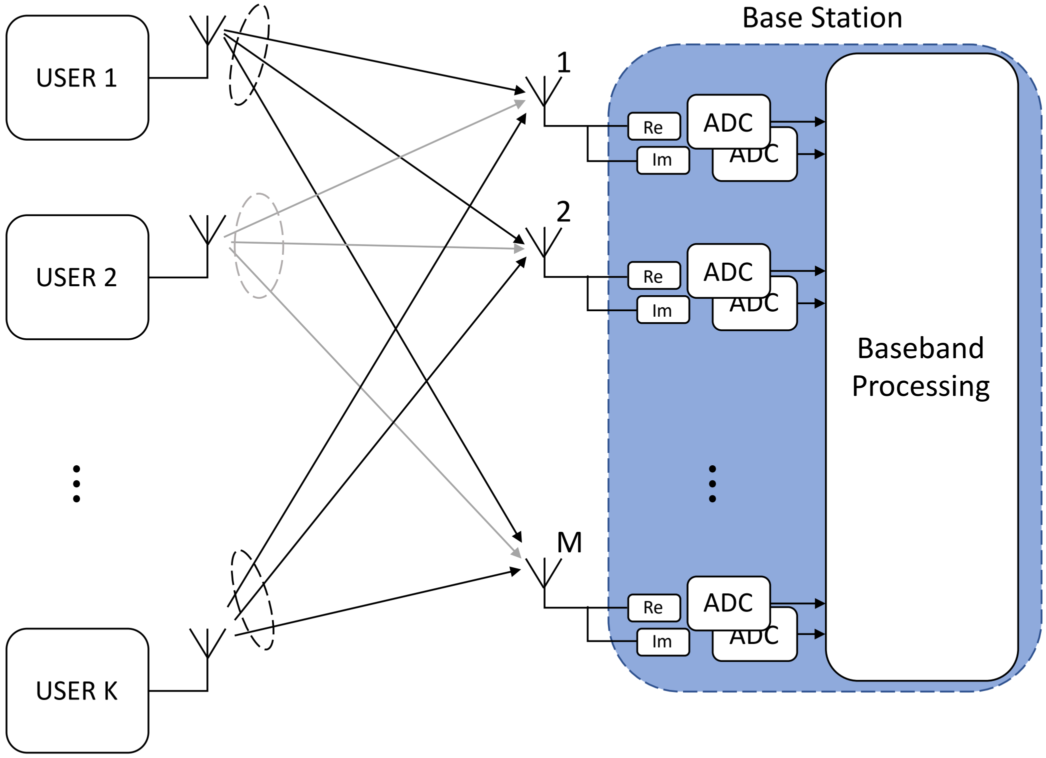

(a). Uplink System.

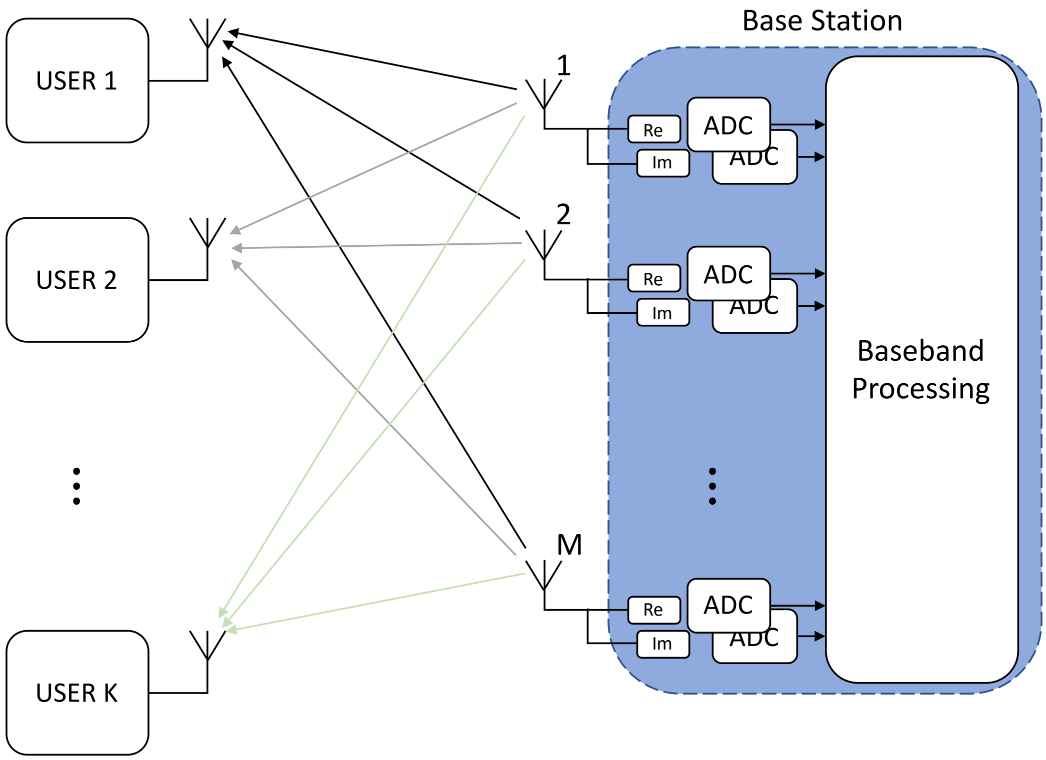

(b). Downlink System.

Figure 1.7: Massive MIMO system.

The transmission rate increment is on the way of 5G, where massive MIMO and the other proposals are believed to be the potential solutions to boost this trend. In massive MIMO, it is proved that with perfect CSI and completely eliminated pilot contamination, one can always achieve a better SNR by simply increasing the transmitter antenna number [33, 34]. Yet another side effect brought about by massive MIMO is that of cellular densification; similar to Cooper's law, the capacity increase will mostly be due to denser and denser cell deployment [35]. With more complex user technologies joining the Internet service in the 5G era, a total redesign of the network architecture will be needed, such as the proposed information centric networking (ICN) [36], software defined radio (SDR) [37], or named network functions virtualization (NFV). In addition, device-to-device (D2D) communications [38], full duplex communication mechanism [39, 40], and collaboration between different users and cells are also believed to be the indispensable elements of 5G.

In MIMO and massive MIMO systems, beamforming, as a signal processing technique that utilizes an antenna array for directional signal transmission or reception, can be used for both the transmitter and the receiver. The array antenna gain provided by beamforming can effectively improve the SNR, suppress the interference in the generalized MIMO system, and solve many technical hitches faced in the system implementation.

Digital Beamforming

In beamforming, base stations use multiple antennas in entirely different ways to increase their coverage as Fig. 1.8 shows. Here, the corresponding mobile device is far from the base station on a line of sight at a right angle to the antenna array. The signals from each antenna reach the designated mobile stations in phase so that they generate constructive interference, and the received signal power is high. On the other hand, other mobile stations are at inclined angles and receive signals from a spare antenna. These signals are destructive interference and the received signal power is low. Therefore, it creates a synthetic antenna beam with the main lobe of the beam pointing at the designated mobile phone and the null beams pointing at the other mobile phones. The beam width is narrower than that of a single antenna and the transmit power is concentrated on the specified mobile phone. The range of the base station in the direction of the designated mobile station is extended.

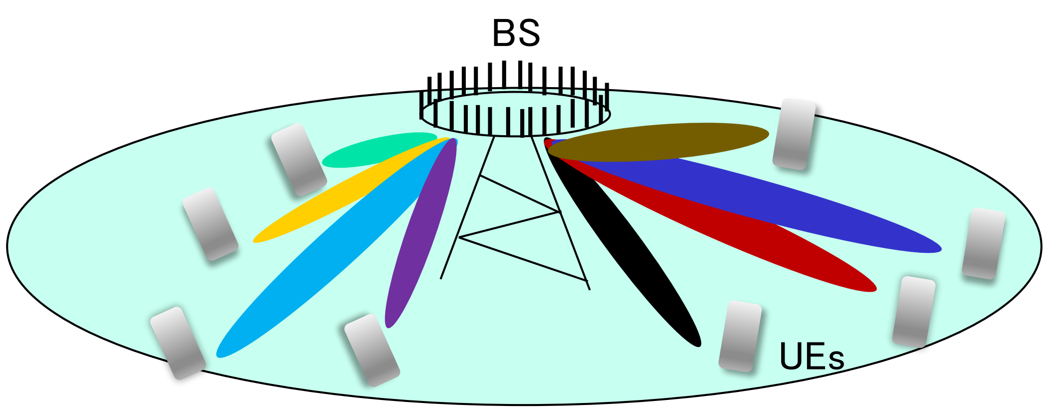

Figure 1.8: Massive MIMO with beamforming.

According to the characteristics of ITU-R 5G, the massive MIMO technology brings at least tenfold improvements in the area throughput by increasing the spectral efficiency while using the same bandwidth and density of base stations as in current networks. These extraordinary gains are achieved by equipping the base stations with arrays of a hundred antennas to enable spatial multiplexing of tens of user terminals. The reason is that multiple antenna ports can be used to provide greater data reliability by transmission diversity or to increase data rate by spatial multiplexing. Based on massive MIMO scenario, space-division multiple access (SDMA) can further be used to enhance the spectral efficiency. The principle is shown in Fig. 1.9.

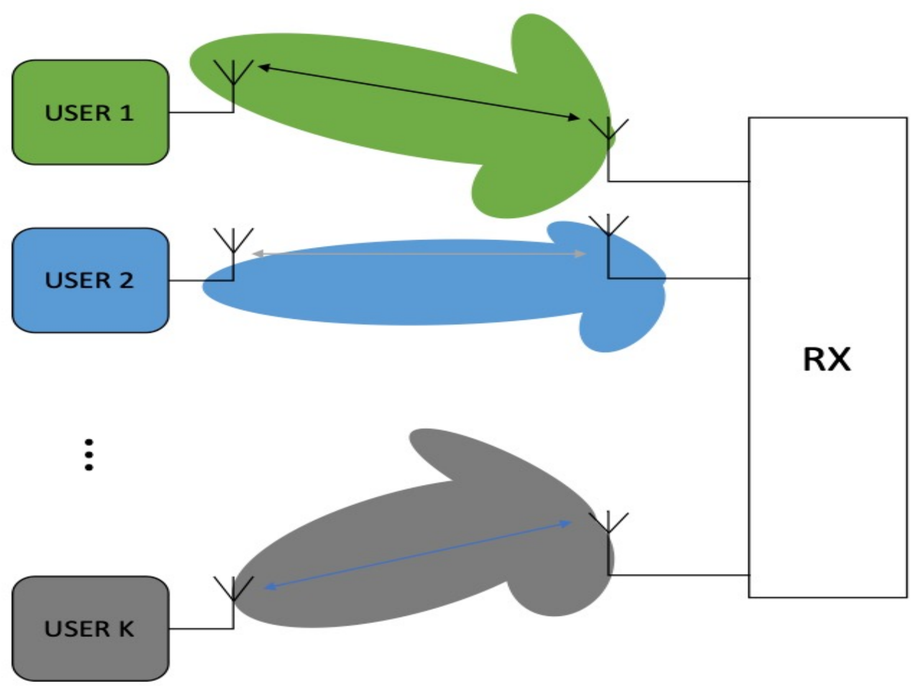

Figure 1.9: Principle of SDMA.

The system can utilize massive MIMO at a receiver to realize space separation. Through SDMA, it can reduce the IUI and then extract the expected signals.

The implementation of massive MIMO can be categorized as full digital beamforming and hybrid beamforming [41,42]. In hybrid beamforming structures, the phase shifters are typically used to determine the angle of the main lobe and its angle changing directly affects the beam width. If the beamwidth is increased, the interference between adjacent users is also increased and it degrades the system performance [43–45]. Full digital beamforming in a massive MIMO system as shown in Fig. 1.10 is considered. The transceiver requires the same number of the DACs and the ADCs as the number of transceiver antenna elements. In the configuration, full-digital massive MIMO achieves better performance based on the digital-precoding using CSI. However, implementing full-digital massive MIMO in the SHF band and EHF band demands higher cost and larger power consumption. For example, it requires lots of expensive DACs and ADCs, consumes relatively larger power due to wider signal bandwidth, and also requires a large-scale RF circuit for its high performance [46]. We use low-resolution ADCs to solve the above problems in Chapter 2 and propose new technical solutions to ensure that the throughput of the system is not affected by low-resolution ADCs.

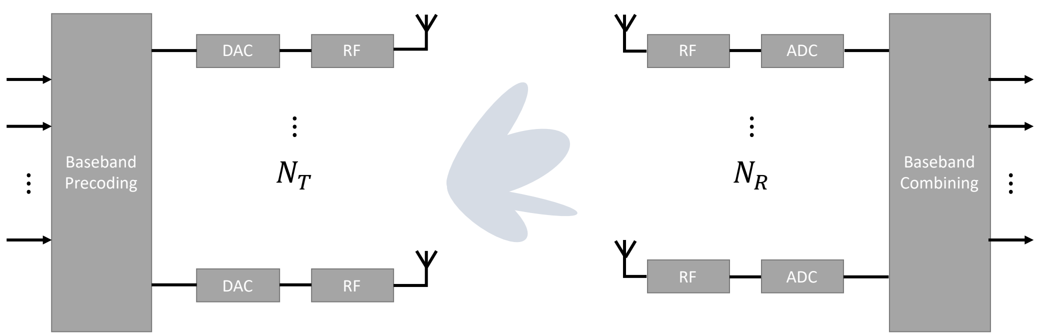

Figure 1.10: Full-digital massive MIMO.

1.3 Research Overview

In Chapter 1, the development of wireless communication is introduced at Section 1.1. At Section 1.2, the evolution of wireless communications and the features of the current 5G and the future 6G are introduced, including the use cases, frequency-band usage allocation, the trend of ADCs as well as its impact on future system performance, and the essential multiple antenna technology. Finally, based on the current research on the massive MIMO system with low-resolution ADCs and the future advanced requirements of communication systems, the author at Section 1.3 puts forward the research motivation, pushes forth related research proposals, and gives a general introduction to subsequent analysis.

1.3.1 Research Motivation

The research motivation in Figure 1.11 has gradually formed according to the following research processing of Chapters 2 and 3.

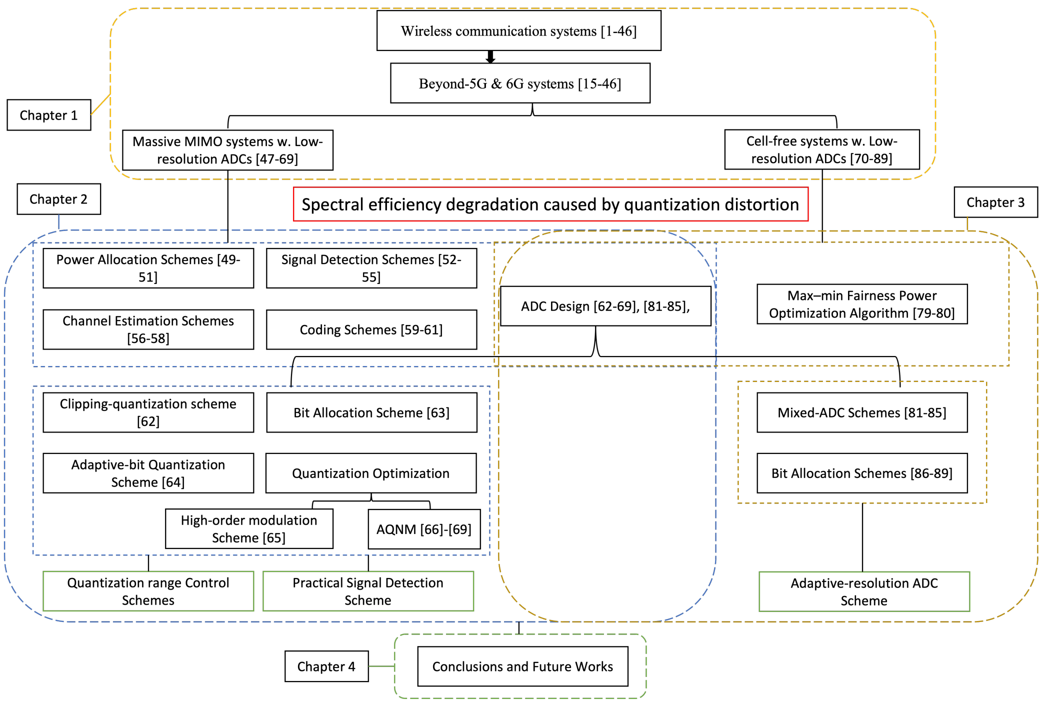

Figure 1.11: Research motivation.

Table 1.2: Research Process

	Solved	Remaining problem
Power Allocation Schemes [49-51]	Reduce the transmit power as much as possible to achieve higher overall data rates	The quantization process of the ADC is not optimized.
Signal Detection Schemes [52-55]	Reduce interference, complexity of detection algorithm	
Channel Estimation Schemes [56-58]	Make the channel response value more accuracy	
Coding Schemes [59-61]	Improve performance by processing the signal before or after the ADC by encoding	
Clipping-Quantization Scheme [62]	Find optimal work point for ADC	MIMO-OFDM is not considered.
Bit Allocation Schemes [63], [86-89]	Allocate bits for each ADC under power constraint to improve performance	Power constraint (no reduction); Hybrid digital-analog system (Interference issue).
Adaptive-Bit Quantization Scheme [64]	Allocate bits for each ADC under power constraint combined with MMSE-based VAMP	
High-Order Modulation Scheme [65] AQNM Schemes [66-69]	Increase throughput by high-Order Modulation; Quantization Analysis by AQNM	The quantization process of the ADC is not optimized.
Cell-free system [70-78]	Coverage gain, high rates, reduce in inter-cell interference	
Max–min Fairness Power Optimization Algorithm [79-80]	Guarantee the priority of the selected user and providing the same rate for the remaining users	
Mixed-ADC Schemes [81-85]	Improve SE by mixing low-bit ADCs and inf-ADCs based on power constraint or max–min Fairness	Quantization bits selection only low resolution and infinite resolution, no judging criteria for allocation ratios.
Chapter 2: Signal Detection Scheme of Massive MIMO Systems with Low-Resolution ADC	Reduce the quantization effects in massive MIMO	Shortcomings in the coverage of users, significantly the user coverage at the cell edge.
	Reduce the complexity of the proposed system	Fixed low resolution.
Chapter 3: Adaptive-Resolution ADC Scheme for Cell-Free Distributed Antenna System	Increase the coverage gain	(Future work) The scalable quantization range scheme for the received signals with different conditions, Selective fading, Optimal SE-EE tradeoff, and compared with cell-free massive MIMO.
	Increase the SE by the adaptive-resolution ADCs	
	The potential method for a tradeoff between SE and EE	

Compared with the previous research, the SE degradation occurred in massive MIMO systems with low-resolution ADCs. Lots of schemes have been proposed for improving the SE in Table 1.2, such as power allocation schemes [49-51], signal detection schemes [52-55], channel estimation schemes [56-58], and coding schemes [59-61]. The above schemes can improve the SE of systems with low-resolution ADCs. However, the low-resolution ADC does not optimize the quantization error of the received signal in these schemes.

Some previous research [62-69] also proposed schemes of ADC design for the overall ADC quantization effect of the system. However, the quantization process of the ADC is not optimized. The proposed quantization range control scheme in Chapter 2 optimizes the related quantization error of the fix-resolution ADC in massive MIMO systems. Meanwhile, a practical signal detection scheme is proposed to simplify the system's complexity. The effect of path loss on the clipping factor is not considered in the multi-user case, and the resolution of the ADC is also fixed when analyzing the impact of quantization error on the performance of the proposed massive MIMO system in Chapter 2. Moreover, although the centralized structure can effectively solve the resource consumption problem of the backhaul line, there are still many deficiencies in the user coverage, especially the user coverage at the cell edge. Since distributed antenna architectures combined with the characteristics of cell-free access [70-78] can improve coverage, distributed antenna architectures in cell-free systems are assumed in Chapter 3. The quantization range control scheme and the MRC algorithm in Chapter 2 are still used to study and analyze how the clipping factor reduces the quantization distortion effect on the received signal considering the propagation loss. Compared with the current research, the related schemes, such as max-min fairness power optimization algorithm [79-80], mixed-ADC schemes [81-85], and bit allocation schemes [86-89], are proposed to improve the SE under the power constraints. According to the received signal under different conditions, an AR-ADC scheme that different resolutions are allocated to the ADC of the AP is proposed in Chapter 3 to improve SE. Further, we provide a potential method to weigh the SE and EE of the system.

1.3.2 Overview of Chapter 2

In future beyond-5G and 6G communication systems, low-resolution ADC components are still used in massive MIMO-based communication systems to improve the EE. Due to beamwidth, hybrid beamforming is only able to provide the limited multi-wave capability while it is sub-optimal compared to digital beamforming. However, in digital beamforming, each antenna component requires a data converter and radio frequency front-end (RFFE). The digital architecture increases complexity and power consumption [47, 48]. Many previous studies used low-resolution ADCs equipped into massive MIMO systems to solve the issues of high cost and high power consumption. However, the quantization noise issue caused by low-resolution ADC components has not yet been resolved. Further, the computing complexity of anti-interference schemes is also an inevitable issue in wireless communication systems. The performance of the communication system is severely limited with the above two aspects.

Based on the current research, various schemes have been proposed to solve the problem on performance degradation by the quantization distortion in massive MIMO systems. They are the schemes of power allocation [49–51], signal detection [52–55], channel estimation [56–58], coding [59–61], and ADC design, respectively. ADC design schemes for massive MIMO scenarios include a clipping-quantization scheme that finds the optimal work points for different ADC resolutions [62] ; a bit-allocation scheme that uses a mean square quantization error (MSQE) minimization problem to allocate a suitable bit for each ADC under power constraint [63]; a adaptive-bit quantization scheme that adaptively allocates a bit for the ADCs based on the effects of imperfect channel state information [64]; and a quantization optimization scheme that increases the number of the antennas based on an AQNM to compensate the quantization distortion and uses high-order constellations based on Bussgang decomposition [65–69]. ADC designs are applied to two parts. One is the mixed resolution ADCs and the other is the quantization error degradation. The related numerical results show that the throughput of the system with low-resolution ADCs can achieve the acceptable target through various methods, such as signal detections, low order modulation, etc. However, the quantization error caused by low-resolution ADCs does not reduce. Moreover, the signal is unfortunately smaller in each received branch and the noise is relatively dominant in the large-scale antenna system. The total noise becomes a severe problem and it affects system performance. Chapter 2 introduces the features of these conventional schemes and focuses on our proposal that reduces the impacts of the quantization distortion through controlling the quantization range and reduces computational complexity through selecting the suitable signal detection schemes.

1.3.3 Overview of Chapter 3

In the full-digital massive MIMO deployment of beyond-5G and 6G, a kind of cell-free network architecture has been investiagted as a user-centric implementation to overcome the propagation loss and inter-cell interference, and to improve the QoS among users [70–78]. However, the path loss is not eliminated in the actual propagation, and it will have a certain impact on ADC quantization at a receiver. Low-resolution ADCs play a key role in the control of power consumption in multi-antenna systems. For the next generation of mobile communications pursuing higher performance, breaking through the system capacity limitation caused by worsening quantization distortion due to the path loss with low-resolution ADCs has become one of the issues of widespread concern at present.

Referring to the existing research, several schemes have been proposed to improve the throughput of systems in premise of ensuring the power consumption. For example, max-min fairness power optimization algorithm utilizes the conventional max-min fairness power control algorithm combined with ADC resolution allocations [79, 80]. In a cell-free system where each antenna is equipped with the same resolution ADC, the resolutions of ADCs are reassigned. High resolution ADCs should be assigned to APs with better channels while the sum of resolutions of ADCs remains constant. The results indicate that employing a large number of antennas can effectively mitigate the detrimental effect of low-resolution ADCs at the APs though it cannot compensate for the rate loss caused by low resolution ADCs of users. The commonly used mixed-ADC schemes [81–85] is the scheme in which the low-resolution ADCs and the infinite-resolution ADCs are dispensed on each antenna of the cell-free system according to a certain proportion. The performance results of the hybrid ADCs indicate that to a certain extent, it does not only solve the power consumption problem caused by infinite-resolution, but also solves the problem of quantization noise introduced by low resolution. Some studies [65, 67, 68] have shown that some composite technologies can also make the system performance of low-resolution ADCs close to that of perfect-resolution ADCs. Therefore, selecting a suitable ADC resolution to optimize SE-EE is still a problem. Bit allocation schemes [86–89] convert the energy distortion caused by hardware impairments into a convex function, making it a convex optimization problem under a sum of ADC bits or a power consumption constraint. In next-generation communication systems using high frequency bands, signal fading will become a worth-mentioned problem. Different received signals from multi-users should be assigned matching resolutions according to their propagation losses. Chapter 3 introduces the cell-free network architecture that can reduce the propagation loss by shortening the distance between the AP and the user, and focuses on a proposed adaptive resolution ADC scheme referring to the path loss parameters, to improve the SE.

1.3.4 Overview of Chapter 4

From research work to modern engineering processes, the high rates of encoded information in multiple signals have forced the data acquisition capabilities of base stations to evelop. A combination of modular hardware and flexible algorithms has become a trend in the wireless communication arrea. These newer modular systems adopt proper ADCs, so the importance of ADCs has been paid more attention to by more scholars. According to recent research, power consumption is one of the major system design constraints today, and low-power ADCs are closely related to their resolution. Under the premise of low power consumption, ensuring or even increasing the throughput of the system will become a major challenge. In order to better adapt to the development of next-generation wireless communication and more effectively accomplish the challenge mentioned above, we extensively refer to and learn the status of ADC application in wireless communication systems and potential quantification problems of the system, and propose our solutions .

Based on the study during the doctoral period, the advantages and scalability of the proposed ADC schemes are fully reflected in different network architectures and multiple scenarios. In Chapter 4, we summarize the relevant conclusions and their implications, and discuss future research work. Future work includes that the proposed ADC scheme still needs to be verified under the remaining real-world communication conditions; the potential advantages of the proposed schemes can be further explored; and the current proposed schemes can be improved according to new technologies in the next generation communication system.

CHAPTER 2
SIGNAL DETECTION SCHEME OF MASSIVE MIMO SYSTEMS WITH LOW-RESOLUTION ADCS

In the current 5G mobile communication system, much higher area data throughput is required to manage the global demand for the continuously growing wireless data traffic. It can achieve a multiple times larger bit rate by improving spectral efficiency (bits/s/Hz/cell) without the need for more bandwidth or additional base stations. Since a large number of the BS antennas effectively averages out noise and fading, and reduces the multi-user interference to a certain extent, massive MIMO is considered as a key technology. Full-digital massive MIMO deployment is difficult to realize because high-resolution ADCs produce primary power consumption. Owing to its favorable property of low cost and low power consumption, low-resolution ADCs ($1 \sim 4$ bits) have also been worth paying attention. Reference [62] proves that an appropriate clipping factor can be found for the optimal work point of a low-resolution ADC in a single-input single-output OFDM system. In [67], the performance of single-carrier modulation in a massive MIMO system with low-resolution ADCs is analyzed while OFDM is assumed. In [90], it is shown that a MMSE algorithm can achieve better bit error rate (BER) using low-resolution ADCs in a hybrid analog-digital system with a large number of BS antennas. MMSE detection demands a large amount of computational complexity for matrix inversion while it achieves near-optimal performance. A MRC detection can also be applied at the receiver of full-digital massive MIMO to achieve the maximum receive signal-to-interference-plus-noise ratio (SINR) [91]. Residual multi-user interference (MUI) caused by low-resolution ADCs limits the system throughput even though MMSE is applied. On the other hand, thermal noise is dominant in a receiver with large-scale antennas. In this Chapter, the achievable uplink rates of MRC and MMSE with the clipping factor are evaluated and compared joint quantization noise and interference effects. In this scenario, MRC achieves comparable throughput performance as that of MMSE. Thus, MRC is more suitable owing to its lower complexity.

The research in Chapter 2 discusses centralized antenna structures in massive MIMO systems. The quantization range control scheme is used to reduce quantization noise in massive MIMO systems with low-resolution ADCs and simplify the system complexity under the constraints of base station receive antennas and clipping factors. In Chapter 2, The effect of different pathloss values on the clipping factor is not included as all the antenna elements are implemented in a base station. The resolution of the ADC is also fixed when analyzing the impact of quantization error on the performance of the proposed massive MIMO system.

2.1 Massive MIMO Systems with Low-resolution ADCs based on Clipping Factor

2.1.1 Uplink System Model of Massive MIMO

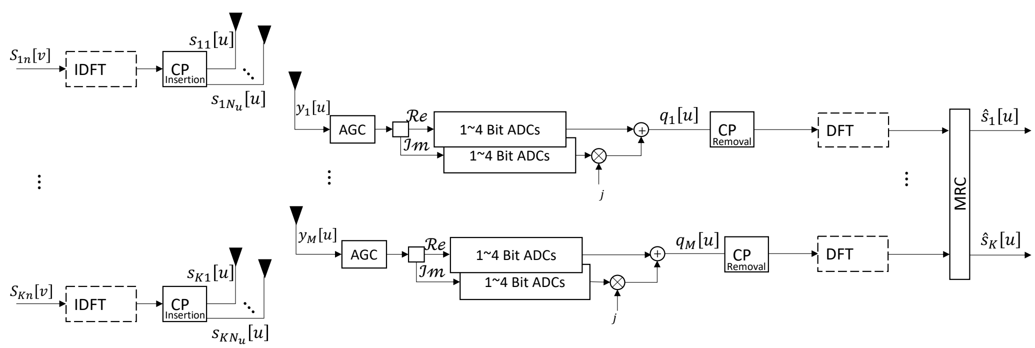

Figure 2.1: Uplink system of massive MIMO with low-resolution ADCs.

The single-cell uplink system shown in Fig. 2.1 is assumed. We consider a full-digital massive MIMO uplink with low-resolution ADCs. There are K users with N_u antennas and one BS equipped with an array of M antennas. Suppose that the size of an inverse discrete Fourier transform (IDFT) is N_{dft} the signal from the nth antenna of the kth user in the uplink is,

$$s_{kn}[u] = \frac{1}{\sqrt{N_{dft}}} \sum_{v=-N_{cp}}^{N_{dft}-1} S_{kn}[v] e^{\frac{j2\pi uv}{N_{dft}}}, \tag{2.1}$$

where $S_{kn}[v]$ is the transmit signal from the nth antenna of user k on the vth subcarrier, N_{cp} is the length of a cyclic prefix, and $s_{kn}[u]$ is the transmit signal at the uth time index. The received signal of the mth antenna of the BS is given as,

$$y_m[u] = \sum_{k=1}^{K} \sum_{n=1}^{N_u} \left(\sqrt{P_k} h_{mkn} s_{kn[u]} \right) + z_m[u], \tag{2.2}$$

where power of $s_{kn}[u]$ is $\mathbb{E}[|\sqrt{P_k} s_{kn}[u]|^2] = 1$, P_k is the transmit power of the kth user, h_{mkn} is the channel response between the nth antenna of the kth user and the mth antenna of the BS, and $z_m[u] \sim \mathcal{N}_{\mathbb{C}}(0, \sigma_n^2)$ is the thermal noise.

With the assumption of identical low-resolution ADCs, the in-phase and quadrature components of the received signal of the mth antenna is quantized by the ADC of $R-$bit resolution as follows,

$$q_m^C[u] = Q^C\left(\Re\left(y_m[u]\right)\right) + jQ^C\left(\Im\left(y_m[u]\right)\right), \tag{2.3}$$

where $Q(\cdot)$ represents quantization, $\Re(\cdot)$ and $\Im(\cdot)$ denote the real and imaginary part, respectively. The quantization through the ADCs worsens the accuracy of channel estimation and deteriorates the system performance.

The quantization noise is given as,

$$e_m^C[u] = q_m^C[u] - y_m[u]. \tag{2.4}$$

The receiver removes the cyclic prefix and put into a discrete Fourier transform (DFT) block. The signal on the vth subcarrier is then given as,

$$Y_m[v] = \sum_{k=1}^{K} \sum_{n=1}^{N_u} \sqrt{P_k} H_{mkn} S_{kn}[v] + (Z_m[v] + E_m[v]) , \tag{2.5}$$

where,

$$H_{mkn} = h_{mkn} e^{\frac{-j2\pi uv}{N_{dft}}} , \tag{2.6}$$

$$S_{kn}[v] = \frac{1}{\sqrt{N_{dft}}} \sum_{u=0}^{N_{dft}-1} s_{kn}[u] e^{\frac{-j2\pi uv}{N_{dft}}} , \tag{2.7}$$

$$Z_m[v] = \frac{1}{\sqrt{N_{dft}}} \sum_{u=0}^{N_{dft}-1} z_m[u] e^{\frac{-j2\pi uv}{N_{dft}}} , \tag{2.8}$$

and the quantization error is expressed as,

$$E_m^C[v] = \frac{1}{\sqrt{N_{dft}}} \sum_{u=0}^{N_{dft}-1} e_m^C[u] e^{\frac{-j2\pi uv}{N_{dft}}} . \tag{2.9}$$

2.1.2 Channel Estimation

Least-square (LS) estimation is employed for channel estimation as follows [92–94]. Suppose that data symbols are transmitted from the (λ)th to the $(\lambda + N_{sc} - 1)$th subcarrier, where N_{sc} is the number of active subcarriers, and a channel response is estimated for each subcarrier. As it is described in Fig. 2.2, the transmit active subcarriers are divided as $B = \left(\frac{N_{sc}}{V}\right)$ blocks in frequency domain, where V is the number of subcarriers in one block. $N_{sym} = \frac{L}{V}$ OFDM symbols are required when the uplink pilots for L streams are inserted at each V subcarriers to estimate channel responses.

The channel in the bth block is estimated during a channel estimation period. The subcarrier index $\{v\}$ in the bth block is from $(b-1)V+\lambda$ to bV. The estimated channel for the bth block is,

$$\hat{H}^{b}_{mkn} = \frac{1}{V} \sum_{v=(b-1)V+\lambda}^{bV-1+\lambda} \left(S_{kn}[v]\right)^{-1} Y_m[v], \tag{2.10}$$

where $S_{kn}[v]$ and $Y_m[v]$ are the orthogonal sequence and the received signals on the vth subcarrier, respectively.

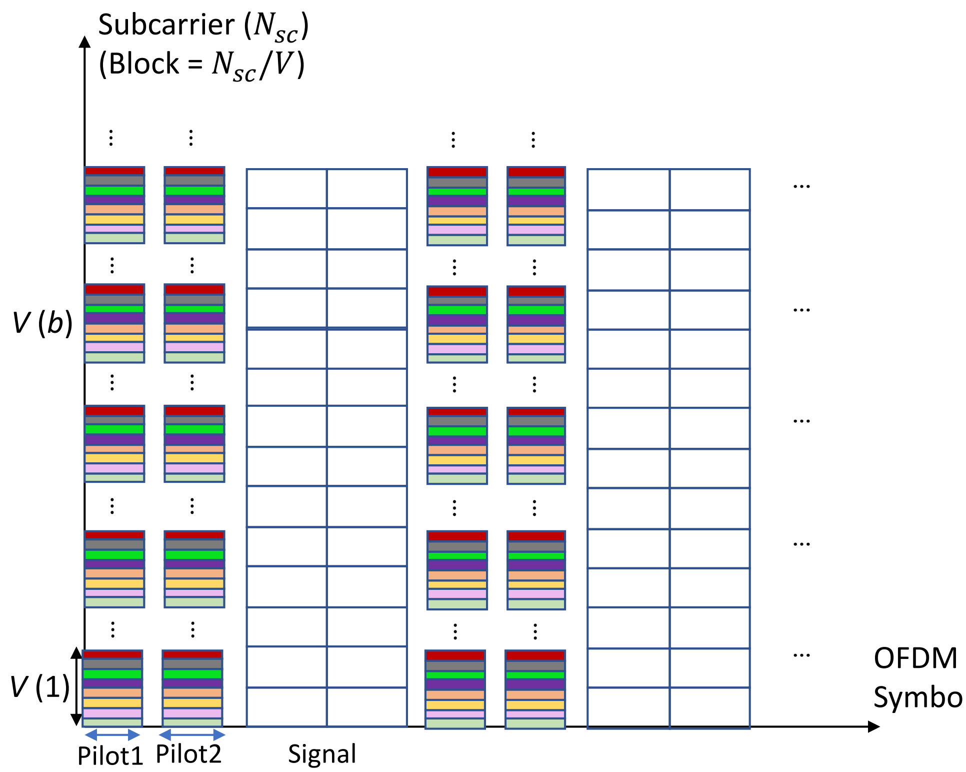

Figure 2.2: Structure of uplink frame.

2.1.3 Scalable Clipping Factor of ADC

To an ADC [95] in a SISO system, a quantization range of a receoved signal is limited in $[-A, A]$, which is shown in Fig. 2.3,

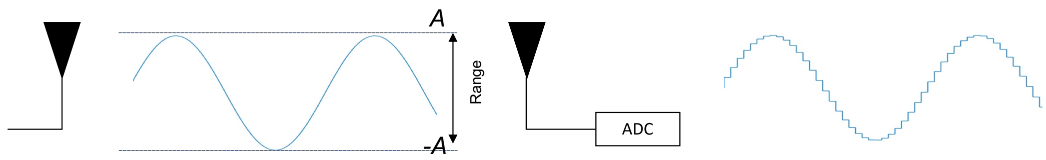

Figure 2.3: Quantization range of an ADC.

Due to the limited range, the quantization distortion can be accurately affected by the thermal noise in the received signal, especially for the existing massive MIMO system, it can be worse. According to the inspiration of reference [62], there can be a suitable clipping factor to achieve the optimal ADC work point. Therefore, we consider a scalable clipping factor to minimize the impact of quantization errors on the massive MIMO system.

The quantization range can be given as,

$$A = C\mathbb{E}\left(|y_m[u]|\right), \tag{2.11}$$

where C is a clipping factor and $|y_m[u]|$ is derived through the output of the power detector equipped in each antenna of the BS. In the massive MIMO-OFDM system, AGC works with symbol duration, and after passing by a fading channel, the range of each OFDM symbol is changed by a clipping factor. Therein, $\mathbb{E}\left(|y_m[u]|\right)$ includes the fading.

The quantization step-size δ is defined as,

$$\delta = \frac{2A}{L_q}, \tag{2.12}$$

which becomes smaller to ensure finer quantization as the number of quantization bits $R = \log_2(L_q)$ increases. Therein, L_q is the quantization level.

The averaging period (the observation time) in Eq. (2.11) for each scalable clipping is one OFDM symbol time (the period is T_s). For example, during one T_s, the range of the received OFDM signal waveform is changed by a clipping factor based on Eq.

(2.11). However, the desired signal waveforms received by massive MIMO branches have correlation and each antenna branch works as a sampling point. This spatial sampling improves the SNR after the MRC combining.

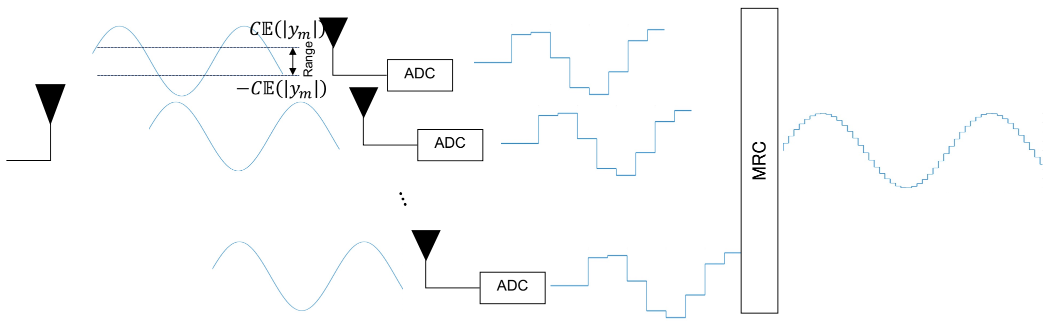

Figure 2.4: Scalable quantization range of an ADC for massive MIMO

The quantization range is adjusted via the clipping factor C. The quantization converts the real input signal to a real-valued output, r_i, for $i = 1, 2, \ldots, 2^R$. The ith output value after ADCs is defined as,

$$q_i = \left(-\frac{2^R}{2} - \frac{1}{2} + i\right)\delta. \tag{2.13}$$

Thus, its value is adjusted for suppressing the extra noise and overcoming the effects of the quantization noise through increasing the quantization accuracy of ADC. The detailed explanation of the principle of noise elimination effect based on the scalable clipping factor is shown in Fig. 2.5.

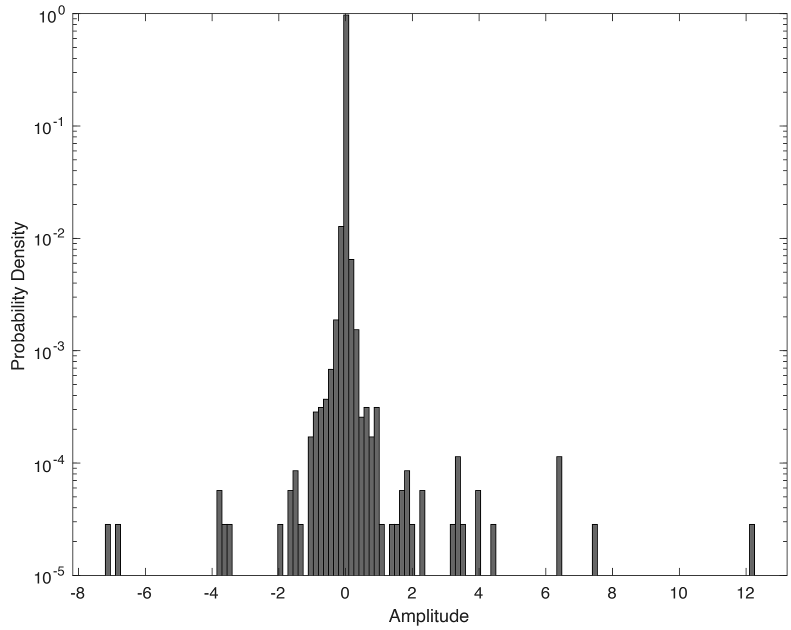

(a). Received Signal.

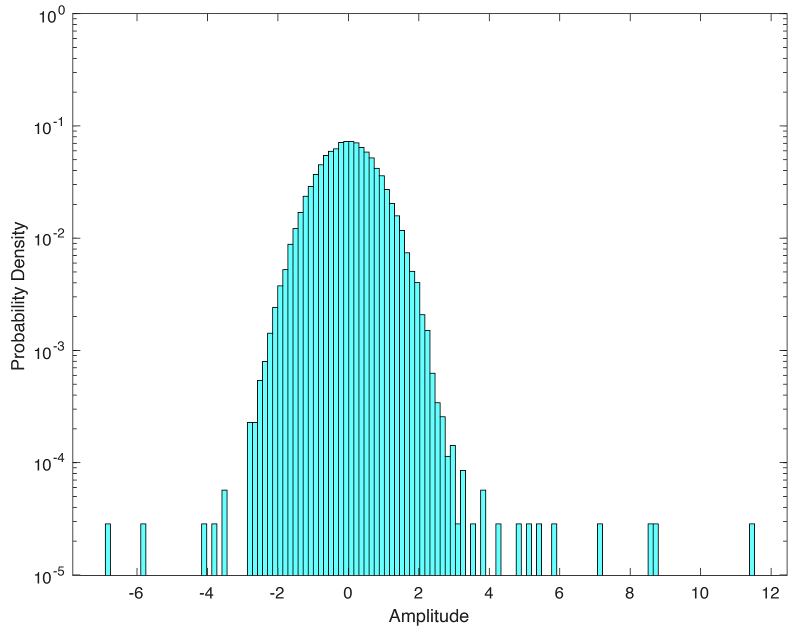

(b). Received Signal with Noise.

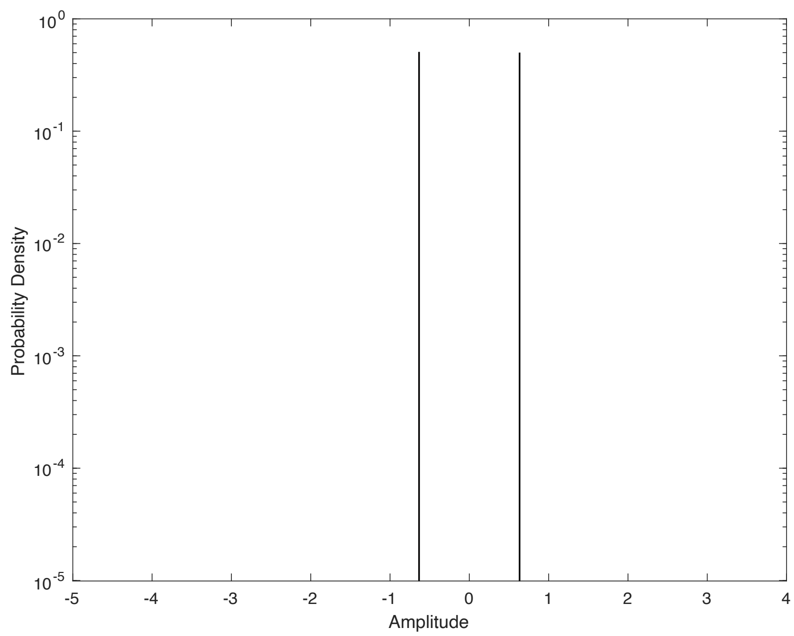

(c). 1−bit ADC Output.

Figure 2.5: Effect of 1−bit ADC (C = 1) under SNR/stream =10dB.

The probability density functions (PDFs) of the real part of the received signal in a time domain are presented in Figs. 2.5(a), 2.5(b), and 2.5(c) to observe the effect of the scalable factor C on the amplitude distribution of the signal during quantization. The amplitude in these figures is normalized by the absolute value of the average amplitude of the received signal with the noise.

From the figures, it is clear that the amplitude in Fig. 2.5(b) includes much more noise as compared with the that of the original signal shown in Fig. 2.5(a). When C is 1, the quantization range is reduced to make the quantized amplitude in Fig. 2.5(c) within the original amplitude distribution range. Thereby the performance of low-resolution ADCs is less affected by the noise.

2.1.4 Uplink Performance of Massive MIMO with Scalable Clipping factor

In the uplink, an ergodic rate per arbitrary user k is,

$$\mathcal{R}_k = \sum_{n=1}^{N} \frac{1}{BV} \sum_{b=1}^{B} \sum_{v=((b-1)V+\lambda}^{bV-1+\lambda} \log_2\left(1 + SINR_{kn}^{v}\right), \tag{2.14}$$

where

$$SINR_{kn}^{v} = \frac{|\mathbb{E}\left\{\mathbf{W}_{kn}^{b}\mathbf{H}_{kn}[v]\right\}|^2}{\sum_{n=1}^{N} \sum_{\substack{i=1\\ i\neq k}}^{K} \mathbb{E}\left\{|\mathbf{W}_{kn}^{b}\mathbf{H}_{in}[v]|^2\right\} + \sum_{\substack{j=1\\ j\neq n}}^{N} |\mathbb{E}\left\{\mathbf{W}_{kn}^{b}\mathbf{H}_{kj}[v]\right\}|^2 + \sigma'}, \tag{2.15}$$

$$\sigma' = \mathbb{E}\left\{\|\mathbf{W}_{kn}^{b}\|^2\right\}\sigma^2 + |\mathbb{E}\left\{\mathbf{W}_{kn}^{b}\mathbf{E}_{m}^{C}[v]\right\}|^2, \tag{2.16}$$

and $\mathbf{W}_{kn}^{b}$ is the MRC coefficient in the vector form, which is given as,

$$\mathbf{W}_{kn}^{b} = \left(\hat{\mathbf{H}}_{kn}^{b}\right)^{\mathrm{H}} = \left(\begin{bmatrix} \hat{\mathrm{H}}_{1kn}^{b} \\ \vdots \\ \hat{\mathrm{H}}_{Mkn}^{b} \end{bmatrix}\right)^{\mathrm{H}}, \tag{2.17}$$

where $\hat{\mathbf{H}}^b_{kn}$ is the channel estimation response of the nth antenna of the kth user, $\mathbf{H}_{ij}[v]$ is the channel responses between the jth antenna of the ith user and the base station antennas in the vector form,

$$\mathbf{H}_{ij}[v] = \begin{bmatrix} \mathrm{H}_{1ij}[v] \\ \vdots \\ \mathrm{H}_{Mij}[v] \end{bmatrix}, \tag{2.18}$$

and $\mathbf{E}^C_m[v]$ is the quantization noise vector is,

$$\mathbf{E}^C[v] = \begin{bmatrix} \mathbf{E}^C_1[v] \\ \vdots \\ \mathbf{E}^C_M[v] \end{bmatrix}. \tag{2.19}$$

Finally, σ' is the sum of the variance of the thermal noise and the quantization noise.

2.1.5 Numerical Results

Simulation Conditions

Computer simulation conditions are presented in Table 2.1. The massive MIMO BS transmits signals with $M = 128$ antenna elements unless it is specified. In a multi-user (MU) transmission, there are eight users that communicate with the BS simultaneously and each user transmits two streams with $N_u = 2$ antennas. The antenna spacing is $0.5\lambda_w$ at the BS and $1.0\lambda_w$ at each user, where λ_w is the wavelength. The number of active subcarriers is 1200 while the DFT size is 2048. The number of blocks is 150 and the number of subcarriers per block is eight. Since the number of symbols for channel estimation is two, the number of signal streams whose channel responses can be estimated with orthogonal sequences is 16. As the orthogonal sequences, Zadoff-Chu sequences with the length of 16 are applied. As a channel mode, independent and identically distributed (i.i.d.) Rayleigh fading are assumed. The resolution of ADCs is selected from one, two, three, four, or infinite bits. The infinite-resolution ADC includes two situations, one is that the quantization range is also infinite; another is that the quantization range is limited. System throughput is the total rate of eight users. The number of trials for each plot is 10000.

Table 2.1: Simulation Conditions.

Number of Antennas of the BS (M)	128
Number of UEs (K)	8
Number of Antennas of each UE (N_u)	2
Antenna spacing at the BS	$0.5\lambda_w$
Antenna spacing at each UE	$1.0\lambda_w$
Number of active subcarriers (N_{sc})	1200
DFT size	2048
Number of blocks for channel estimation	150
Number of subcarriers per block	8
Number of symbols for channel estimation	2
Pilot sequence	Zadoff-Chu sequence
Channel model	i.i.d. Rayleigh fading
ADC resolution	$1- \sim 4-$bit
Number of trials	10000 channel response/plot

Quantization Error Analysis

The MSDE is defined here as the average amount of the quantization error and the noise, which is normalized by the power of the noise and is given as,

$$MSDE = \frac{1}{M} \sum_{m=1}^{M} \frac{\mathbb{E}\left\{|y_m[u] - q_m^C[u]|^2\right\}}{\sigma^2}, \tag{2.20}$$

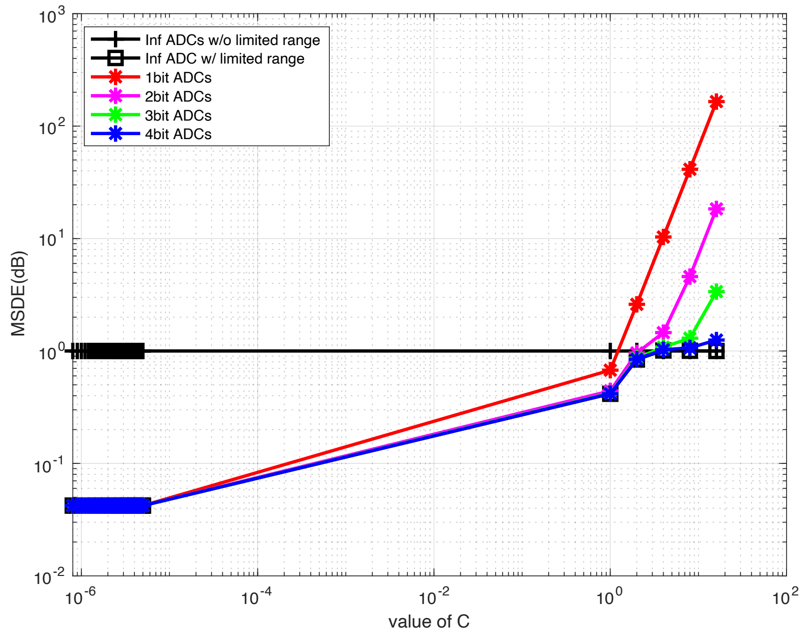

(a). Case: SNR/stream is 10dB.

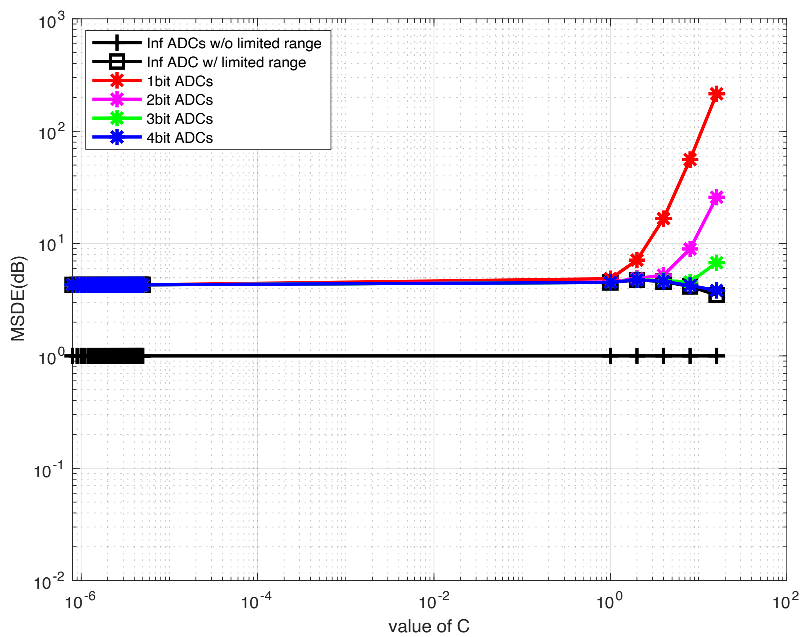

(b). Case: SNR/stream is 30dB.

Figure 2.6: MSDE versus scalable clipping factor C.

The MSDEs versus the quantization range for SNRs of 10dB and 30dB are shown in

Figs. 2.6(a) and 2.6(b). The SNR is defined as the signal-to-noise ratio per stream. The MSDE is normalized by the noise power.

Taking the conclusion shown in Fig. 2.6 as an example, Fig. 2.6(a) shows that when the SNR for each stream is 10dB, which means each receive antenna stays in a low-SNR environment and the noise dominates the received signal at each branch, the MSDEs in low-resolution ADCs are smaller than that in nonscalable situation as C is less than 1. The noise clipping happens even with infinite-resolution ADC and the range limit produces the smaller MSDE. The MSDEs with $1-$, $2-$, $3-$, and $4-$bit ADCs can also achieve their smallest values, respectively, at the different values of C. In addition, larger MSE happens for the infinite-resolution ADC with range limit due to over-clipping, which means a part of signal amplitude is clipped by the clipping factor.

Detection Performance Analysis

The BS receives the $N \times K$ uplink pilot signals from users. Thereby, 16 symbols (eight subcarriers $\times$ two symbol slots) are assigned for channel estimation in the uplink system. The MSE of channel estimation with the thermal noise and the quantization error per each branch is adopted as the performance metric, which is normalized by the power of the received signal and is defined as,

$$MSE = \frac{1}{M} \sum_{m=1}^{M} \frac{1}{B} \sum_{b=1}^{B} \frac{\mathbb{E}\left\{ \|\mathbf{H}_m^b - \hat{\mathbf{H}}_m^b\|^2 \right\}}{\mathbb{E}\left\{ \|\mathbf{H}_m^b\|^2 \right\}}, \tag{2.21}$$

where

$$\mathbf{H}_m^b = \left[\frac{1}{V} \sum_{v=(b-1)V+\lambda}^{bV-1+\lambda} H_{m11}[v], \ldots, \frac{1}{V} \sum_{v=(b-1)V+\lambda}^{bV-1+\lambda} H_{mKN_u}[v] \right]^T \tag{2.22}$$

and

$$\hat{\mathbf{H}}_m^b = \left[\hat{H}_{m11}^b, \ldots, \hat{H}_{mKN_u}^b \right]^T. \tag{2.23}$$

The relationship between the MSE with the low-resolution ADCs and the quantization range is shown in Fig. 2.7. After the channel estimation, when the SNR is low, by taking the clipping factor C less than or equal to 1, the performance of the low-resolution ADCs is better than that of the infinite-resolution ADCs with range limit. When the SNR is high, there is the appropriate value of C to realize the optimal performance. For the 1−bit ADC, when C is equal to 1.0, the BS achieves the best MSE; for the other low-resolution ADCs, $C = 2.0$ is the best.

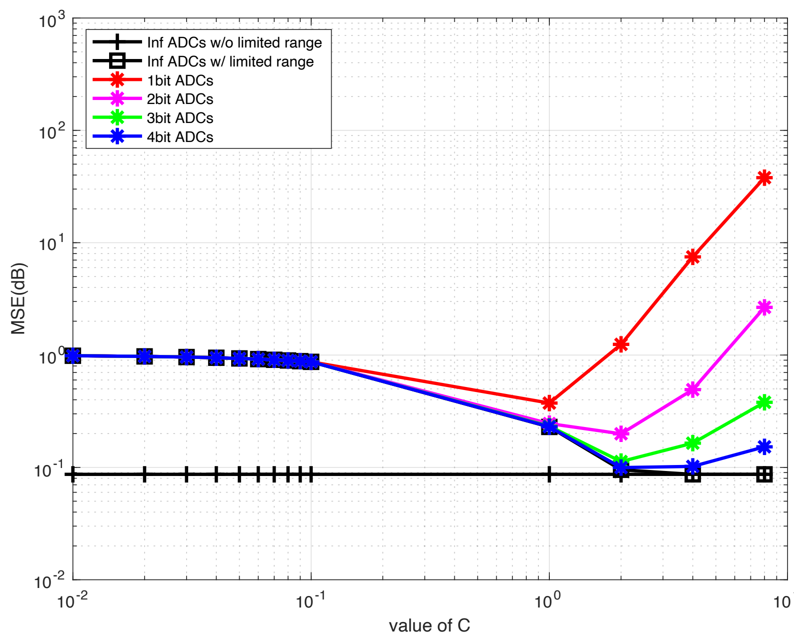

(a). Case: SNR/stream is 20dB.

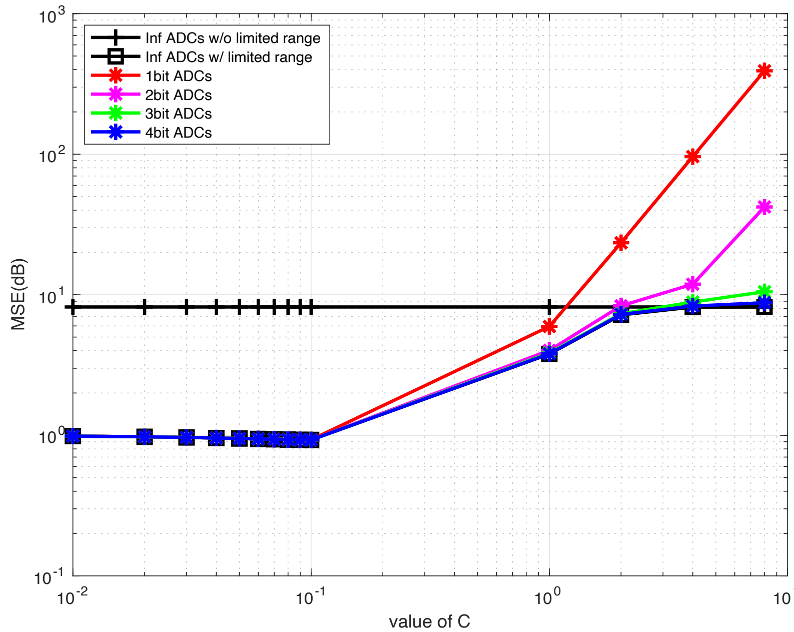

(b). Case: SNR/steam is 0dB.

Figure 2.7: MSE versus scalable clipping factor C.

From the figures, when the SNR is 20dB, the amplitude of the signal is clipped too much as compared with the amplitude of the original signal if the clipping factor C is too small. Although the distortion is smaller in average, the over-clipping of the original signal deteriorates the channel estimation accuracy.

Through this comparison between the infinite-resolution ADCs and the range-limited any-resolution ADC, the range limit of the ADC plays a key role for performance improvement. The noise elimination by range limit realizes the equivalent throughput of the system with low-resolution ADCs as that with the infinite-resolution ADCs.

Throughput of Uplink System

The system throughputs of the uplink with MRC versus SNR for $C = 1$ and 2 are shown in Figs. 2.8(a) and 2.8(b), respectively. The number of users is eight. MRC means infinite range and infinite resolution in the ADCs and MRC with infinite ADCs implies range limit in the infinite-resolution ADCs.

In Fig. 2.8(a), C is set as 1 for more clipping. When the SNR per stream is lower than 15dB, low-resolution ADCs can realize better performance than the infinite-resolution ADCs without range limit and they can keep appropriate throughputs in the large SNR. In Fig. 2.8(b), when C is enlarged, $2- \sim 4-$bit ADCs can achieve the near-optimal throughputs relative to that with the infinite-resolution ADCs. Meanwhile, it is confirmed here that the low-resolution ADCs can be adopted in a full-digital massive MIMO system as the system throughput degradation with $2-$bit ADCs is limited when $C = 1$ or 2.

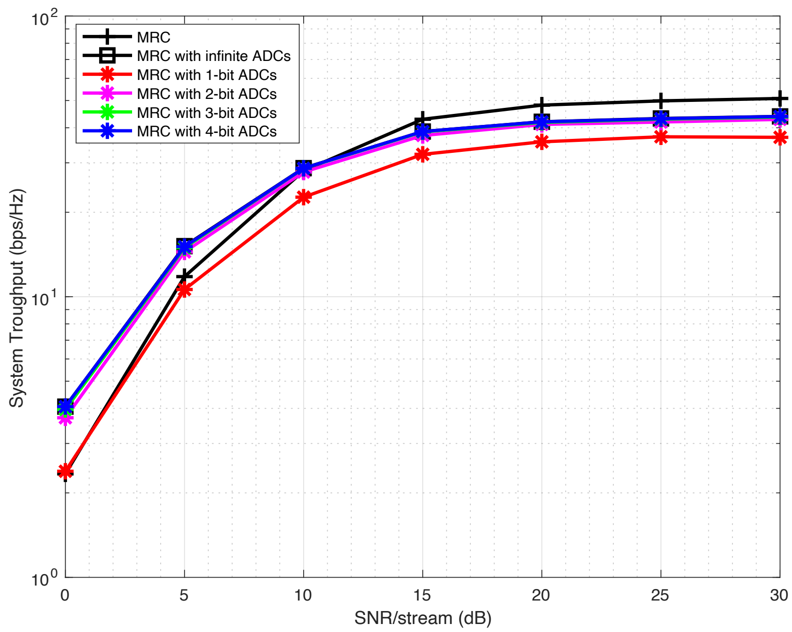

(a). Case: $C = 1$.

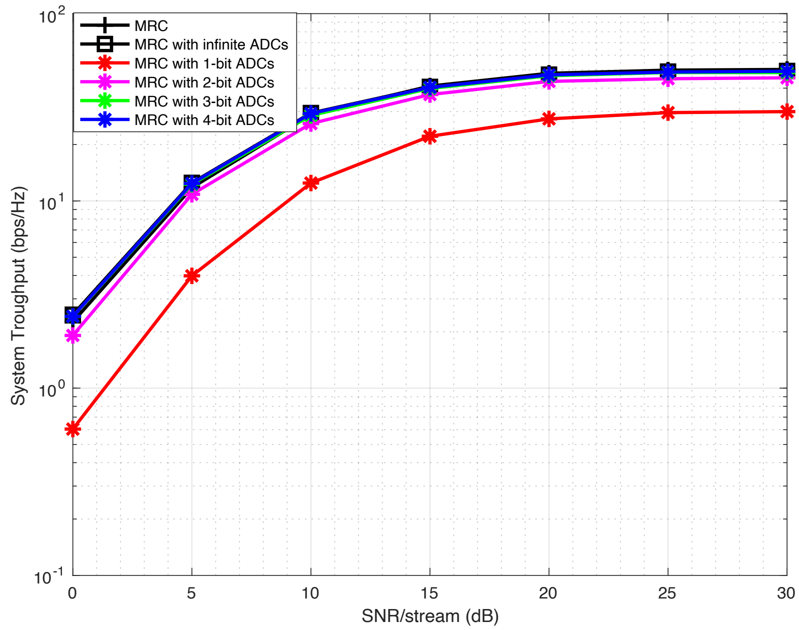

(b). Case: $C = 2$.

Figure 2.8: Throughput of uplink with MRC scheme.

Number of Antennas Effects

The system throughputs versus the number of antennas are presented in Figs. 2.9(a) and 2.9(b). The number of users is eight. As shown in these figures that the system throughput improves when the number of antennas increases. According to our previous analysis, setting as C=1 can make the achievable rate of low-resolution ADCs exceeds that of infinite-resolution ADCs without range limit no matter how many receive antennas are equipped as the system stays in a low SNR environment.

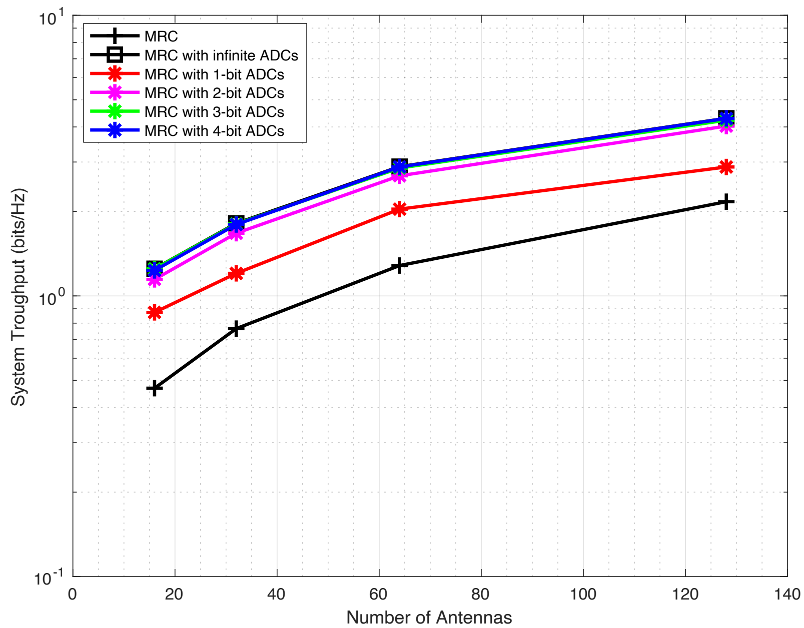

(a). Case: SNR/stream is 0dB and $C = 1$.

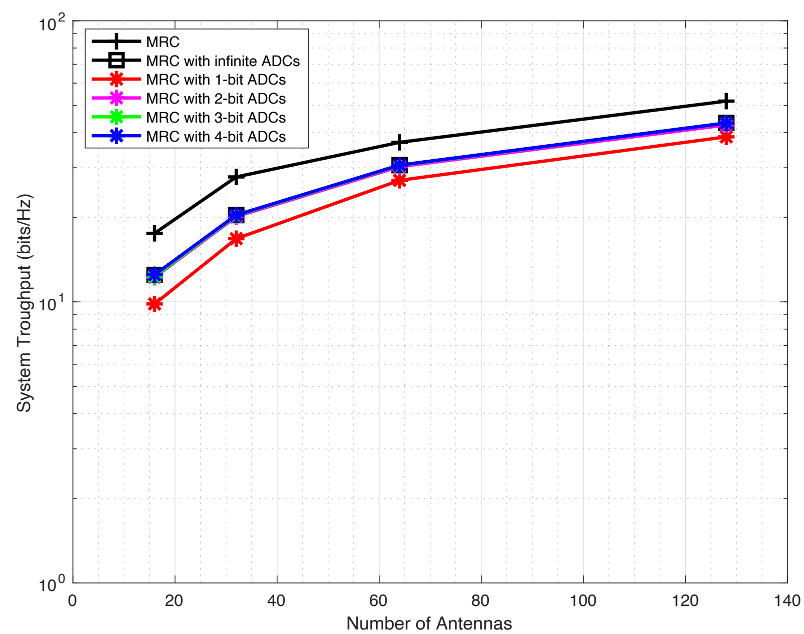

(b). Case: SNR/stream is 30dB and $C = 2$.

Figure 2.9: Performance of uplink vs. no. of antennas.

Number of UEs Effects

The system throughput versus the number of users is shown in Figs. 2.10(a) and 2.10(b). The number of antennas is 128. The SNR is 0dB or 30dB and the clipping factor is $C = 1$. When the number of users increases, the system throughput can be improved as well. Moreover, the throughput of the low-resolution ADCs can be equivalent to that of the range-limited infinite-resolution case even if the SNR is 30dB. Thus, it is also confirmed that the low-resolution ADCs can be adopted in a full-digital massive MIMO system.

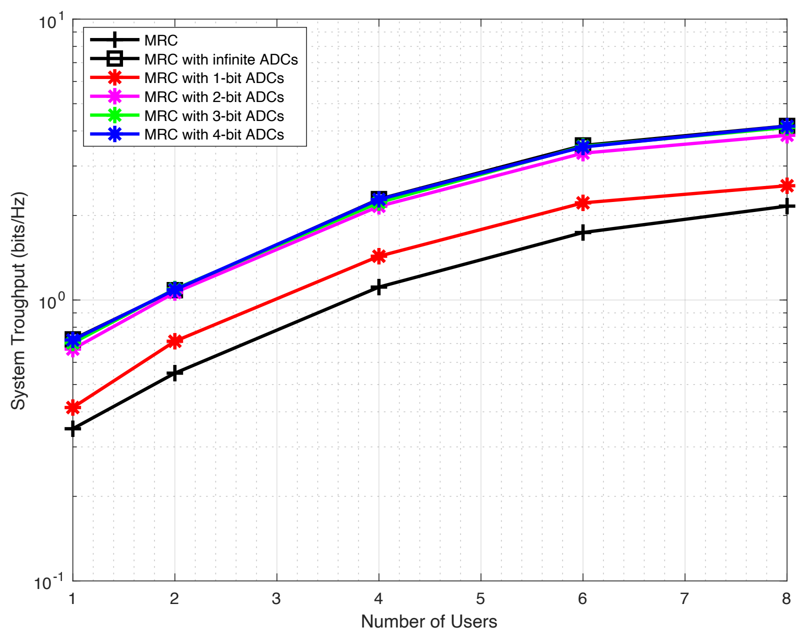

(a). Case: SNR/stream is 0dB and $C = 1$.

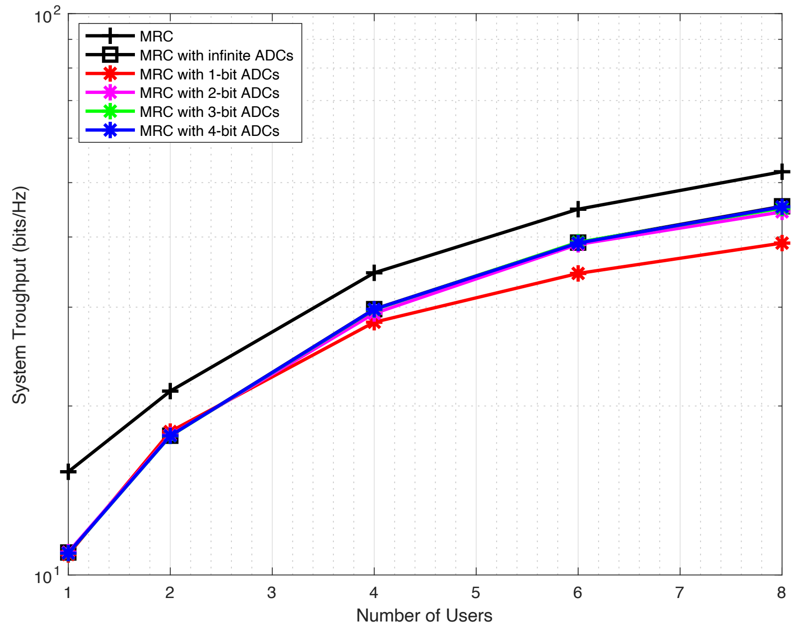

(b). Case: SNR/stream is 30dB and $C = 2$.

Figure 2.10: Performance of uplink vs. no. of UEs.

The system throughput versus the number of users is shown in Figs. 2.10(a) and 2.10(b). The number of antennas is 128. The SNR is 0dB or 30dB and the clipping factor is $C = 1$. When the number of users increases, the system throughput can be improved as well. Moreover, the throughput of the low-resolution ADCs can be equivalent to that of the range-limited infinite-resolution case even if the SNR is 30dB. Thus, it is also confirmed that the low-resolution ADCs can be adopted in a full-digital massive MIMO system.

Low-resolution ADCs are still a good choice to apply in a massive MIMO system and our proposal is for fulfilling to make up the weakness of this case on the throughput of the system. In this paper, we have investigated the novel ADC design scheme. Observed from the ratio of the improvement, a smaller clipping factor, C, can make greater gains in the system throughput under a low SNR environment. Meanwhile, the achievable rate of the 1−bit ADC exceeds that of infinite-resolution ADC without a range limit. Even though the SNR is larger, the system throughput degradation with low-resolution ADCs is limited with our ADC design. In the premise of low power consumption, the system performance breaks through the original limits. From numerical results obtained through computer simulation, the low-resolution ADC becomes a better option to improve the performance of the Massive MIMO system.

2.2 Detection-selection scheme in Massive MIMO systems with Clipping Factor

The primary purpose of the signal detection schemes is to more accurately recover the transmitted signal from the received signal after the channel estimation at the receiver. Among the detection schemes, the error detection performance of the MAP algorithm is optimal. When the transmitter transmits signals using the equal probability, the maximum a posteriori (MAP) algorithm is equivalent to the maximum likelihood (ML) algorithm, which is also further equivalent to searching for the point where the Euclidean distance between all transmitted signals and the received signal is the smallest. If the receiver antennas are fully used for spatial multiplexing, it will result in an exponentially increasing relationship between the complexity of the MAP (ML) and the number of transmit antennas and the constellation orders. Therefore, in the scene of large-scale antennas, the linear detection algorithms have been widely used. For example, MMSE converts a MIMO channel into multiple parallel, uncorrelated channels for eliminating mutual interference.

2.2.1 Uplink Performance based on MMSE/MRC

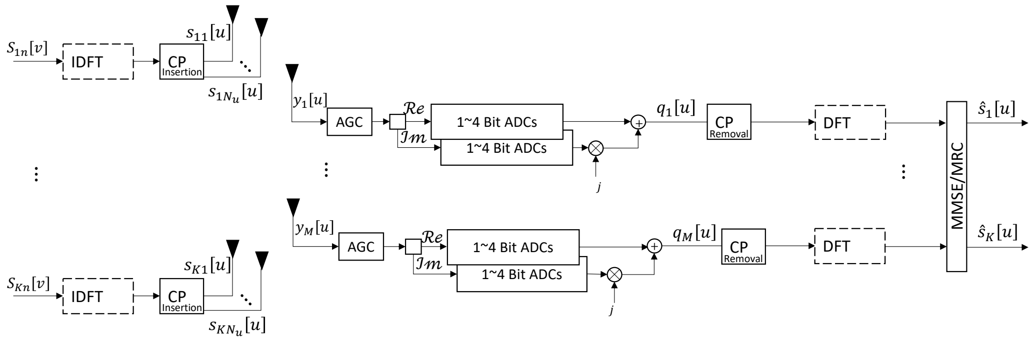

Figure 2.11: MRC/MMSE detection schemes in the massive MIMO with low-resolution ADCs.

In this comparison of signal detection schemes, we analyze the performance based on the MMSE algorithm or the MRC algorithm of the proposed system in Sect. 2.1. And leveraging on the equations (2.15), (2.16) and (2.17), the throughput of the system with MMSE can be obtained. Therein, the coefficient $\mathcal{W}_{kn}^{b}$ of the MMSE algorithm is given as,

$$\mathcal{W}_{kn}^{b} = \left(\left(\hat{\mathbf{H}}^{b}\right)^{\mathrm{H}}\left(\hat{\mathbf{H}}^{b}\right) + \sigma'^{2}\mathbf{I}\right)^{-1}\left(\hat{H}_{kn}^{b}\right)^{\mathrm{H}}. \tag{2.24}$$

Here, it is assumed that channel responses,

$$\hat{\mathbf{H}}^{b} = [\hat{H}_{111}^{b}, \ \ldots, \ \hat{H}_{MKN_u}^{b}]^{T}, \tag{2.25}$$

are known to the receiver through channel estimation with pilot signals and the variance of the thermal noise, σ^2, as well as the quantization noise vector, $\mathbf{E}_m^C[v]$, can be estimated through the pilot signals. MRC also requires the channel response.The MMSE signal detection algorithm involves matrix inversion $\left(\left(\hat{\mathbf{H}}^{b}\right)^{\mathrm{H}}\left(\hat{\mathbf{H}}^{b}\right) + \sigma'^{2}\mathbf{I}\right)^{-1}$ with the complexity of $O\left((KN_u)^3\right)$, while MRC demands the complexity of $O\left((KN_u)^2\right)$.

2.2.2 Numerical Results

Simulation Conditions

Computer simulation conditions for this section are that the massive-MIMO BS transmits signals with $M = 128$ and 1024 antenna elements, respectively, unless it is specified, and the remaining conditions are listed in Table 2.1.

Uplink Throughput based on MRC/MMSE

The performance of MRC and MMSE with low-resolution ADCs based on 128 antennas is presented in Fig. 2.12. As shown in Figs. 2.12(a) and 2.12(b), when the clipping factor $C = 4$, the performance with infinite-resolution ADCs is not only limited by MUI, but also the over-clipping of the original signal deteriorates the channel estimation accuracy. With inf-ADCs, MMSE detection is better due to MUI elimination.

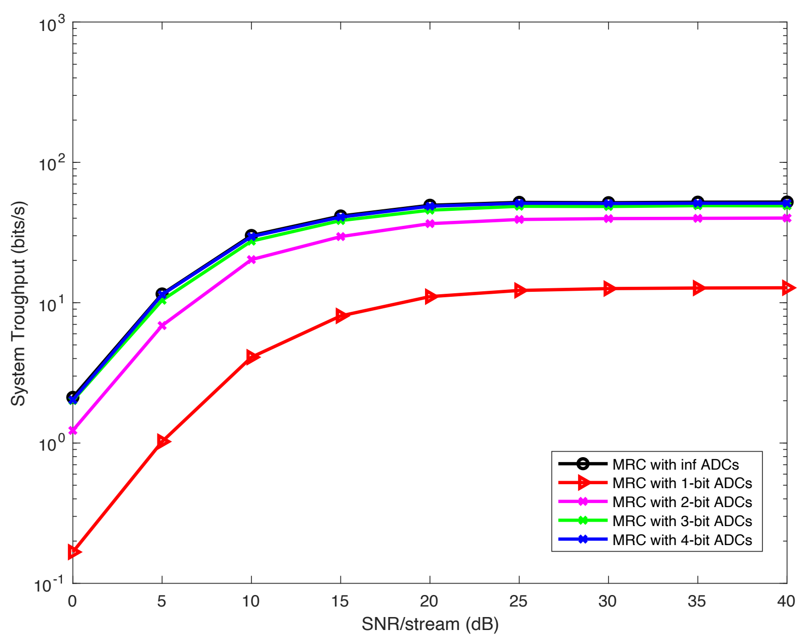

(a). System with MRC and $C = 4$.

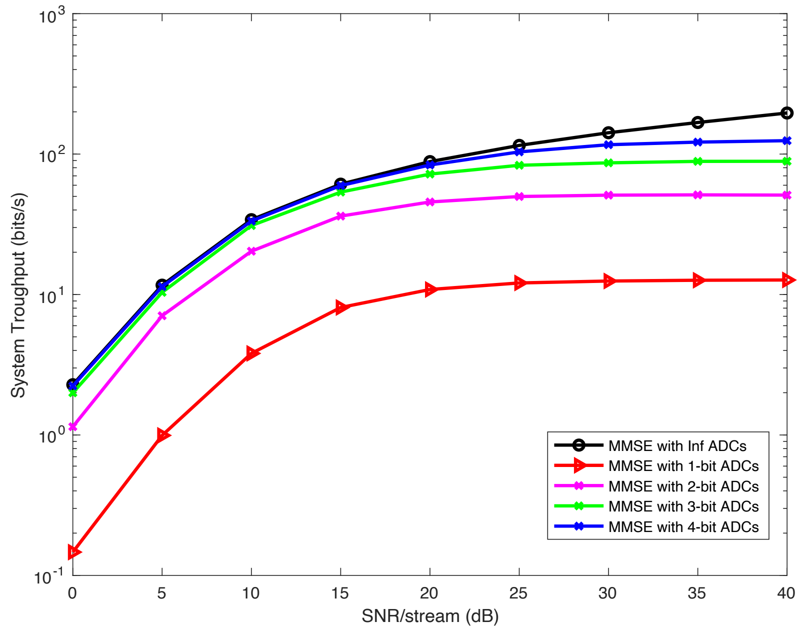

(b). System with MMSE and $C = 4$.

Figure 2.12: Performance of uplink system with 128 antennas.

Because of a limited number of BS antennas, low-resolution ADCs have produced a severe BER in a TDD OFDM system. In a massive MIMO system, a large number of BS antennas can be equipped to reduce the BER. However, the MMSE signal detection algorithm involves matrix inversion with large complexity (especially in massive MIMO). MRC can avoid complicated matrix inversion. In Figs. 2.13(a) and 2.13(b), they are clear that the performance of MRC with 1024 antennas is as good as MMSE. MRC can achieve even better performance than that of MMSE with $1-, 2-, 3-$bit ADCs.

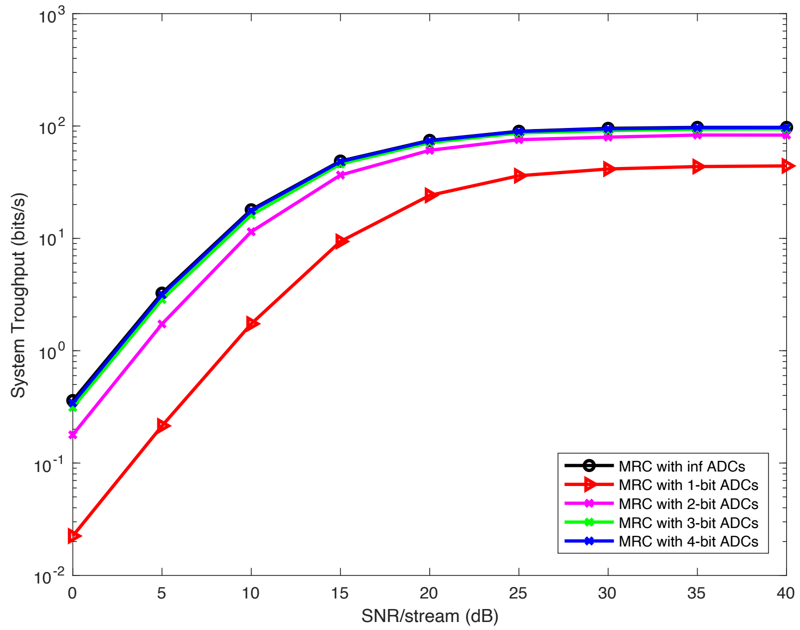

(a). System with MRC and $C = 4$.

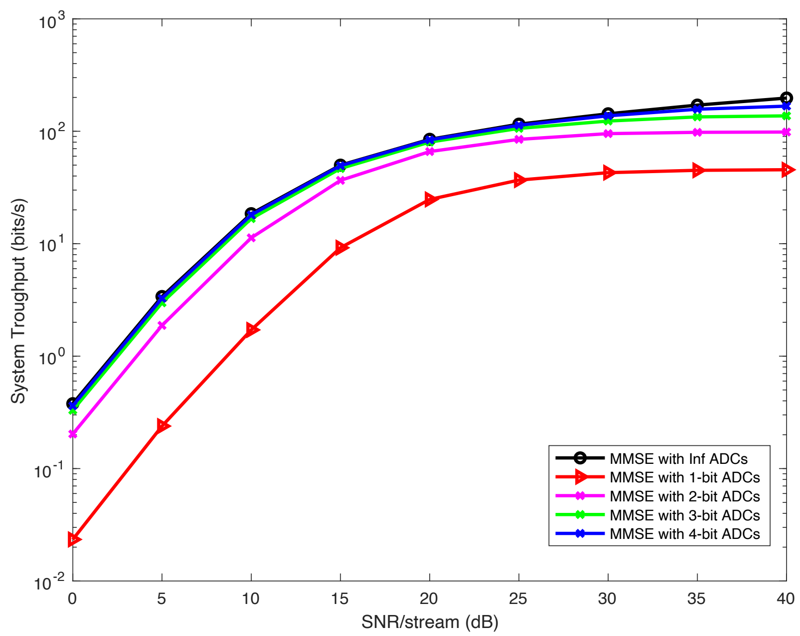

(b). System with MMSE and $C = 4$.

Figure 2.13: Performance of uplink system with 1024 antennas.

When the clipping factor C is reduced to 1 for two different antennas scenarios, it is clear that in the case of $2-, 3-, 4-$bit ADCs in Figs. 2.14 and 2.15, the performance of the MRC is almost as good as that of the MMSE. At low SNR, MRC can achieve higher performance. Because it increases the signal gains through the diversity combining and more noise is removed through reducing the clipping factor C, although the interference still exists after the MRC. When the noise is more dominant than the interference, the effect is particularly outstanding.

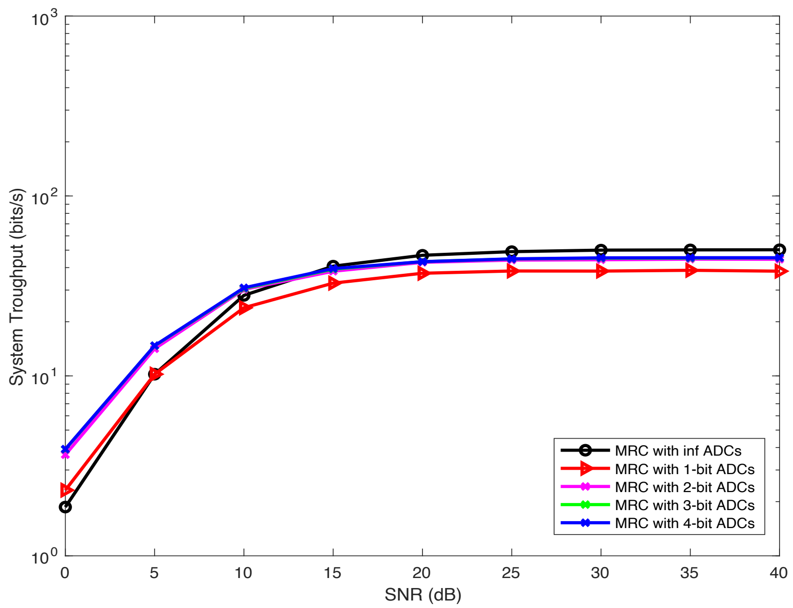

(a). System with MRC and $C = 1$.

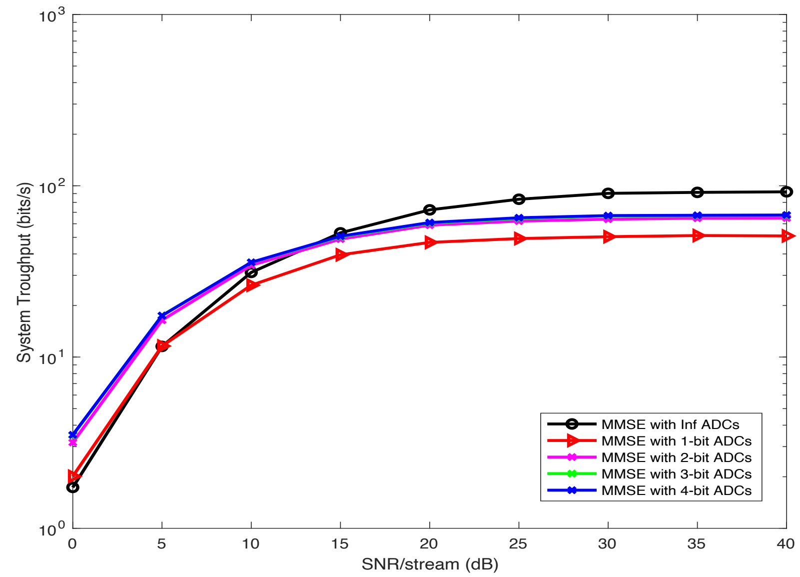

(b). System with MMSE and $C = 1$.

Figure 2.14: Performance of uplink system with 128 antennas.

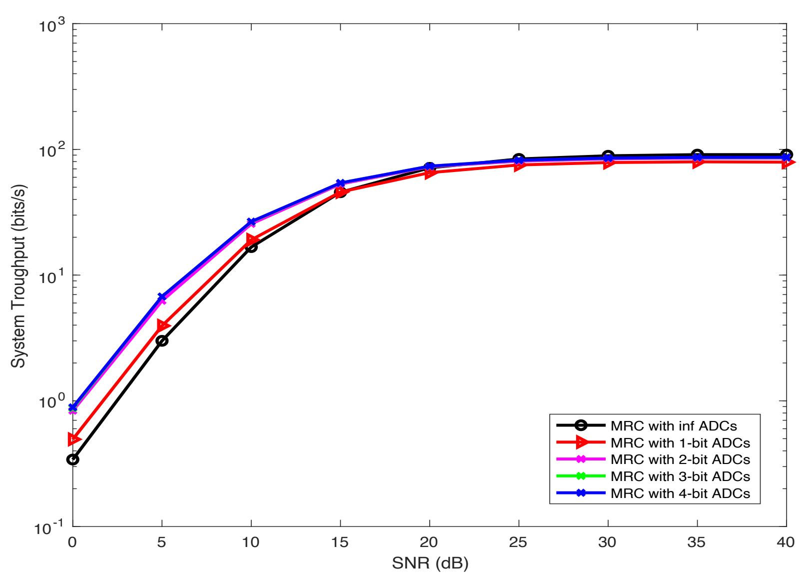

(a). System with MRC and $C = 1$.

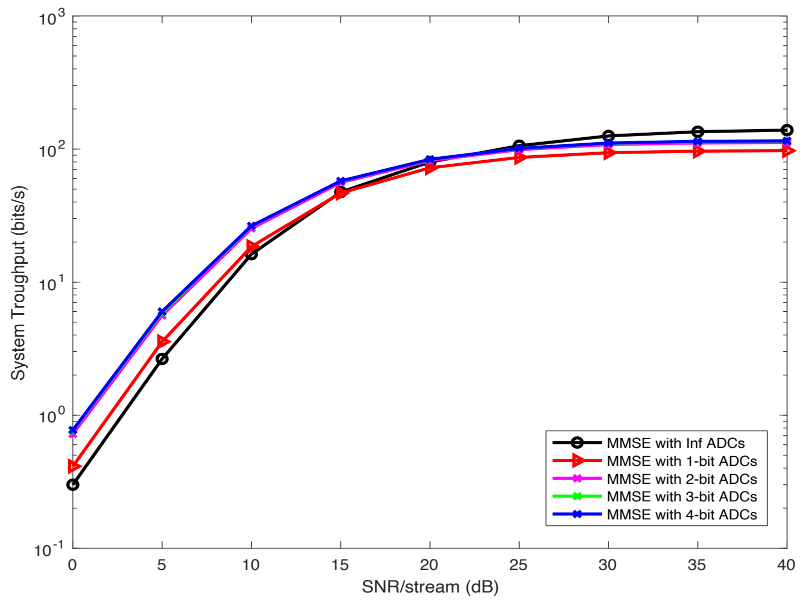

(b). System with MMSE and $C = 1$.

Figure 2.15: Performance of uplink system with 1024 antennas.

In the massive MIMO system with conventional low-resolution ADCs, MMSE is still a good interference rejection scheme according to the performance analysis. We propose that a simple MRC algorithm is used to guarantee performance and reduce system complexity. In this section, we compare and analyze the advantages and disadvantages of the MMSE algorithm and the MRC algorithm based on the proposed ADC design mentioned in Sect. 2. Since the smaller clipping factor C can eliminate a large amount of noise in a low SNR environment, the MRC originally affected by the dominant effect of the noise is outstanding in improving the SNR of the system. Even if the performance based on the MMSE algorithm is also improved, the MRC algorithm almost achieves the same system throughput. In the premise of high performance, the complexity of the system is greatly reduced, especially for the large-scale antennas scenario. The numerical results prove that the MRC algorithm is a better choice to improve the overall performance of the massive MIMO system.

2.3 Conclusion

The quantization factor of an ADC can be selected to clipping the noise under a massive anttenna system. Based on this principle, the different signal detection algorithms used by the uplink receiver in a multi-user massive MIMO system are compared. Under a large number of BS antennas, MMSE with higher resolution ADCs is better than MRC, although the matrix inversion operation demands a large amount of computational complexity. On the other hand, MRC can achieve equivalent or even better performance, especially with low-resolution ADCs. The system throughput realized in MRC with 2-bit ADCs is almost the same as that with infinite resolution ADCs and MRC can achieve better performance than MMSE with $1-, 2-, 3-$bit ADCs. In addition, it requires less computational complexity. Therefore, MRC is more suitable as the number of BS antenna elements increases in a full-digital massive MIMO with low-resolution ADCs.

CHAPTER 3

ADAPTIVE-RESOLUTION ADC SCHEME FOR CELL-FREE DISTRIBUTED ANTENNA SYSTEM

The 2nd chapter of the study discussed a centralized-antenna structure in massive MIMO systems. this chapter studies a distributed-antenna structure in cell-free systems. The quantization range control scheme and the MRC algorithm in Chapter 2 are used to study and analyze how the clipping factor reduces the quantization distortion effect on the received signal considering the propagation loss. Chapter 2 adopted the massive MIMO system because its centralized structure can effectively solve the resource consumption problem of the backhaul line, and there are still many deficiencies in the user coverage, especially the user coverage at the cell edge. Moreover, the general rule for the centralized-massive MIMO is that one always uses all the antennas to serve all the users. In a distributed system, some antennas close to a user to provide services for it. The coverage gain is increased and these antennas are allocated more appropriate ADC to further analyze system performance. Since distributed antenna architectures combined with the characteristics of cell-free access can supplement the deficiencies of the massive MIMO, we consider distributed antenna architectures in cell-free systems in Chapter 3. According to the received signal under different conditions, especially large differences in the propagation loss, and different resolutions are allocated to the ADCs of the APs to improve SE. Further, a potential method to weigh the SE and the EE of the system is provided.

Existing radio and television networks are challenging to meet users' needs to upgrade their consumption experience, and 5G links have become an important communication channel for radio and television media. A 5G mixed mode for multicast-broadcast services is promoted by 3GPP R17 [103]. Small towers in the future broadcasting system (i.e., mobile communication base stations) should have low power, low site, and substantial flexibility to make themselves more suitable for small-scale temporary broadcasting and TV services. For these reasons, the network architecture and technologies in the beyond-5G and 6G can satisfy the requirements of high spectrum efficiency and low power consumption in the future broadcasting system since these critical aspects on 6G play a vital role [96, 97, 104]. A DAS has a large number of independently controlled antennas, such as a large number of irregularly distributed APs, and they are connected to a CPU through the fronthaul network. As the distance between a UE and an AP decreases, this network architecture helps improve SE and EE and resist shadow fading. [73, 98, 99].

The current research on a distributed antenna network is more focused on a cell-free structure [24, 105–110]. Cell-free concept is introduced in [24] and in that concept all APs with a single antenna connect to a central processing unit via a backhaul network to form a large single cell. The advantages of a cell-free network compared with small cells is also discussed in [24]. [107] discusses a pilot assignment scheme based on a topological structure. A two-stage channel estimation scheme in a cell-free IoT network for massive random access is proposed in [108]. Resource allocation over multiple clusters of APs is investigated in [109]. [110] proposes an improved iterative robust precoder of a cell-free system.

Recently, the performance of cell-free systems with low-resolution ADCs is studied [111–113]. The research [111] takes full-duplex technology into cell-free massive MIMO systems with low-resolution ADCs, [112] analyzes max-min fairness power control optimization problems based on a fronthaul-capacity constrained cell-free systems with low-resolution ADCs, and [113] applies a max-min fairness power control optimization algorithm on a Rician channel in cell-free systems with low-resolution ADCs. However, no ADC resolution optimization has been investigated. These research works have shown that the implementation of low-resolution ADCs in APs inevitably leads to severe quantization distortion, especially under high SNR conditions. To compensate for the degradation of the SE performance due to quantization errors, the hybrid ADC architecture has also been widely studies in massive MIMO systems [82, 84], and has also been applied to cell-free systems [76, 81]. It replaces a small fraction part of low-resolution ADCs with inf-ADCs, and explores the ratio of inf-ADCs in a mixed-ADC architecture. It has a better SE-EE tradeoff as compared with inf-ADCs or low-resolution ADCs. Nevertheless, they force the antenna to make a selection between a small bit (i.e., 1−bit) ADC and an inf-ADC, which is far from an energy-saving architecture. This is because the total ADC power consumption is dominated by a few high-resolution ADCs. Moreover, since only the ratio of different resolution bits at each AP is considered and no received signal strength is taken into account. In this case, when an AP receives a signal from a UE in a long distance and noise is the dominant component in the received signal, an ADC with a high resolution will not improve the SE-EE tradeoff. In a cell-free network, there are more and more line-of-sight (LOS) components in between a UE and an AP [77], which means the 'short distance'. In this case, a low-resolution ADC causes serious quantization distortion in the received signal of a short-distance UE. More suitable ADC selection remains to be resolved and we propose an AR-ADC scheme. The adaptive resolution capability of the ADC can be realized by a successive approximation register (SAR) structure, in which N stages are needed to process the $N-$bit resolution [100]. Therefore, the AR-ADC needs to adjust its quantization bit according to the proposed AR selection algorithm. Therein, based on an AQNM [67], the clipping factor of each resolution of the ADC is derived so that the ADCs with the different resolutions at different SINRs can obtain the corresponding optimal signal-to-interference-plus-quantization-and-noise ratios (SIQNRs).

None of the above-mentioned literature focused on an OFDM receiver. In [62] the clipping-quantization theory is revised by means of an exact joint analysis in the case where a Gaussian input signal is present. An adaptive quantization range with the use of automatic gain control (AGC) inserted before ADC is assumed in this research, which is the case of real receiver implementation. The proposed AR-ADC scheme provides a potential energy-efficient OFDM receiver for a cell-free DAS architecture through minimizing the

ADC resolution bits. This is because the inf-ADC limits the EE even though its ratio is relatively small. The proposed AR-ADC scheme improves the EE as compared with the other schemes except the system with only $1-$bit ADCs. Moreover, the SE performance is improved by allocating more resolution bits to the APs closer to each UE with the proposed criterion.

Furthermore, the proposed AR-ADC can reduce the correlation of quantization errors. This Chapter derives the performance of a cell-free distributed antenna network based on the theory of [62] and shows that the assumption of the AGC improves the accuracy of a linear quantization model in a multi-antenna system.

3.1 System Model of Cell-free Distributed Antenna Systems

The assumed system model is shown in Fig. 3.1. A multiuser cell-free DAS is deployed. The geographically-distributed single-antenna APs within a serving range (SR) supports each UE. Leveraging on an AR selection algorithm and an allowable quantization distortion, Δ, the resolutions of ADCs in APs are selected.

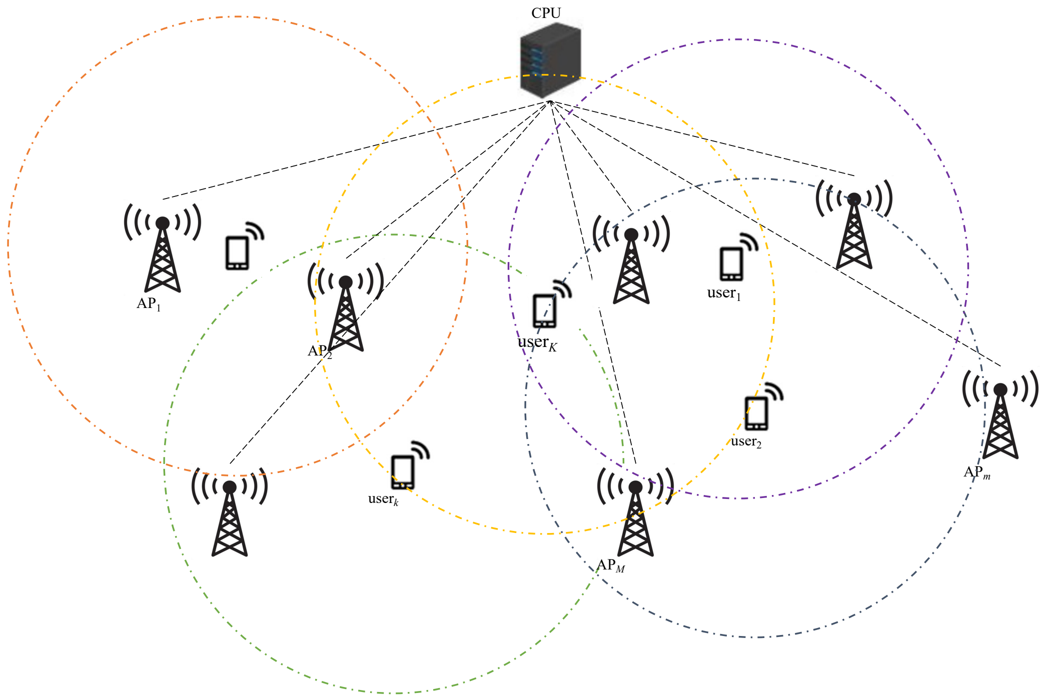

Figure 3.1: Distribution antenna system.

3.1.1 Tranceiving in the Uplink

In the cell-free DAS, there are L_{ap} single-antenna APs randomly distributed within a coverage area and they are connected by means of fronthaul links to a CPU to serve K single-antenna UEs simultaneously. An arbitrary desired UE should be served by M APs ($M \leq L_{ap}$) among the distributed APs. Moreover, in the uplink, the MRC is applied at the CPU to the received signals collected by the fronthual.

It is assumed that all the UEs transmit OFDM signals to their surrounding APs in the uplink. Suppose that the size of an IDFT is N_{dft}, a transmit signal from the kth single-antenna UE in the uplink is expressed as the same as Eq. (2.1).

In this Chapter, the Rayleigh fading and Rician fading as a classic stochastic model is used. The kth input signal at the mth AP is,

$$r_m = g_{mk} s_k[u], \tag{3.1}$$

where g_{mk} is the channel response, which is subject to a Rayleigh distribution or a Rician distribution if the UE is located in a LOS or non-line-of-sight (NLOS) location from the AP. The received signal at the mth AP as the ADC input is given as,

$$y_m[u] = \sum_{k=1}^{K} (g_{mk} s_k[u]) + z_m[u], \tag{3.2}$$

where $z_m[u] \sim \mathcal{N}_{\mathbb{C}}(0, \sigma_n^2)$ is the thermal noise.

Leveraging on the LOS model and the NLOS propagation model [101], the path loss α_{mk} included in g_{mk} can be calculated more accurately. The propagation model is defined by,

$$PL[\mathrm{dB}] \triangleq \begin{cases} 28.0 + 22.0 \log_{10}(d_{mk}) + 20 \log_{10}(f_c) & \text{LOS}, \\ 22.7 + 36.7 \log_{10}(d_{mk}) + 26 \log_{10}(f_c) & \text{NLOS}, \end{cases} \tag{3.3}$$

where d_{mk} is the distance between the kth UE and the mth AP, and f_c is the carrier frequency. The LOS probability model is considered as,

$$P_{\mathrm{LOS}}(d_{mk}) = \min\left(\frac{18}{d_{mk}}, 1\right)\left(1 - \exp\left(\frac{-d_{mk}}{d_{\mathrm{LOS}}}\right)\right) + \exp\left(\frac{-d_{mk}}{d_{\mathrm{LOS}}}\right), \tag{3.4}$$

where d_{LOS} is the distance between the AP and the user under the LOS condition.

3.1.2 Analog-to-Digital Conversion with optimal clipping factor

The received OFDM signal given in Eq. (3.2) is amplified by a low noise amplifier that is controlled by the AGC and put into an ADC. The ADC output is limited in the range of $[-A, A]$, which is scalable through the range limit factor C against the impact of quantization and clipping [62]. According to Sect. 2.1, the step-size δ becomes smaller to ensure finer quantization. Similarly, when the resolution bit R is constant, we can see that fine quantization can also be achieved by adjusting the clipping factor C.

The quantization through the ADCs worsens the accuracy of channel estimation and deteriorates the system performance. The quantized output based on AQNM is expressed as

$$
\begin{aligned}
q_m^C[u] &= \mu y_m[u] + n_m[u] \\
&= \mu \sum_{k=1}^{K} g_{mk} s_k[u] + \mu z_m[u] + n_m[u],
\end{aligned}
\tag{3.5}
$$

where μ is the attenuated factor, which can be calculated as [23], $y_m[u]$ is the ADC input at the mth AP, and $n_m[u]$ is the additive Gaussian quantization noise at the uth time index, respectively. The quantization distortion including the additive Gaussian quantization noise can be derived as,

$$
e_m^C[u] = q_m^C[u] - y_m[u]. \tag{3.6}
$$

The digital OFDM demodulator removes the cyclic prefix and put into a DFT block. The signal on the vth subcarrier is then given as,

$$
Y_{q_m}[v] = \sum_{k=1}^{K} (G_{mk}[v] S_k[v]) + (E_m^C[v] + Z_m[v]), \tag{3.7}
$$

where, $G_{mk}[v]$ is the channel response including pathloss between the kth user and the mth AP, and $Z_m[v]$ is the thermal noise in the mth AP on the vth subcarrier, respectively. These are given as, is expressed as,

$$
G_{mk}[v] = \mu g_{mk} e^{\frac{-j2\pi uv}{N_{dft}}}. \tag{3.8}
$$

and

$$
Z_m[v] = \frac{1}{\sqrt{N_{dft}}} \sum_{u=0}^{N_{dft}-1} \mu z_m[u] e^{\frac{-j2\pi uv}{N_{dft}}}. \tag{3.9}
$$

3.2 Adaptive-Resolution Selection Scheme

Based on [62], the corresponding optimal clipping factors with the best signal-to-distortion-quantization noise ratio (SDQNR) performances for different resolutions can be found. For different received SNRs, the performance characteristics of the ADC with the optimal clipping factor under different resolutions are analyzed. For the assumed DAS system, IUI needs to be taken into consideration. Therefore, we need to re-establish the analysis model of the optimal clipping factor for the quantization distortion of the ADC.

3.2.1 SIQNR Analysis

In order to accurately analyze the impact of quantization distortion on system performance, we use different received SINRs and their corresponding SIQNRs to find the optimal clipping factors for different resolutions. The article [114] has pointed out that the SIQNR is inaccurate in a MIMO system because of correlation between the quantization errors on different received branches. However, with the application of the adaptive range in the proposed scheme, the correlation between the quantization errors on different branches is small enough to apply the Bussgang decomposition. It will be discussed with numerical results in Section: *Correlation between Quantization Noises on Different APs*.

Based on the Bussgang theorem, the ADC output of the mth AP can be treated as an undistorted component that is proportional to an input signal and a noise distortion,

$$q_m^C[u] = \mu y_m[u] + \theta_m[u], \tag{3.10}$$

where $y_m[u]$ is the ADC input at the mth AP, $\theta_m[u]$ is the filtered distortion noise and is not correlated to $y_m[u]$ at the uth time index, respectively, and the coefficient μ is,

$$\mu = \frac{1}{\sqrt{2\pi\sigma_{y_m}^2}} \int_{-\infty}^{\infty} \frac{yQ_b(y)}{\sigma_{y_m}^2} e^{-\frac{y^2}{2\sigma_{y_m}^2}} dy, \tag{3.11}$$

where $\sigma_{y_m}^2$ is the ADC input power of the mth AP.

At the mth AP, the power of the undistorted signal component is expressed as,

$$P_{q_m^C}(C) = \frac{1}{2\pi}\left\{\sum_{i=-L/2+1}^{L/2} q_i\left[e^{\frac{\hat{y}_{mi}C}{\sqrt{2}}} - e^{\frac{\hat{y}_{m(i-1)}C}{\sqrt{2}}}\right]\right\}^2, \tag{3.12}$$

where $\hat{y}_{mi}$ is the ith original quantization threshold value and q_i is the amplitude of the ith original quantization interval. Accoriding to Eq. (3.10), it can be transformed to $P_{q_m^C}(C) = \sigma_{y_m}^2\mu^2$.

The total power of the output of the quantizer at the mth AP is given as,

$$\sigma_{q_m^C}^2 = \frac{1}{2}\sum_{-L/2+1}^{L/2} q_i^2 \cdot \left[\operatorname{erfc}(\frac{\hat{y}_{mi}C}{\sqrt{2}}) - \operatorname{erfc}(\frac{\hat{y}_{m(i-1)}C}{\sqrt{2}})\right], \tag{3.13}$$

where $\operatorname{erfc}(\cdot)$ is the complementary error function.

The SINR can be given as,

$$SINR = \frac{\sigma_{y_{mk}}^2}{\sigma_{y_m}^2 - \sigma_{y_{mk}}^2}, \tag{3.14}$$

where $\sigma_{y_{mk}}^2$ is the ADC input power of the signal from the kth UE at the mth AP.

The SIQNR can be derived as the ratio between the undistorted signal power and the sum of the interference power, the thermal noise power, and quantization noise power as

$$SIQNR(C) = \frac{P_{q_{mk}^C}(C)}{\sigma_{q_m^C}^2 - P_{q_{mk}^C}(C)}, \tag{3.15}$$

which can obtain the optimal value at different resolutions used by the kth UE on the mth AP by adjusting the clipping factor C and $P_{q_{mk}^C}$ is the power of the kth undistorted received signal component at the mth AP.

To more accurately investigate the impact of lower resolution on system performance in various SINR environments, we evaluated the characteristics of the SIQNR with a resolution from one bit to six bits, respectively. In Fig. 3.2, the behavior of the SIQNR function of C is explored. For each number of bit resolution, there is a suitable value of the clipping factor C to optimize the corresponding SIQNR. If C is smaller than the optimum point, the SIQNR decreases as the quantization noise increases. If C is larger than the optimum point, the clipping phenomena becomes dominant. The optimum work point depends on the resolution of the ADC under a certain SINR.

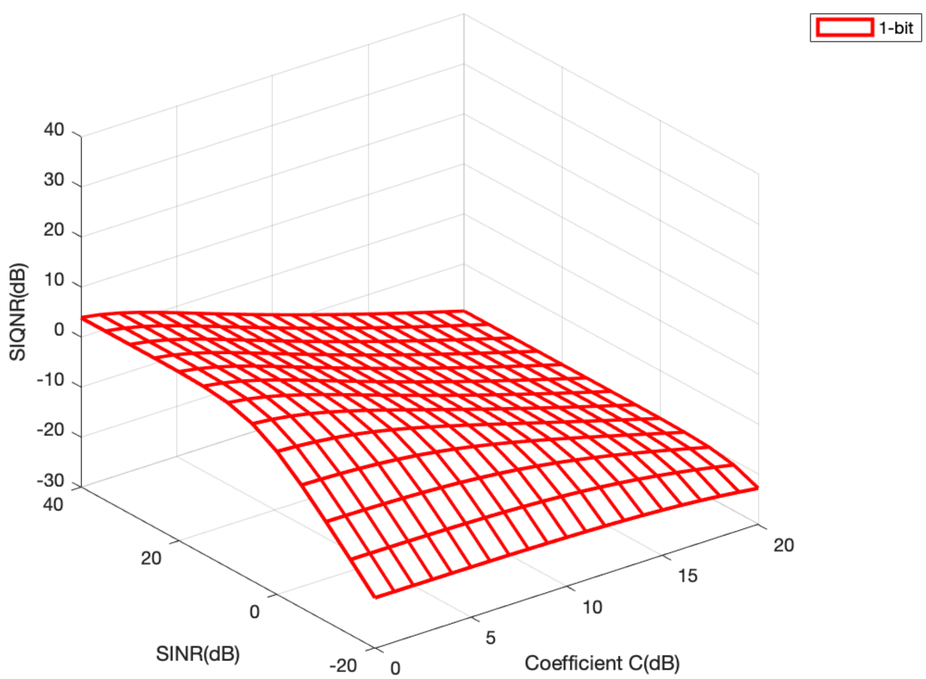

(a). Case: 1−bit ADC.

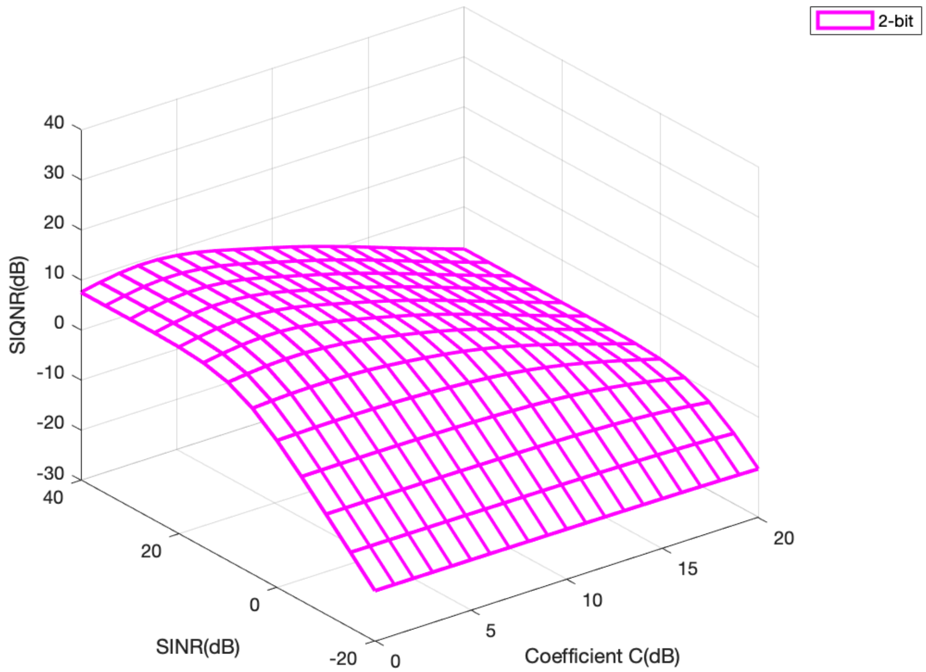

(b). Case: 2−bit ADC.

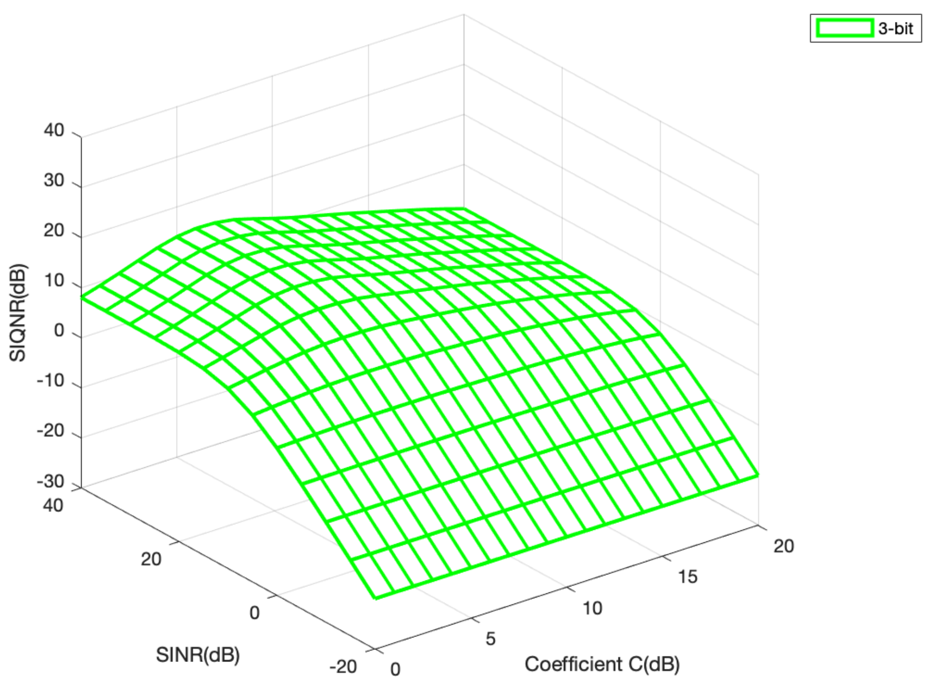

(c). Case: 3−bit ADC.

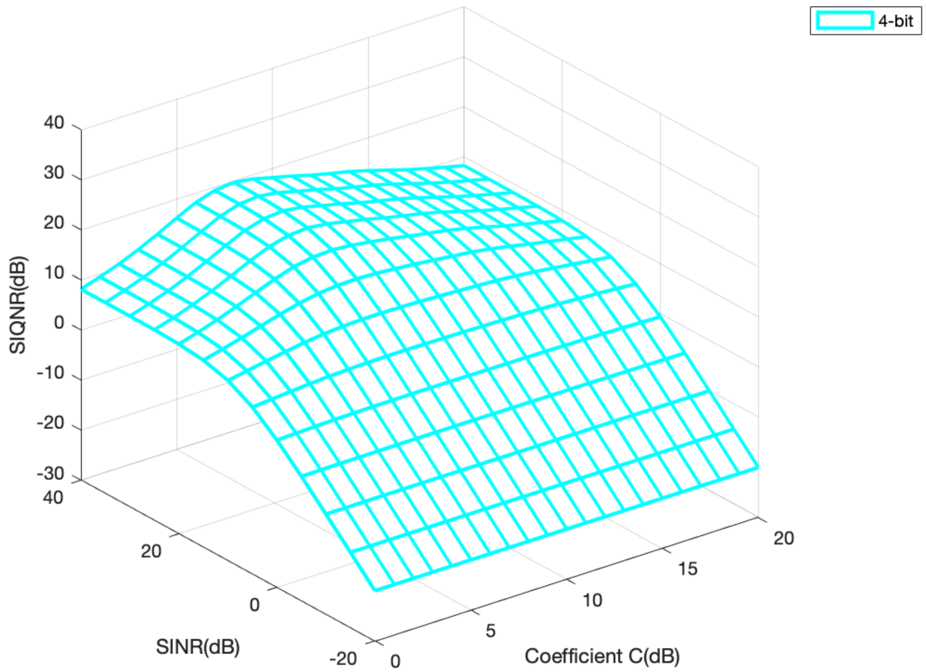

(d). Case: 4−bit ADC.

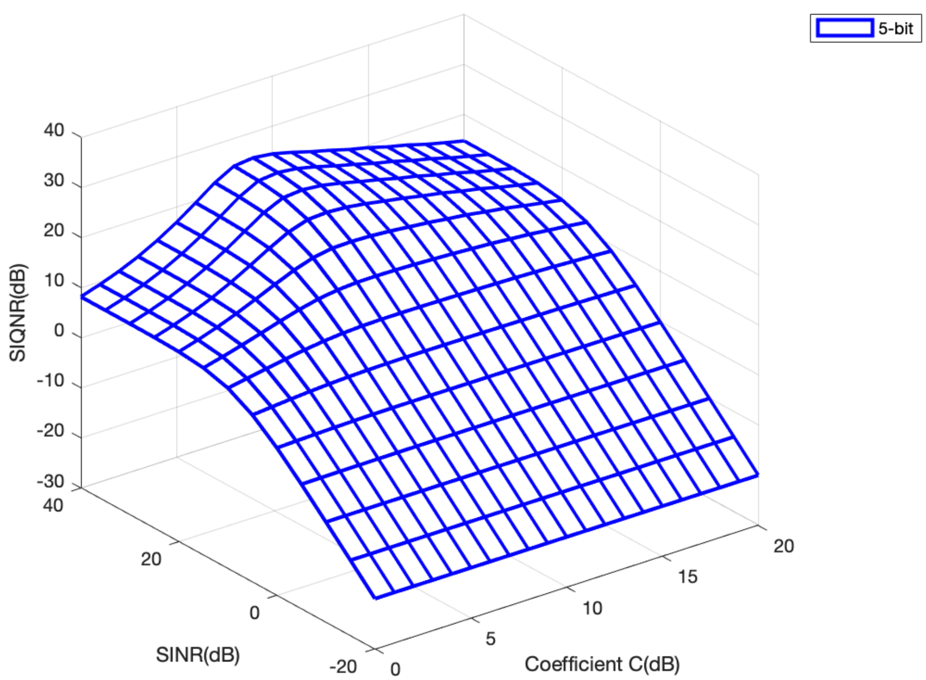

(e). Case: 5−bit ADC.

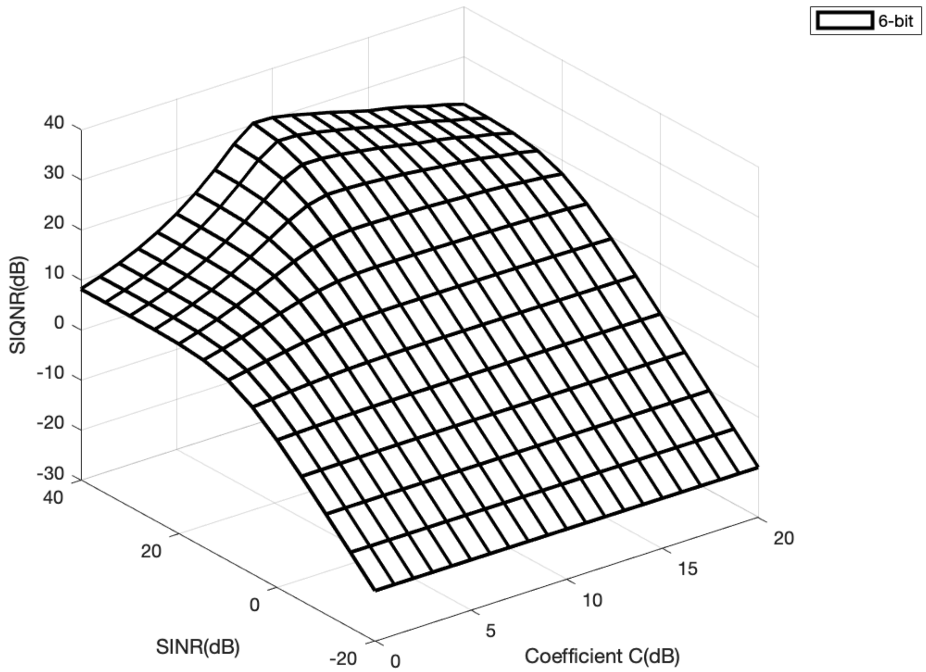

(f). Case: 6−bit ADC.

Figure 3.2: SIQNR versus clipping factor C for different bits of an ADC in different SINR conditions.

3.2.2 Adaptive-Resolution Selection Scheme

According to the evaluation of the SIQNR, we know the optimal clipping factor of the ADC under the existence of the IUI. The related SINR and clipping factor C based on Eqs. (3.13) and (3.14) can be pre-calculated before the signal reception. Therefore, the receiver simply needs a large memory to store this data for the simple calculation of the AR selection scheme so that the AR selection scheme selects the appropriate ADC resolution at each serving AP for the desired UE.

For better EE, the resolution needs to be a lower number of bits within one bit to six bits. Therein, an allowable quatization error in dB is used as a criterion. Based on Fig. 3.2, the resolution of each ADC, R, is obtained with the following.

Criterion:

$$\begin{aligned}&\text{minimize } R\\&\text{s.t.}\quad SINR[\text{dB}] - \max_{C} SIQNR(R, C)[\text{dB}] < \Delta[\text{dB}],\end{aligned} \tag{3.16}$$

where $SIQNR(R, C)$ is the SIQNR of a $R-$bit ADC with a clipping factor of C.

From this criterion, each AR-ADC is able to select the minimum resolution. The optimal clipping factor C is selected for the calculation of the SIQNR. If this criterion is not satisfied with the given Δ, R is set to one.

In our proposed system, referring to objective SINR after channel estimation, the optimal SIQNR for each resolution ADCs with the related C can be found as well according to Fig. 3.2. Based on Eq. (3.16), we can select the corresponding maximum SIQNR value from the best SIQNRs by a Δ limit so that the AR-ADC can know the corresponding resolution bits and C value. The parameter Δ is set with a selected range as one of the evaluation criteria.

3.3 Performance of Cell-free Distributed Antenna Systems

Suppose that channel estimation is ideally carried out, the estimate of $S_k[v]$ at AP m can be computed as,

$$\begin{aligned}\hat{S}_k[v] =& W_{mk}^{\mathrm{H}} G_{mk} S_k[v] + \sum_{\substack{i=1\\i\neq k}}^{K} W_{mk}^{\mathrm{H}} G_{mi} S_i[v]\\&+ W_{mk}^{\mathrm{H}} Z_m[v],\end{aligned} \tag{3.17}$$

where $W_{mk} = G_{mk}$ as MRC coefficient is the actual receive combining vector for APs that serve UE k.

3.3.1 Spectral Efficiency

The instantaneous SIQNR of the MRC output of the kth UE is expressed as,

$$\Omega_k\left(\mathcal{B}, C_{op}\right) = \frac{p_k^{ul}\mathbb{E}\left\{\left|\sum_{m=1}^{M} W_{mk}^{\mathrm{H}}[v] G_{mk}[v]\right|^2\right\}}{\sum_{\substack{i=1\\i\neq k}}^{K} p_i^{ul}\mathbb{E}\left\{\left|\sum_{m=1}^{M} W_{mk}^{\mathrm{H}}[v] G_{mi}[v]\right|^2\right\}} \tag{3.18}$$

$$\overline{+\mathbb{E}\left\{\|W_{mk}^{\mathrm{H}}[v]\|^2\right\}\left(\sigma_{q_m^C}^2 - \sigma_{y_m}^2\right)}$$

$$\overline{+\mathbb{E}\left\{\|W_{mk}^{\mathrm{H}}[v]\|^2\right\}\sigma_n^2},$$

where $\mathcal{B}$ is the resolution set of ADCs of different APs serving UE K, and C_{op} is the set of different clipping coefficients C corresponding to $\mathcal{B}$. p_k^{ul} and p_i^{ul} are UEs' transmit power.

An achievable uplink SE is derived based on Eq. (3.15) as,

$$SE = \sum_{k=1}^{K} \log_2\left(1 + \Omega_k\left(\mathcal{B}, C_{op}\right)\right). \tag{3.19}$$

3.3.2 Energy Efficiency

In the system performance analysis, the utilization efficiency of energy resources is also an important indicator. The sources of power consumption are mainly considered as ADC components and the power consumption model of the ADC is introduced,

$$PC_k = \sum_{m=1}^{M} FOM_W \cdot f_s \cdot 2^{R_{mk}}, \tag{3.20}$$

where PC_k expresses the power consumption of ADCs of M serving-APs for the desired UE k, FOM_W is the Walden's figure-of-merit [12], f_s is the Nyquist sampling rate and R_{mk} is the quantized bit of the mth AP serving UEk in $\mathcal{B}$ of the AR-ADC.

The calculation of the ADC power consumption based on [76], the formula can be simplified to the following,

$$PC_k = \sum_{m=1}^{M} 3 \times 10^{-5} \times 2^{R_{mk}} + 0.002\beta$$
$$\begin{cases} R_{mk} = 1 \text{ for } \beta = 0, \\ R_{mk} > 1 \text{ for } \beta = 1, \end{cases} \tag{3.21}$$

$$PC_k = 0.1229M, \quad \text{Inf-ADC case} \tag{3.22}$$

where β is a flag parameter associated with the quantization R_{mk}. From Eqs. (3.18) and (3.19), obviously the power consumption is dominated by the inf-ADC.

The EE is defined as the ratio of the sum uplink SE and the ADC power consumption [78],

$$\eta_{EE} = \sum_{k=1}^{K} \frac{SE}{PC_k}. \tag{3.23}$$

3.3.3 Numerical Results

Simulation Conditions

Computer simulation conditions are presented in Table 3.1. In the cell-free DAS, all the APs are randomly distributed within a circular coverage area with a radius of 500 meters to serve eight UEs simultaneously, i.e. the coverage area is $500^2\pi$ square meters. The SR in this simulation is set as a circular area from a desired UE and all the APs in the SR processes the received signal from the desired UE. The center frequency of a transmission band is 5.2 GHz, its bandwidth is 20 MHz, and the transmit power from each UE is 0 dBm. The OFDM signal bandwidth is 20 MHz, the DFT size is 2048, and the number of subcarriers is 1200. The niose spectrum density at each AP is -174 dBm/Hz. The average number of APs is determined by an average inter-antenna distance (IAD) as each AP covers the area of $(\mathrm{IAD}/2)^2\pi$, where the average number of APs is calculated as $500^2/(\mathrm{IAD}/2)^2$. As a channel model, a path loss model with Rician fading (a Rician $\mathcal{K}-$factor of 10 dB) is assumed for LOS and an ideal pathloss model with Rayleigh (IPL-Rayleigh) fading is assumed [102] for NLOS. The reference distance of the LOS condition is 36 meters. The resolution of ADC can be selected from one bit to six bits based on the criterion parameter Δ. The number of trials is 5000.

Table 3.1: Simulation Conditions.

Coverage area (S)	$\pi \times 500^2$ m^2
Number of UEs (K)	8
Center frequency (f_c)	5.2 GHz
Used frequency bandwidth (BW)	20 MHz
Transmit power from each UE (p^{ul})	0 dBm
DFT size	2048
Number of active subcarriers (N_{sc})	1200
Noise spectrum density	-174 dBm/Hz
Channel models for LOS & NLOS	Rician fading with $\mathcal{K}$ = 10 dB IPL-Rayleigh fading
Distance in LOS (d_{LOS})	36 m
ADC resolution	$1- \sim 6-$bit
Allowable quantization distortion (Δ)	0 ~ 20 dB
Number of trials	5000

Correlation between Quantization Noises on Different APs

In [114], a 4×4 MIMO channel matrix, each element of which is subject to an independent complex Gaussian distribution ($\mathcal{N}_{\mathbb{C}}(0, 1)$), is assumed. It means the 1-bit ADC output in [114], +1 or −1, corresponds to the same level as the whole average of each element of the received signal even though some of those elements might be so huge (with a smaller probability). On the other hand, with the adaptive-range scheme given in Eq. (2.12), the 1-bit ADC output, +1 or −1, is adjusted with the received signal level.

To analyze the correlation of the element of $\theta_m[u]$ with 1−bit ADC after Bussgang decomposition, the cumulative probability functions of correlation values are shown in Fig. 3.3. The analysis of the correlation is based on three conditions; i.e., the fixed-range ADC with Rayleigh fading model, the adaptive-range ADC with Rayleigh fading model, and the adaptive-range ADC with Rician fading model ($\mathcal{K}$ = 10 dB), respectively.

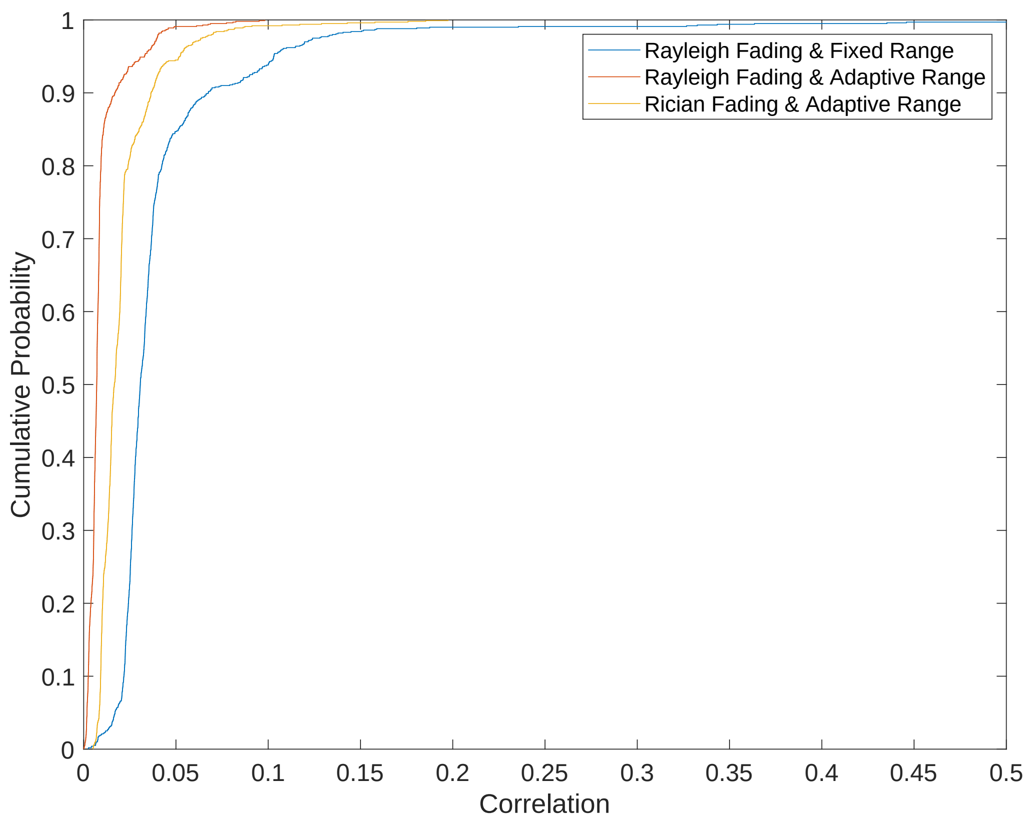

Figure 3.3: Cumulative probability function of the correlation coefficient between elements in $\theta_m[u]$.

The numerical results in Fig. 3.3 show high correlation values like [114] with the fixed-range ADC on the Rayleigh fading model. Bussgang theorem may be inaccurate to 1-bit ADCs because the fixed-range ADC quantizes the received signal with an average amplitude over the whole fading variation. However, the adaptive-range ADC in our proposed scheme quantizes the received signal based on the instantaneous fading variation. With the Rayleigh fading model in NLOS cases, lower correlation values appear and Bussgang decomposition may be applicable. With the adaptive-range ADC in our proposed scheme with the Rician fading model in LOS cases, a little higher correlation values appear. However, Bussgang decomposition can also be applicable to LOS cases since the SINR should be relatively high in the LOS cases and high-resolution ADCs should be selected and the high-resolution ADC leads to lower correlation values.

Spectral Efficiency and Energy Efficiency for Different Inter-antenna Distances

The SE and the EE of the uplink system versus the average IAD are shown in Figs. 3.4 and 3.5. The SR is 500 meters, and allowable distortion parameter through quantization Δ = 10dB. The performance curves of the proposed AR-ADC algorithm and a current hybrid ADC scheme as well as a low-resolution ADC scheme are presented. In the hybrid ADC scheme, low-resolution ADCs and infinite-resolution ADCs are used and the ratio of the low-resolution ADCs to all the ADCs is set to ρ. Moreover, the performance of infinite-resoultion ADC scheme in the same scenario is included as a reference in these comparisons. Furthermore, we also explored the impact of the number of APs on system performance in different IAD scenarios.

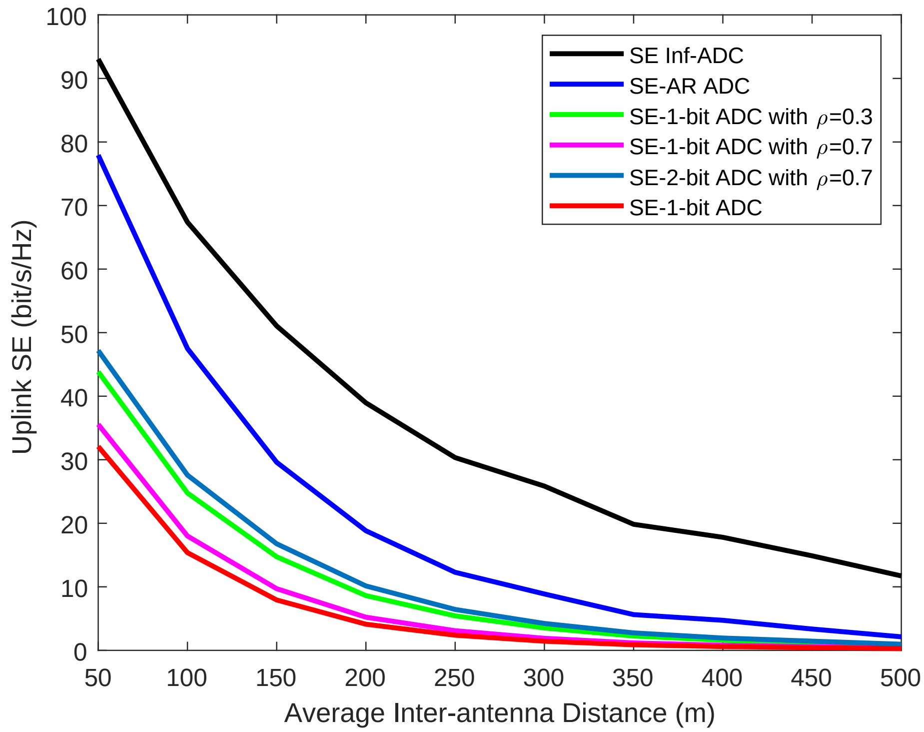

Figure 3.4: SE versus IAD.

The numerical results in Fig. 3.4 shows that the larger system throughput can be realized if more ADC bits are available. The 1−bit ADC limits the system throughput even though its ratio is only 0.3. As AP density increases, i.e., the IAD reduces, the growth rate of the system throughput with the AR-ADC is getting more and more obvious. This is because more resolution bits should be allocated to the ADCs of the APs that are closer to the UE, instead of simply applying the inf-ADC components at the APs in the low-resolution system to enhance the SE performance.

The larger system throughput can be realized if more ADC bits are available. Compared blue curve and black curve, due to more bits for ADC, the SE of inf-ADC is better than that of AR-ADC. Compared AR-ADC and mix-ADC cases, the SE of AR-ADC is better than that of mix-ADC cases. This is because under the parameter Δ = 10dB, AR-ADC minimizes the effect of quantization noise, while the inf-ADC suffers from the stronger IUI.

It is not necessary to allocate more total resolution bits to achieve the higher SE. The total resolution bits of AR-ADC (max bit is 6) is less than that of the mixed-ADC case with $\rho = 0.3$, even 0.7.

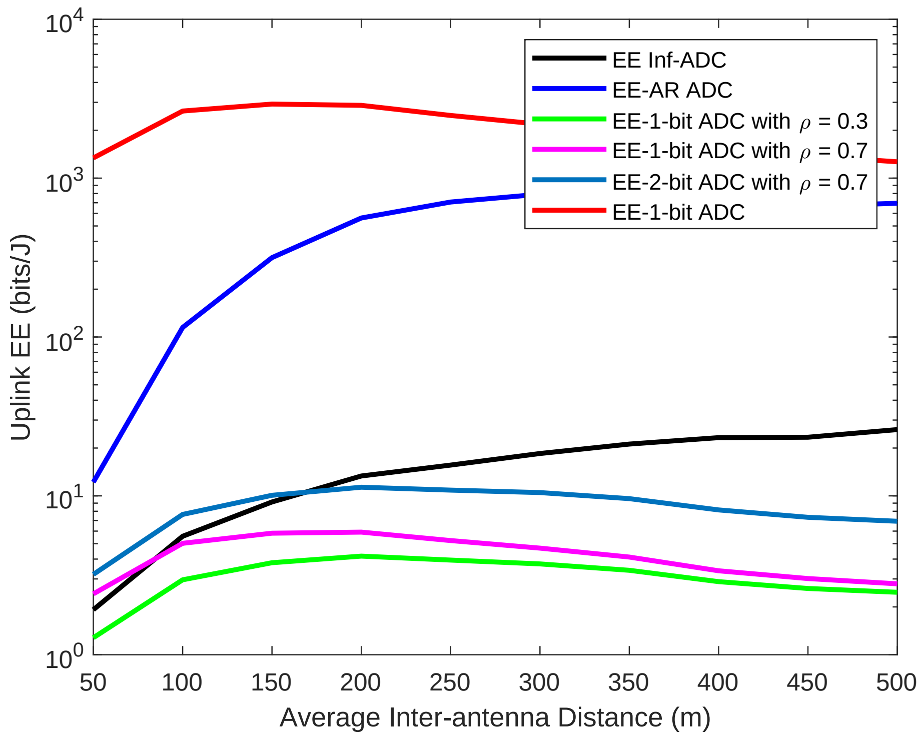

Figure 3.5: EE versus IAD.

In Fig. 3.5, the numerical results show that the larger energy efficiency can be realized if lower resolution bits are applied. By comparing the magenta curve and the dark blue curve, the infinite-resolution ADCs limit the EE even though its ratio is only 0.3 ($\rho = 0.7$). Obviously, the EE increases as the number of APs decreases. This is because the low-resolution ADCs limit the SE severely and the SE in Eq. (3.23) becomes small. On the other hand, the increase in power consumption can be justified by the improvement of the SE with infinite-resolution ADCs. Under a certain average inter-antenna distance, it may occur that the EE of the mixed-ADC is smaller than that of the infinite-resolution ADC and mix-ADC cases when the lower resolution reduces the throughput more significantly than the power consumption. By comparing the blue curve and the black curve, the EE of the AR-ADC is better than that of the inf-ADC because fewer bits. By comparing the AR-ADC and mix-ADC cases, the EE of the AR-ADC is better than that of the inf-ADC. There are two reasons. For smaller IAD situation, it is the growth rates of throughputs are faster than that of the corresponding power consumption. For larger IAD situation, the total resolution bits of AR-ADC are fewer than that of mixed-ADC cases.

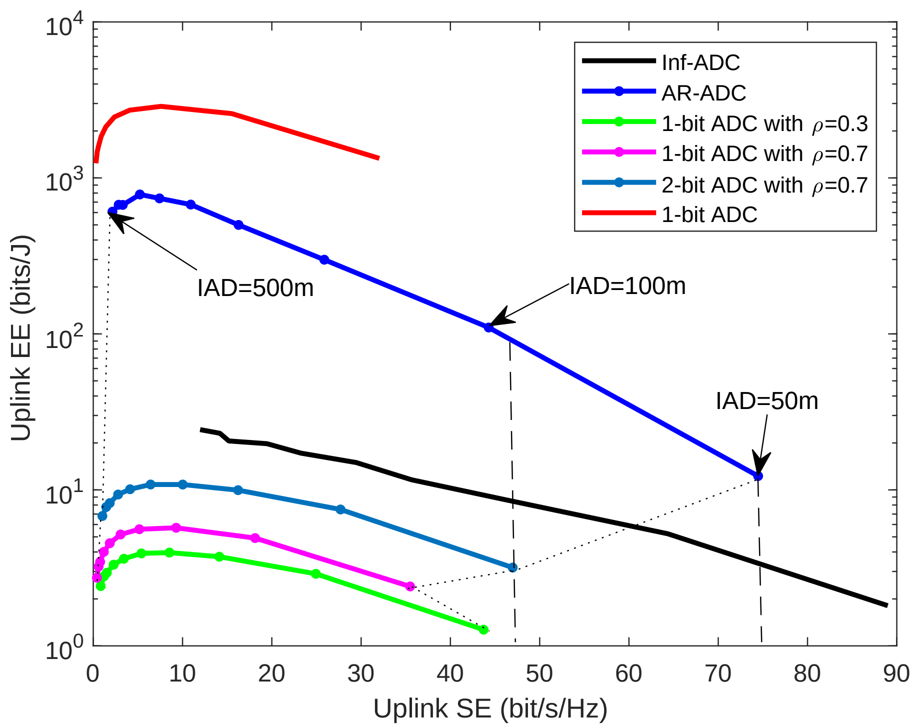

Figure 3.6: EE versus SE based on IAD conditions.

(IAD=50-500 m, SR=500 m, Δ = 10dB)

In Fig. 3.6, under the same IAD condition, the EE of the proposed AR-ADC is better than that of the conventional mixed-ADC cases at the same SE. This is because more and fewer resolution bits should be allocated to ADCs of APs closer and farther from the UE, respectively when the parameter Δ is appropriately chosen to be 10dB. Moreover, the SE can be up to 70 bit/s/Hz in the proposed scheme while it can reach only up to 45 bit/s/Hz in the conventional mixed-ADC cases. It means that the resolution bits are selected for the proposed AR-ADC to keep higher SE and realize better EE according to Eq. (3.16) (Δ = 10dB) when IAD is set between 450 meters and 500 meters. If the SE of the one-bit ADC is less than 30 bit/s/Hz, the one-bit ADC case will be the best choice in terms of the EE. However, higher SE is better. Observed from this figure, the proposed AR-ADC is the best choice when the SE of the AR-ADC is less than 75 bit/s/Hz.

Spectral Efficiency and Energy Efficiency for Different Serving Ranges

The SE and the EE of the uplink system versus the SR are shown in Figs. 3.7 and 3.8. The average IAD is 50 meters, and allowable distortion parameter through quantization Δ = 10dB.

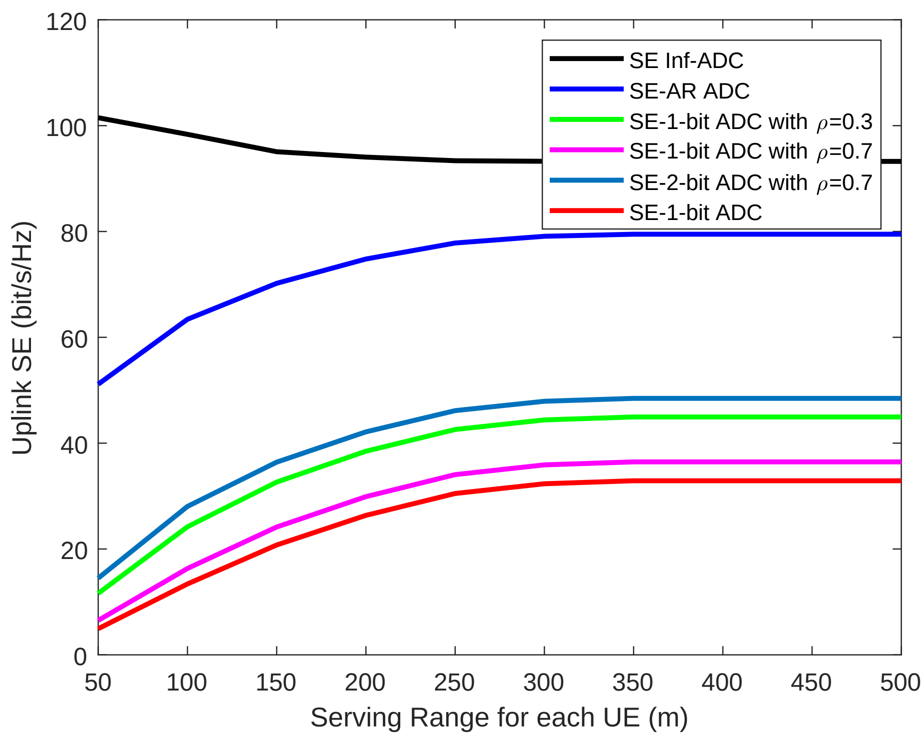

Figure 3.7: SE versus SR.

The curves in Fig. 3.7 shows that the SE increases with the low-resolution ADCs while it decreases with the inf-ADCs. The reason is that quantization distortion reduces more with a large number of APs. On the other hand, the IUI increases with the inf-ADCs when the APs increase. By comparing the black curve and the blue curve, the SE of the inf-ADC is better than that of the AR-ADC because of more resolution bits allocation. By comparing the AR-ADC and mixed-ADC cases, the SE of the AR-ADC is better than that of mix-ADCs. This is because, under the parameter $\Delta = 10$dB, AR-ADC minimizes the effect of quantization noise, while the inf-ADC suffers from the stronger IUI.

The numerical results in Fig. 3.8 show that the shorter SR is better in terms of the EE if the IAD is small enough such as 50 meters though the better system throughput is realized with the larger SR if quantization is applied. This is because a larger number of APs improve the SIQNR more with larger power consumption. This can be explained as the $SIQNR - SINR$ relationship for 1-bit ADC since it improves in the low SINR region. Compared blue curve and red curve, fewer resolution bits can bring higher EE. Compared the AR-ADC and mixed-ADC cases, the EE of the AR-ADC is better than that of mixed-ADC cases. This is because under the parameter $Dleta = 10$dB, AR-ADC minimizes the effect of quantization noise, and the stronger IUI comes from inf-ADC.

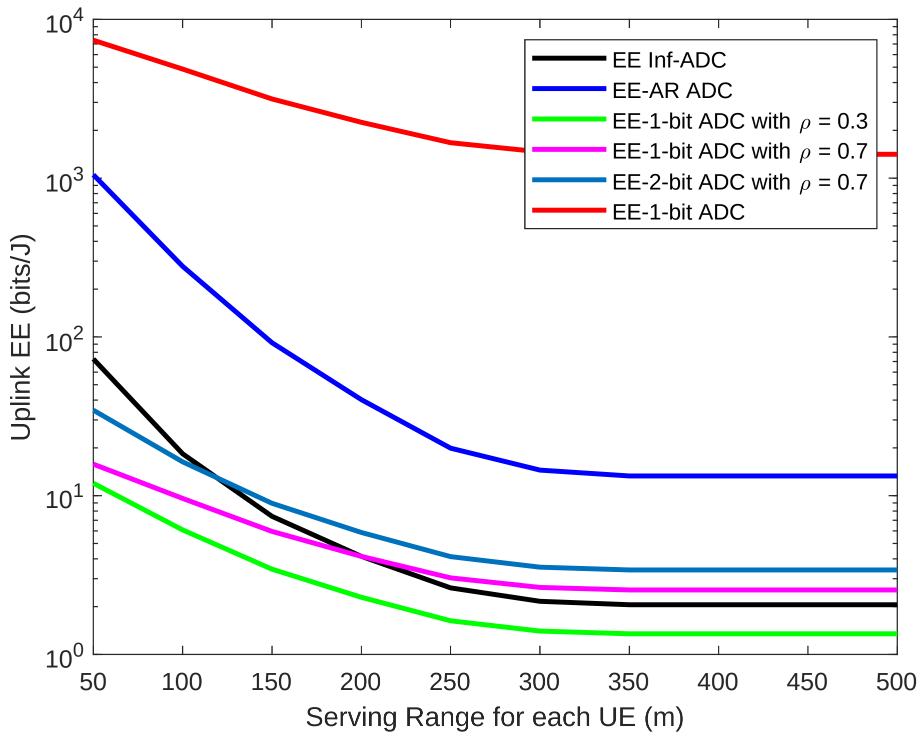

Figure 3.8: EE versus SR.

Moreover, the EE is worse as the SR increases. This is because that the growth rates of the power consumption are faster than that of the corresponding throughputs.

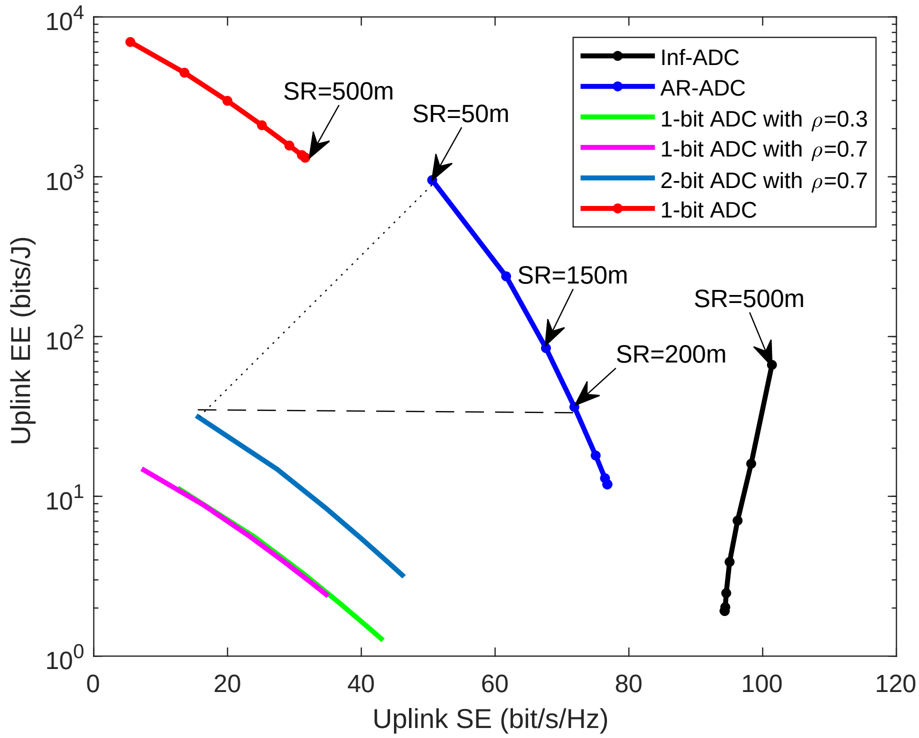

Figure 3.9: EE versus SE based on SR conditions.

(IAD=50 m, SR=50-500 m, Δ = 10dB)

In the same SR condition, the EE and the SE of the proposed AR-ADC is better than that of the conventional mixed-ADC cases in Fig. 3.9. Since the growth rates of the power consumption are faster than that of the corresponding throughputs, the system with AR-ADC (SR=50m) can meet almost the same EE and the higher SE as that with one-bit ADC (SR=500m). Meanwhile, the system with inf-ADC (SR=500m) can meet almost the same EE and the higher SE as that with AR-ADC (SR=150m).

Spectral Efficiency and Energy Efficiency for Allowable Distortion Parameter through Quantization

In Figs. 3.10 and 3.11, the SE and the EE of the uplink system versus the allowable distortion parameter through quantization are shown. The average IAD is 50 meters and the SR is

500 meters.

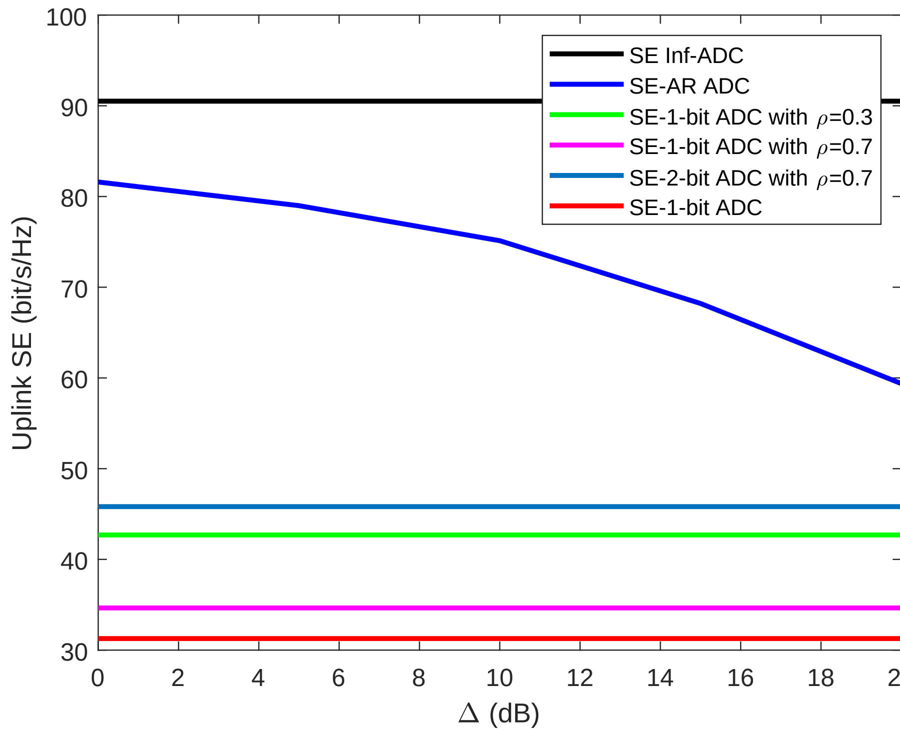

Figure 3.10: SE versus allowable distortion parameter through quantization Δ.

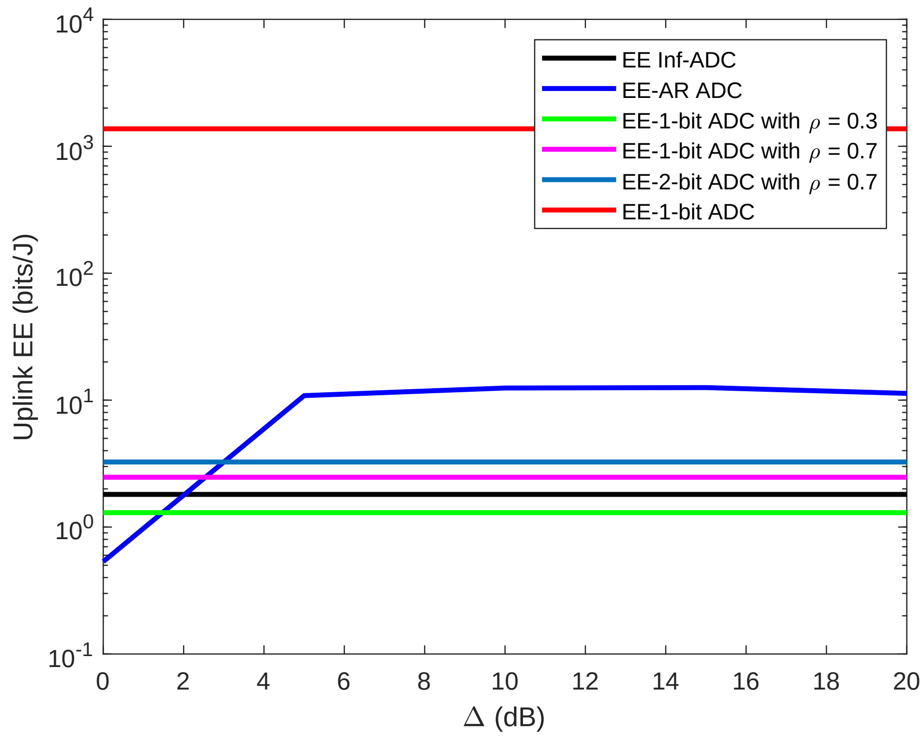

Figure 3.11: EE versus allowable distortion parameter through quantization Δ.

The parameter Δ acts only on the proposed AR-ADC. The SE and EE of the proposed AR-ADC after Δ adjusting cannot reach that of one-bit ADC and inf- ADC case, respectively, but its SE and EE can far exceed that of the conventional mixed-ADC cases at some suitable Δ values.

The SE performance with the AR-ADC decreases and the EE increases as Δ increases. This is because that more ADC bits would be required, if Δ is small. With a large Δ, the probability of small resolution bits being selected would grow to realize better EE. Moreover, the EE converges at a parameter Δ of around 5dB. However, inappropriate resolution selection results in the reduction of the EE more with the low-resolution ADC than with the inf-ADC as Δ is smaller than 2dB. This has important implications for the SE-EE trade-off.

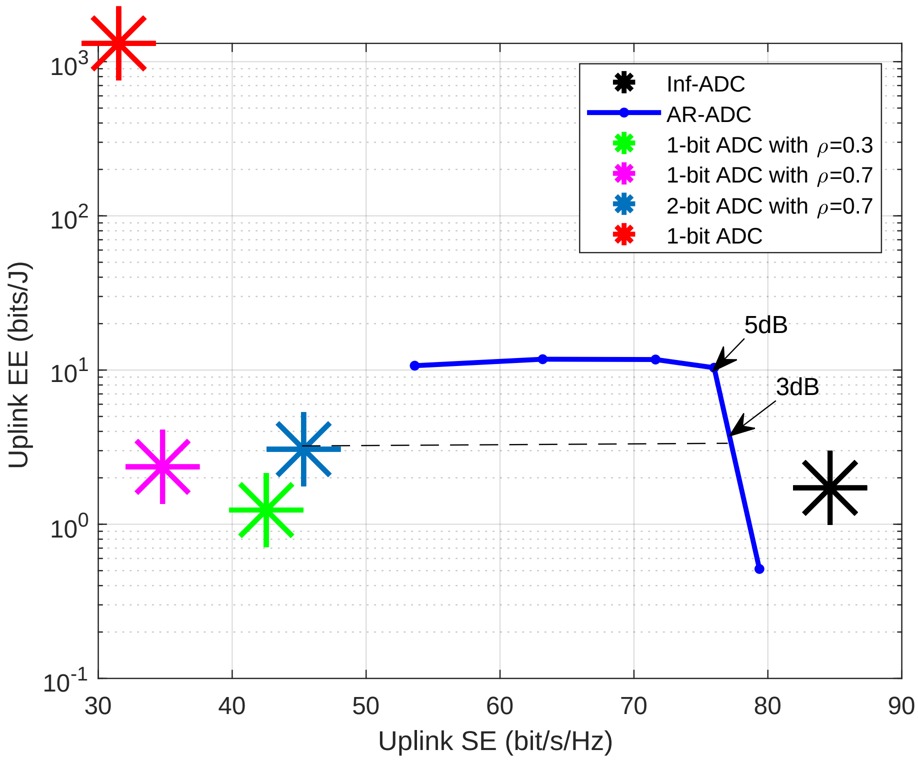

Figure 3.12: EE versus SE based on Δ conditions.

(IAD=50 m, SR=500 m, $\Delta = 0 - 20$dB)

In Fig. 3.12, the parameter Δ acts only on the proposed AR-ADC. The EE of the proposed AR-ADC for any Δ values cannot reach that of one-bit ADC case though, its SE and EE are far better than that of the conventional mixed-ADC cases at some suitable Δ values ($\Delta \leq 15$dB). Meanwhile, the SE of the proposed AR-ADC after Δ adjusting cannot reach that of inf-ADC case though, it can provide better EE at close to SE of the inf-ADC.

3.4 Conclusion

The cell-free DAS architecture with the AR-ADCs to provide the potential energy-efficient OFDM receiver architecture through minimizing the ADC resolution bits has been proposed. The EE performance is improved by the proposed AR-ADC scheme more than tenfold as compared with the other schemes except for the system with only 1−bit ADCs. The reason is that the infinite-resolution ADC deteriorates the EE even though its ratio is relatively small. Moreover, the SE performance is improved by allocating more resolution bits to the APs closer to each UE with the proposed criterion. The proposed AR-ADC doubles the SE as compared with the system with only $1-$bit ADCs.

CHAPTER 4

OVERALL CONCLUSIONS AND FUTURE WORK

To achieve higher data rates, the current standard approach is to use classical linear modulation techniques like MIMO-OFDM and extending the cardinality of modulation as well as the number of antennas. This comes at a severe cost in terms of power consumption per bit, not only due to requiring higher SNR, but also due to reaching limits of the ADC. The most energy efficient ADC per quantization bin is the 1-bit converter. This particular ADC only detects zero crossings, and therefore little-to-no power-consuming AGC circuit needs to be implemented. In some cases, $1-$bit ADCs can be applied instead of inf-ADCs based on our scheme to maintain system performance and reduce power consumption. However, a pure $1-$bit ADC system is still not satisfied with higher performance requirements. Through research and analysis, we found that a reasonable allocation scheme of different resolutions in low-resolution ADCs can not only achieve a large gain in hardware EE, but also improve SE.

4.1 Detection-Selection Scheme for Massive MIMO Systems

In Chapter 2, considering the reduction of power consumption and components cost, the MMSE algorithm and the MRC algorithm are simultaneously considered as the signal detection schemes for the problem of the interference and noise of the current popular massive MIMO system with low-resolution ADCs. Conventionally, MRC uses a diversity combining technique to increase the gains of the received signal, so that the interference and noise are relatively weakened to improve system performance. Also, the computational complexity of MRC is low and is widely used in multi-antenna systems. Due to the multi-channel characteristics of the MIMO system, the received signal at the receiver consists of multiple signals at the transmitter. If the transmitter does not transmit the same data streams, the various data streams will be superimposed at the receiver. Therefore, the data are stripped, and it is crucial to restore each of them. The zero-forcing (ZF) algorithm and the MMSE algorithm are considered as interference cancellation schemes. However, the MMSE algorithm can be seen as a compromise between ZF and MRC according to the previous introduction, because it not only eliminates interference but also does not cause noise enhancement. In theory, MMSE can achieve suboptimal reception but has to be at the expense of higher computational complexity. In a massive MIMO system, the noise is dominant because of the multipath and path loss, as the signal received on each branch of the receiver (BS), which means that the noise power is much larger than the received signal power. At the same time, because the system adopts low-resolution ADC components, the quantization noise generated will harm the detection effect of MMSE. In this way, the performance of the system with low-resolution ADCs will be significantly reduced. First of all, the authors proposed to break through the quantization range limit by controlling the scalable clipping factor C to ensure system throughput.

The numerical results and theoretical analysis show that in this scenario, reducing the quantization range of the ADC can ensure the throughput of the system. Moreover, if shrinking the quantization range of the ADC in a poor SNR environment, not only the throughput of the system will be guaranteed, but also the target of low power consumption and low cost will be realized, and the system performance in the 1-bit ADCs configuration will exceed that in the ideal ADCs (inf-ADCs) configuration. The conclusion is the same when the number of users or the number of antennas in a single cellular system increases.

On the ther hand, the MMSE algorithm and the MRC algorithm have been compared and analyzed based on the above conditions. The numerical results and theoretical analysis show that MMSE detection is better than MRC in the low-resolution ADCs system with the conventional quantization range. The system performance of the MRC is limited by IUI and IAI. If the system is based on the quantization range control scheme of the ADC, the MRC can achieve the same detection effect as the MMSE in the base station of 1024 receive antennas since the noise is clipped. However, 1024 or even a larger number of antennas makes the MMSE algorithm hardly implement in practice. In this scenario, MRC can be used as a better signal detection scheme.

4.2 Aadptive-Resolution ADC Scheme for Cell-Free Distributed Antenna Systems

In Chapter 3, considering a more uniform quality of service (QoS) among users, the AR-ADC scheme has been proposed for application in a cell-free network architecture. It is well known that the cell-free massive MIMO network architecture provides diversity gain due to active deployment densification. In addition, it is no longer restricted by conventional cells, and provides users with better link reliability and QoS. Since the resolution of ADC components used in a system is usually fixedly allocated, i.e., some systems use a uniform resolution, and some systems use an average resolution under power constraints. However, in practice, as the number of the serving APs as well as the distance from the serving APs and UEs continue to change, the performance of the above systems will fluctuate. In order to ensure the optimal performance and stability of the system, it can be achieved through the adaptive allocation resolution to ADCs. First, the author combines path loss and quantization effects to find the clipping factor C that makes each ADC component reach its optimal work point. Furthermore, a quantitative analysis was made on the selection of ADC resolution.

Numerical results and theoretical analysis show that in the cell-free system, the ADC of each AP has its corresponding clipping factor C. In a certain area, the proposed AR-ADC scheme can achieve higher SE in massive MIMO; but with a small number of antennas, the EE of the system can also be improved. Moreover, in the proposed system, the SR of the SE and EE of the system converged to a range of about 300 meters.

Furthermore, massive and ultra-massive MIMO may be applied to next-generation communication systems. Numerical results and theoretical analysis show that the allowable distortion parameter Δ can enable the ADC to select a suitable resolution while meeting requirements for SE and EE. The author's proposal has great potential in the SE-EE trade-off.

4.3 Future Work

In current research, for simple analysis, we assume that the received signals from different UEs are equivalent at the base station in the case of massive MIMO, so only the scaling of the superimposed signals is assumed. The following work plan will consider a scalable quantization range scheme for the received signals with different conditions. Moreover, it is only assumed a case of flat fading in performance evaluation for simplicity since the LOS signal component contributes more significantly to the SE as well as the EE. We also would like to focus on the performance evaluation of the cell-free DAS with adaptive resolution ADC on frequency selective fading in a near future.

In addition, maximizing SE and EE under limited conditions has always been the goal pursued by communication systems. However, the both of them must restrict each other, how to find the best SE-EE trade-off conditions? Moreover, only the massive MIMO and cell-free distributed antenna systems are currently considered. Compared with a cell-free centralized antenna system, which system architecture is more suitable for future communications based on the proposed solution is also an interesting topic.

Appendices

APPENDIX A
ADAPTIVE-RESOLUTION ADC SCHEME FOR CELL-FREE DISTRIBUTED ANTENNA SYSTEM

The derivation of μ in Eq. (3.10) is given in the appendix.

Based on [115], the relationship of the $y_m[u]$, the output q_m^C, and the nonlinear characteristic $Q_b^C(y_m[u])$ is given as

$$q_m^C[u] = Q_b^C(y_m[u]). \tag{A.1}$$

Let $y_m[u]$ be a stationary, Gaussian random variable. Based on Bussgang theorem, the cross-correlation between the input and the output has the same shape as the autocorrelation of input,

$$\mathbb{E}\left\{y_m[u+\tau]q_m^C[u]\right\} = \mu\mathbb{E}\left\{y_m[u+\tau]y_m[u]\right\}. \tag{A.2}$$

From Eq. (A.2) and $\tau = 0$ for the nature of quantization,

$$\begin{aligned}\mu &= \frac{\mathbb{E}\left\{y_m[u]q_m^C[u]\right\}}{\mathbb{E}\left\{y_m[u]y_m[u]\right\}} \\ &= \frac{1}{\sqrt{2\pi\phi[0]}}\int_{-\infty}^{\infty}\frac{y}{\phi[0]}e^{-\frac{y^2}{2\phi[0]}}Q_b^C(y)dy \\ &= \frac{1}{\sqrt{2\pi\sigma_{y_m}^2}}\int_{-\infty}^{\infty}\frac{y}{\sigma_{y_m}^2}e^{-\frac{y^2}{2\sigma_{y_m}^2}}Q_b^C(y)dy,\end{aligned} \tag{A.3}$$

where

$$\phi[\tau] = \mathbb{E}\left\{y_m[u+\tau]y_m[u]\right\}. \tag{A.4}$$

REFERENCES

[1] J. A. del Peral-Rosado, R. Raulefs, J. A. López-Salcedo, and G. Seco-Granados, "Survey of Cellular Mobile Radio Localization Methods: From 1G to 5G," *IEEE Communications Surveys & Tutorials*, vol. 20, no. 2, pp. 1124-1148, Secondquarter 2018.

[2] L. C. Godara, "Application of antenna arrays to mobile communications. II. Beam-forming and direction-of-arrival considerations," *Proceedings of the IEEE*, vol. 85, no. 8, pp. 1195-1245, Aug. 1997.

[3] E. Björnson, E. G. Larsson, and M. Debbah, "Massive MIMO for Maximal Spectral Efficiency: How Many Users and Pilots Should Be Allocated?," *IEEE Transactions on Wireless Communications*, vol. 15, no. 2, pp. 1293-1308, Feb. 2016.

[4] H. Taub, Principles of Communication Systems, McGraw-Hill Education (India), Sep. 2008.

[5] Y. L. Lee, D. Qin, L. -C. Wang, and G. H. Sim, "6G Massive Radio Access Networks: Key Applications, Requirements and Challenges," *IEEE Open Journal of Vehicular Technology*, vol. 2, pp. 54-66, 2021.

[6] K. Kitao A. Benjebbour, and H. Atarashi, “IMT-2020 Radio Interface Standardization Trends in ITU-R,” *NTT DOCOMO Technical Journal*, Jan. 2018.

[7] M. Giordani, M. Polese, M. Mezzavilla, S. Rangan, and M. Zorzi, "Toward 6G Networks: Use Cases and Technologies," *IEEE Communications Magazine*, vol. 58, no. 3, pp. 55-61, Mar. 2020.

[8] B. Shihada S. Dang O. Amin, and M. S. Alouini, “What should 6G be?” *Nature Electronics 3*, pp. 20–29, Jan. 2020.

[9] M. Haenggi, J. G. Andrews, F. Baccelli, O. Dousse, and M. Franceschetti, "Stochastic geometry and random graphs for the analysis and design of wireless networks," *IEEE Journal on Selected Areas in Communications*, vol. 27, no. 7, pp. 1029-1046, Sep. 2009

[10] Q. Nadeem, A. Kammoun, and M. Alouini, "Elevation Beamforming With Full Dimension MIMO Architectures in 5G Systems: A Tutorial," *IEEE Communications Surveys & Tutorials*, vol. 21, no. 4, pp. 3238-3273, Fourthquarter 2019

[11] [Online] Available: www.soumu.go.jp/main$_c$ontent/000538001.pdf

[12] R. H. Walden, "Analog-to-digital converter survey and analysis," *IEEE Journal on Selected Areas in Communications*, vol. 17, no. 4, pp. 539-550, Apr. 1999.

[13] Y. Sanada, "Performance of Full Digital Massive MIMO with Low-resolution Analogto-Digital Converters," *IEICE Technical Report, RCS2019-200*, pp. 121–126, Oct. 2019.

[14] R. H. Walden, Analog-to-digital conversion in the early twenty-first century, Wiley Online Library, Sep. 2008.

[15] R. C. Mathes, "Cover Sheet for Technical Memoranda-A Technique in Information Exchange," *Proceedings of the IRE*, pp. 912–913, Aug. 1949.

[16] T. L. Marzetta, E. G. Larsson, H. Yang, and H. Q. Ngo, Fundamentals of Massive MIMO, In Chap. Multi-Cell Systems, Cambridge University Press, pp. 77–96, 2016.

[17] T. Nakamura, "5G Evolution and 6G," *IEEE Symposium on VLSI Technology*, Dec. 2020.

[18] H. Holma and A. Toskala, WCDMA for UMTS: HSPA Evolution and LTE, Wiley Publishers (5th Edition), 2010

[19] X. Liang, H. Liu, and Q. Wang, "4G Heterogeneous Networks Base Station Planning Using Evolutionary Multi-objective Algorithm," *11th International Conference on Computational Intelligence and Security (CIS)*, pp. 248-252, Feb. 2016.

[20] E. G. Larsson, O. Edfors, F. Tufvesson, and T. L. Marzetta, "Massive MIMO for next generation wireless systems," *IEEE Communications Magazine*, vol. 52, no. 2, pp. 186-195, Feb. 2014.

[21] J. Hoydis, S. ten Brink, and M. Debbah, "Massive MIMO in the UL/DL of Cellular Networks: How Many Antennas Do We Need?," *IEEE Journal on Selected Areas in Communications*, vol. 31, no. 2, pp. 160-171, Feb. 2013.

[22] E. Björnson, L. Sanguinetti, J. Hoydis, and M. Debbah, "Optimal Design of Energy-Efficient Multi-User MIMO Systems: Is Massive MIMO the Answer?," *IEEE Transactions on Wireless Communications*, vol. 14, no. 6, pp. 3059-3075, Jun. 2015.

[23] E. Björnson, J. Hoydis, M. Kountouris, and M. Debbah, "Massive MIMO Systems With Non-Ideal Hardware: Energy Efficiency, Estimation, and Capacity Limits," *IEEE Transactions on Information Theory*, vol. 60, no. 11, pp. 7112-7139, Nov. 2014.

[24] H. Q. Ngo, A. Ashikhmin, H. Yang, E. G. Larsson, and T. L. Marzetta, "Cell-Free Massive MIMO Versus Small Cells," *IEEE Transactions on Wireless Communications*, vol. 16, no. 3, pp. 1834-1850, Mar. 2017.

[25] H. Q. Ngo, L. Tran, T. Q. Duong, M. Matthaiou, and E. G. Larsson, "On the Total Energy Efficiency of Cell-Free Massive MIMO," *IEEE Transactions on Green Communications and Networking*, vol. 2, no. 1, pp. 25-39, Mar. 2018.

[26] G. Interdonato, E. Björnson, H. Q. Ngo, P. Frenger, and E. G. Larsson, “Ubiquitous Cell-free Massive MIMO Communications,” *EURASIP Journal on Wireless Communications and Networking*, article no. 197, Aug. 2019.

[27] J. Zhang, S. Chen, Y. Lin, J. Zheng, B. Ai, and L. Hanzo, "Cell-Free Massive MIMO: A New Next-Generation Paradigm," *IEEE Access*, vol. 7, pp. 99878-99888, Jul. 2019.

[28] A. Paulraj and D. Gore R. Nabar, Introduction to Space-Time Wireless Communications (First ed.) Cambridge University Press (United Kingdom), May. 2003.

[29] G. J. Foschini, "Layered space-time architecture for wireless communication in a fading environment when using multi-element antennas," *Bell Labs Technical Journal*, pp. 41–59, Oct. 1996.

[30] T. L. Marzetta, "Noncooperative Cellular Wireless with Unlimited Numbers of Base Station Antennas," *IEEE Transactions on Wireless Communications*, vol. 9, no. 11, pp. 3590-3600, Nov. 2010.

[31] T. L. Marzetta and A. Ashikhmin, "MIMO system having a plurality of serviceantennas for data transmission and reception and method thereof," *US Patent 8.594*, p. 215, 2011.

[32] L. Lu, G. Y. Li, A. L. Swindlehurst, A. Ashikhmin, and R. Zhang, "An Overview of Massive MIMO: Benefits and Challenges," *IEEE Journal of Selected Topics in Signal Processing*, vol. 8, no. 5, pp. 742-758, Oct. 2014.

[33] F. Rusek, D. Persson, B. K. Lau, E. G. Larsson, T. L. Marzetta, O. Edfors, and F. Tufvesson, "Scaling Up MIMO: Opportunities and Challenges with Very Large Arrays," *IEEE Signal Processing Magazine*, vol. 30, no. 1, pp. 40-60, Jan. 2013.

[34] J. Hoydis, S. ten Brink, and M. Debbah, "Massive MIMO: How Many Antennas Do We Need?," *49th Annual Allerton Conference on Communication, Control, and Computing (Allerton)*, pp. 545-550, Sep. 2011.

[35] J. G. Andrews, X. Zhang, G. D. Durgin, and A. K. Gupta, "Are We Approaching the Fundamental Limits of Wireless Network Densification?," *IEEE Communications Magazine*, vol. 54, no. 10, pp. 184-190, Oct. 2016.

[36] C. Fang, F. R. Yu, T. Huang, J. Liu and Y. Liu, "A Survey of Green Information-Centric Networking: Research Issues and Challenges," *IEEE Communications Surveys & Tutorials*, vol. 17, no. 3, pp. 1455-1472, Thirdquarter 2015.

[37] A. L. Garcia Reis, A. F. Barros, K. Gusso Lenzi, L. G. Pedroso Meloni, and S. E. Barbin, "Introduction to the Software-defined Radio Approach," *IEEE Latin America Transactions*, vol. 10, no. 1, pp. 1156-1161, Jan. 2012.

[38] K. Jayasinghe, P. Jayasinghe, N. Rajatheva, and M. Latva-Aho, "Linear Precoder-Decoder Design of MIMO Device-to-Device Communication Underlaying Cellular Communication," *IEEE Transactions on Communications*, vol. 62, no. 12, pp. 4304-4319, Dec. 2014.

[39] S. Hong, J. Brand, J. I. Choi, M. Jain, J. Mehlman, S. Katti, and P. Levis, "Applications of Self-interference Cancellation in 5G and Beyond," *IEEE Communications Magazine*, vol. 52, no. 2, pp. 114-121, Feb. 2014.

[40] X. Zhang, W. Cheng, and H. Zhang, "Full-duplex Transmission in Phy and Mac Layers for 5G Mobile Wireless Networks," *IEEE Wireless Communications*, vol. 22, no. 5, pp. 112-121, Oct. 2015.

[41] A. Li and C. Masouros, "Energy-Efficient SWIPT: From Fully Digital to Hybrid Analog–Digital Beamforming," *IEEE Transactions on Vehicular Technology*, vol. 67, no. 4, pp. 3390-3405, Apr. 2018.

[42] J. Shen S. Suyama T. Obara, and Y. Okumura, “Influence of Analog Beamforming Configuration on Massive MIMO with Hybrid Beamforming in High Frequency Bands,” *IEICE Technical Report*, pp. 213–218, Mar. 2015.

[43] B. Allen and M. Ghavami, Adaptive Array Systems: Fundamentals and Applications (First ed.), John Wiley and Sons (USA), Feb. 2006.

[44] B. P. Lathi and Z. Ding, Modern Digital and Analog Communication Systems (Fourth ed.), Oxford University Press (USA), Jan. 2009.

[45] P. Robertson and S. Kaiser, "The Effects of Doppler Spreads in OFDM(A) Mobile Radio Systems," *IEEE VTS 50th Vehicular Technology Conference*, vol.1, pp. 329-333, Sep. 1999.

[46] C. H. Doan, S. Emami, D. A. Sobel, A. M. Niknejad, and R. W. Brodersen, "Design Considerations for 60 GHz CMOS Radios," *IEEE Communications Magazine*, vol. 42, no. 12, pp. 132-140, Dec. 2004.

[47] J. Zhang, L. Dai, S. Sun, and Z. Wang, "On the Spectral Efficiency of Massive MIMO Systems With Low-Resolution ADCs," *IEEE Communications Letters*, vol. 20, no. 5, pp. 842-845, May 2016.

[48] C. Mollén, J. Choi, E. G. Larsson, and R. W. Heath, "Uplink Performance of Wideband Massive MIMO With One-Bit ADCs," *IEEE Transactions on Wireless Communications*, vol. 16, no. 1, pp. 87-100, Jan. 2017.

[49] M. Tang, M. Vehkapera, X. Chu, and R. Wichman, "Power Allocation for Multipair Massive MIMO FD Relay Systems with Low Resolution ADCs," *16th International Symposium on Wireless Communication Systems (ISWCS)*, pp. 505-510, Aug. 2019.

[50] P. Dong, H. Zhang, W. Xu, and X. You, "Efficient Low-Resolution ADC Relaying for Multiuser Massive MIMO System," *IEEE Transactions on Vehicular Technology*, vol. 66, no. 12, pp. 11039-11056, Dec. 2017.

[51] C. Kong, C. Zhong, S. Jin, S. Yang, H. Lin, and Z. Zhang, "Full-Duplex Massive MIMO Relaying Systems With Low-Resolution ADCs," *IEEE Transactions on Wireless Communications*, vol. 16, no. 8, pp. 5033-5047, Aug. 2017.

[52] S. Wang, Y. Li, and J. Wang, "Multiuser Detection in Massive Spatial Modulation MIMO With Low-Resolution ADCs," *IEEE Transactions on Wireless Communications*, vol. 14, no. 4, pp. 2156-2168, Apr. 2015.

[53] T. Liu, J. Tong, Q. Guo, J. Xi, Y. Yu, and Z. Xiao, "Energy Efficiency of Massive MIMO Systems With Low-Resolution ADCs and Successive Interference Cancellation," *IEEE Transactions on Wireless Communications*, vol. 18, no. 8, pp. 3987-4002, Aug. 2019.

[54] Y. Xiong, N. Wei, and Z. Zhang, "A Low-Complexity Iterative GAMP-Based Detection for Massive MIMO with Low-Resolution ADCs," *IEEE Wireless Communications and Networking Conference (WCNC)*, Mar. 2017.

[55] S. Moon, I. Kim, D. Kam, D. Jee, J. Choi, and Y. Lee, "Massive MIMO Systems With Low-Resolution ADCs: Baseband Energy Consumption vs. Symbol Detection Performance," *IEEE Access*, vol. 7, pp. 6650-6660, Jan. 2019.

[56] J. Choi, J. Mo, and R. W. Heath, "Near Maximum-Likelihood Detector and Channel Estimator for Uplink Multiuser Massive MIMO Systems With One-Bit ADCs," *IEEE Transactions on Communications*, vol. 64, no. 5, pp. 2005-2018, May 2016.

[57] S. Yoshioka, S. Suyama, T. Okuyama, J. Mashino, and Y. Okumura, "5G massive MIMO with Digital Beamforming and Two-stage Channel Estimation for Low SHF Band," *Wireless Days*, pp. 107-112, 2017.

[58] Y. Xiong, N. Wei, Z. Zhang, B. Li, and Y. Chen, "Channel Estimation and IQ Imbalance Compensation for Uplink Massive MIMO Systems With Low-Resolution ADCs," *IEEE Access*, vol. 5, pp. 6372-6388, Apr. 2017.

[59] O. B. Usman, H. Jedda, A. Mezghani, and J. A. Nossek, "MMSE precoder for massive MIMO using 1-bit quantization," *IEEE International Conference on Acoustics, Speech and Signal Processing (ICASSP)*, pp. 3381-3385, Mar. 2016.

[60] J. Xu, W. Xu, F. Gong, H. Zhang, and X. You, "Optimal Multiuser Loading in Quantized Massive MIMO Under Spatially Correlated Channels," *IEEE Transactions on Vehicular Technology*, vol. 68, no. 2, pp. 1459-1471, Feb. 2019.

[61] T. Liu, J. Tong, Q. Guo, J. Xi, Y. Yu, and Z. Xiao, "On the Performance of Massive MIMO Systems With Low-Resolution ADCs and MRC Receivers Over Rician Fading Channels," *IEEE Systems Journal*, vol. 15, no. 3, pp. 4514-4524, Sep. 2021.

[62] D. Dardari, "Joint Clip and Quantization Effects Characterization in OFDM Receivers," *IEEE Transactions on Circuits and Systems I: Regular Papers*, vol. 53, no. 8, pp. 1741-1748, Aug. 2006.

[63] J. Choi, B. L. Evans and A. Gatherer, "ADC Bit Allocation Under A Power Constraint for MmWave Massive MIMO Communication Receivers," *IEEE International Conference on Acoustics, Speech and Signal Processing (ICASSP)*, pp. 3494-3498, Mar. 2017.

[64] H. Chen, C. Chou, and L. Golubchik, "Adaptive-bit Quantized Massive MIMO Systems with MMSE-based Variational Approximate Message Passing," *16th IEEE Annual Consumer Communications & Networking Conference (CCNC)*, Feb. 2019.

[65] S. Jacobsson, G. Durisi, M. Coldrey, U. Gustavsson, and C. Studer, "Throughput Analysis of Massive MIMO Uplink With Low-Resolution ADCs," *IEEE Transactions on Wireless Communications*, vol. 16, no. 6, pp. 4038-4051, Jun. 2017.

[66] O. Orhan, E. Erkip, and S. Rangan, "Low Power Analog-to-digital Conversion in Millimeter Wave Systems: Impact of Resolution and Bandwidth on Performance," *Information Theory and Applications Workshop (ITA)*, pp. 191-198, Oct. 2015.

[67] L. Fan, S. Jin, C. Wen, and H. Zhang, "Uplink Achievable Rate for Massive MIMO Systems With Low-Resolution ADC," *IEEE Communications Letters*, vol. 19, no. 12, pp. 2186-2189, Dec. 2015.

[68] Y. Dong and L. Qiu, "Spectral Efficiency of Massive MIMO Systems With Low-Resolution ADCs and MMSE Receiver," *IEEE Communications Letters*, vol. 21, no. 8, pp. 1771-1774, Aug. 2017.

[69] M. Srinivasan and S. Kalyani, "Analysis of Massive MIMO With Low-Resolution ADC in Nakagami- *m* Fading," *IEEE Communications Letters*, vol. 23, no. 4, pp. 764-767, Apr. 2019.

[70] E. Nayebi, A. Ashikhmin, T. L. Marzetta, and H. Yang, "Cell-Free Massive MIMO systems," *49th Asilomar Conference on Signals*, Systems and Computers, pp. 695-699, Feb. 2016.

[71] X. Bai, M. Zhou, X. Qiao, Y. Zhang, and L. Yang, "Uplink Performance Analysis of Cell-Free MIMO with Low-Resolution ADCs and ZF Receiver," *22nd International Conference on Advanced Communication Technology (ICACT)*, pp. 125-129. Apr. 2020.

[72] E. Björnson and L. Sanguinetti, "Scalable Cell-Free Massive MIMO Systems," *IEEE Transactions on Communications*, vol. 68, no. 7, pp. 4247-4261, Jul. 2020.

[73] H. Masoumi and M. J. Emadi, "Performance Analysis of Cell-Free Massive MIMO System With Limited Fronthaul Capacity and Hardware Impairments," *IEEE Transactions on Wireless Communications*, vol. 19, no. 2, pp. 1038-1053, Feb. 2020.

[74] Z. Chen and E. Björnson, "Channel Hardening and Favorable Propagation in Cell-Free Massive MIMO With Stochastic Geometry," *IEEE Transactions on Communications*, vol. 66, no. 11, pp. 5205-5219, Nov. 2018.

[75] X. Hu, C. Zhong, X. Chen, W. Xu, H. Lin, and Z. Zhang, "Cell-Free Massive MIMO Systems With Low Resolution ADCs," *IEEE Transactions on Communications*, vol. 67, no. 10, pp. 6844-6857, Oct. 2019.

[76] Y. Zhang, M. Zhou, H. Cao, L. Yang, and H. Zhu, "On the Performance of Cell-Free Massive MIMO With Mixed-ADC Under Rician Fading Channels," *IEEE Communications Letters*, vol. 24, no. 1, pp. 43-47, Jan. 2020.

[77] Ö. Özdogan, E. Björnson, and J. Zhang, "Performance of Cell-Free Massive MIMO With Rician Fading and Phase Shifts," *IEEE Transactions on Wireless Communications*, vol. 18, no. 11, pp. 5299-5315, Nov. 2019.

[78] Y. Zhang, M. Zhou, X. Qiao, H. Cao, and L. Yang, "On the Performance of Cell-Free Massive MIMO With Low-Resolution ADCs," *IEEE Access*, vol. 7, pp. 117968-117977, Aug. 2019

[79] Y. Zhang, H. Cao, S. Wu, M. Zhou, and L. Yang, "Max-Min Fairness for Cell-Free Massive MIMO with Low-Resolution ADCs," *IEEE 8th Global Conference on Consumer Electronics (GCCE)*, pp. 199-200, Feb. 2020.

[80] S. Chakraborty, E. Björnson, and L. Sanguinetti, "Centralized and Distributed Power Allocation for Max-Min Fairness in Cell-Free Massive MIMO," *2019 53rd Asilomar Conference on Signals, Systems, and Computers*, pp. 576-580, Mar. 2020

[81] Y. Zhang, Y. Cheng, M. Zhou, L. Yang, and H. Zhu, "Analysis of Uplink Cell-Free Massive MIMO System With Mixed-ADC/DAC Receiver," *IEEE Systems Journal*, pp. 1-12, Jun. 2020.

[82] J. Zhang, L. Dai, Z. He, S. Jin, and X. Li, "Performance Analysis of Mixed-ADC Massive MIMO Systems Over Rician Fading Channels," *IEEE Journal on Selected Areas in Communications*, vol. 35, no. 6, pp. 1327-1338, Jun. 2017.

[83] N. Liang and W. Zhang, "Mixed-ADC Massive MIMO," *IEEE Journal on Selected Areas in Communications*, vol. 34, no. 4, pp. 983-997, Apr. 2016.

[84] J. Zhang, L. Dai, Z. He, B. Ai, and O. A. Dobre, "Mixed-ADC/DAC Multipair Massive MIMO Relaying Systems: Performance Analysis and Power Optimization," *IEEE Transactions on Communications,* vol. 67, no. 1, pp. 140-153, Jan. 2019.

[85] W. Tan, S. Jin, C. Wen, and Y. Jing, "Spectral Efficiency of Mixed-ADC Receivers for Massive MIMO Systems," *IEEE Access*, vol. 4, pp. 7841-7846, Aug. 2016.

[86] W. B. Abbas, F. Gomez-Cuba, and M. Zorzi, "Bit Allocation for Increased Power Efficiency in 5G Receivers With Variable-resolution ADCs," *Information Theory and Applications Workshop (ITA)*, Aug. 2017

[87] D. Verenzuela, E. Björnson, and M. Matthaiou, "Optimal Per-Antenna ADC Bit Allocation in Correlated and Cell-Free Massive MIMO," *IEEE Transactions on Communications*, vol. 69, no. 7, pp. 4767-4780, Jul. 2021.

[88] J. Choi, B. L. Evans, and A. Gatherer, "ADC Bit Allocation Under A Power Constraint for MmWave Massive MIMO Communication Receivers," *IEEE International Conference on Acoustics, Speech and Signal Processing (ICASSP)*, pp. 3494-3498, Jun. 2017.

[89] I. Z. Ahmed, H. R. Sadjadpour, and S. Yousefi, "An Optimal Low-Complexity Energy-Efficient ADC Bit Allocation for Massive MIMO," *IEEE Transactions on Green Communications and Networking*, vol. 5, no. 1, pp. 61-71, Mar. 2021.

[90] T. E. Bogale, L. B. Le, and X. Wang, "Hybrid Analog-Digital Channel Estimation and Beamforming: Training-Throughput Tradeoff," *IEEE Transactions on Communications*, vol. 63, no. 12, pp. 5235-5249, Dec. 2015.

[91] M. Karlsson and E. G. Larsson, "On the Operation of Massive MIMO With And Without Transmitter CSI," *IEEE 15th International Workshop on Signal Processing Advances in Wireless Communications (SPAWC)*, Nov. 2014.

[92] J. Heiskala and J. Terry, OFDM Wireless LAN: A Theoretical and Practical Guide, SAMS (first ed.), Dec. 2001.

[93] R. V. Nee and R. Prasad, OFDM for Wireless Multimedia Communications, Artech House Publisher (first ed.), 2000.

[94] S. Coleri, M. Ergen, A. Puri and A. Bahai, "Channel Estimation Techniques Based on Pilot Arrangement in OFDM Systems," *IEEE Transactions on Broadcasting*, vol. 48, no. 3, pp. 223-229, Sep. 2002.

[95] K. H. Lundberg, “Analog-to-Digital Converter Testing,” 2002.

[96] T. S. Rappaport, Y. C. Xing, O. Kanhere, S. H. Ju, A. Madanayake, S. Mandal, A. Alkhateeb, and G. C. Trichopoulos, "Wireless Communications and Applications Above 100 GHz: Opportunities and Challenges for 6G and Beyond," *IEEE Access*, vol. 7, pp. 78729-78757, Jun. 2019.

[97] U. Gustavsson, P. Frenger, C. Fager, T. Eriksson, H. Zirath, F. Dielacher, C. Studer, A. Pärssinen, R. Correia, J. N. Matos, D. Belo, and N. B. Carvalho, "Implementation Challenges and Opportunities in Beyond-5G and 6G Communication," *IEEE Journal of Microwaves*, vol. 1, no. 1, pp. 86-100, Jan. 2021.

[98] D. Wang, J. Wang, X. You, Y. Wang, M. Chen, and X. Hou, "Spectral Efficiency of Distributed MIMO Systems," *IEEE Journal on Selected Areas in Communications*, vol. 31, no. 10, pp. 2112-2127, Oct. 2013.

[99] A. Salem, L. Musavian, and K. A. Hamdi, "Wireless Power Transfer in Distributed Antenna Systems," *IEEE Transactions on Communications*, vol. 67, no. 1, pp. 737-747, Jan. 2019.

[100] Y. Zhu, C. H. Chan, U. F. Chio, S. W. Sin, S. P. U, R. P. Martins, and F. Maloberti, "A 10-bit 100-MS/s Reference-Free SAR ADC in 90 nm CMOS," *IEEE Journal of Solid-State Circuits*, vol. 45, no. 6, pp. 1111-1121, Jun. 2010.

[101] T. S. Rappaport, Y. Xing, G. R. MacCartney, A. F. Molisch, E. Mellios, and J. Zhang, "Overview of Millimeter Wave Communications for Fifth-Generation (5G) Wireless Networks—With a Focus on Propagation Models," *IEEE Transactions on Antennas and Propagation*, vol. 65, no. 12, pp. 6213-6230, Dec. 2017.

[102] S. Y. Han, N. B. Abu-Ghazaleh, and D. Lee, "Efficient and Consistent Path Loss Model for Mobile Network Simulation," *IEEE/ACM Transactions on Networking*, vol. 24, no. 3, pp. 1774-1786, Jun. 2016.

[103] E. Garro, M. Fuentes, J. L. Carcel, H. Chen, D. Mi, F. Tesema, J. J. Gimenez, and D. Gomez-Barquero, "5G Mixed Mode: NR Multicast-Broadcast Services," *IEEE Transactions on Broadcasting*, vol. 66, no. 2, pp. 390-403, June 2020.

[104] Y. L. Lee, D. Qin, L. -C. Wang, and G. H. Sim, "6G Massive Radio Access Networks: Key Applications, Requirements and Challenges," *IEEE Open Journal of Vehicular Technology*, vol. 2, pp. 54-66, Jan. 2020.

[105] L. Yu, J. Wu, A. Zhou, E. G. Larsson, and P. Fan, "Massively Distributed Antenna Systems With Nonideal Optical Fiber Fronthauls: A Promising Technology for 6G Wireless Communication Systems," *IEEE Vehicular Technology Magazine*, vol. 15, no. 4, pp. 43-51, Dec. 2020.

[106] H. A. Ammar, R. Adve, S. Shahbazpanahi, G. Boudreau, and K. V. Srinivas, "User-centric Cell-free Massive MIMO Networks: A Survey of Opportunities, Challenges and Solutions," *IEEE Communications Surveys & Tutorials*, vol. 24, no. 1, pp. 611-652, Firstquarter 2022.

[107] H. Yu, X. Yi, and G. Caire, "Topological Pilot Assignment in Large-Scale Distributed MIMO Networks," *IEEE Transactions on Wireless Communications*, Early Access.

[108] X. Wang, A. Ashikhmin, Z. Dong, and C. Zhai, "Two-Stage Channel Estimation Approach for Cell-Free IoT with Massive Random Access," *IEEE Journal on Selected Areas in Communications*, Early Access.

[109] H. A. Ammar, R. Adve, S. Shahbazpanahi, G. Boudreau, and K. V. Srinivas, "Distributed Resource Allocation Optimization for User-Centric Cell-Free MIMO Networks," *IEEE Transactions on Wireless Communications*, Early Access.

[110] V. M. T. Palhares, A. R. Flores, and R. C. de Lamare, "Robust MMSE Precoding and Power Allocation for Cell-Free Massive MIMO Systems," *IEEE Transactions on Vehicular Technology*, vol. 70, no. 5, pp. 5115-5120, May 2021.

[111] P. Anokye, R. K. Ahiadormey, and K. -J. Lee, "Full-Duplex Cell-Free Massive MIMO With Low-Resolution ADCs," *IEEE Transactions on Vehicular Technology*, vol. 70, no. 11, pp. 12179-12184, Nov. 2021.

[112] G. Femenias and F. Riera-Palou, "Fronthaul-Constrained Cell-Free Massive MIMO With Low Resolution ADCs," *IEEE Access*, vol. 8, pp. 116195-116215, Jun. 2020.

[113] Y. Zhang, L. Yang, and H. Zhu, "Cell-Free Massive MIMO Systems With Low-Resolution ADCs: The Rician Fading Case," *IEEE Systems Journal*, Early Access.

[114] O. T. Demir and E. Bjornson, "The Bussgang Decomposition of Nonlinear Systems: Basic Theory and MIMO Extensions [Lecture Notes]," *IEEE Signal Processing Magazine*, vol. 38, no. 1, pp. 131-136, Jan. 2021.

[115] H. E. Rowe, "Memoryless Nonlinearities with Gaussian Inputs: Elementary Results," *The Bell System Technical Journal*, vol. 61, no. 7, pp. 1519-1525, Sep. 1982.